ACS Energy LETTERS

http://pubs.acs.org/journal/aelccp

REVIEW

Colloidal Quantum Dot Photovoltaics: Current Progress and Path to Gigawatt Scale Enabled by Smart Manufacturing

Ahmad R. Kirmani,* Joseph M. Luther, Milad Abolhasani, and Aram Amassian*

Cite This: *ACS Energy Lett.* 2020, 5, 3069–3100

Read Online

ACCESS | Metrics & More | Article Recommendations

ABSTRACT: Colloidal quantum dots (QDs) have lately been pursued with intense vigor for optoelectronic applications such as photovoltaics (PV), flexible electronics, displays, mid-infrared photodetectors, lasers, and single-photon emitters. These nanometer-sized semiconducting crystals can be suitably mass-produced and size-tuned via cost-effective solution-based synthetic routes to operate in the quantum size confinement regime, endowing them with a wide array of exotic optical and electronic properties. While the first potential market entry could be in displays and in niche applications such as "internet-of-things", ultimately, the technology has the potential to influence large-scale terrestrial power generation, because it is amenable to high-throughput synthesis from Earth-abundant materials and large-area solution-based coating techniques and can be air-stable. In this Review, we chronicle the recent advances that have propelled QD PV toward commercialization and highlight potential areas for further progress. We present an account of the material compositions being explored as QDs and their various benefits, major chemical passivation and doping strategies that have been developed to allay QD surface traps, and advanced device designs deployed to maximize charge extraction. We also discuss pathways to >20% efficient QD PV and describe recent advances in high-precision and autonomous synthesis of such materials. With recent demonstrations of scalable synthesis of high-quality QDs, smart manufacturing of QDs and QD solids, and fabrication of stable solar cells under ambient conditions, we suggest that the technology is on the road to achieving maturity and technological relevance and that gigawatt per year distributed panel production sites may be within reach.

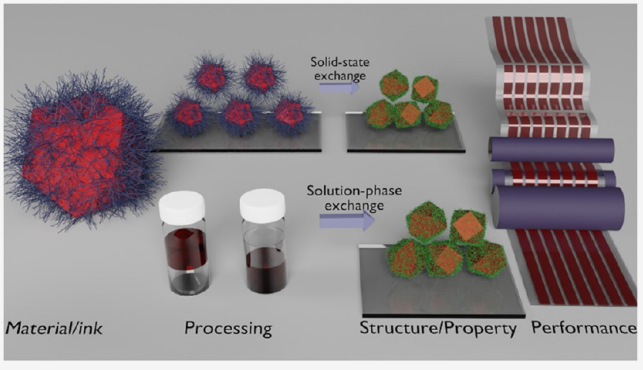

Colloidal quantum dots (QDs) are solution-synthesized nanocrystals of almost any semiconductor compound, with the added benefit of size, shape, and surface chemistry-tunable optical and electronic properties. Conventionally, QDs are synthesized as colloids in organic solvents using the hot-injection method stabilized with long hydrocarbon surface ligands (surfactants). Synthesizing QDs with diameter smaller than the Bohr exciton radius leads to confinement of the photogenerated exciton, which allows the QD bandgap to be precisely tuned by controlling the size of the nanocrystals.[1] Some modern semiconductor nanocrystals, such as metal halide perovskites, have many of the benefits of QDs, including tunability, but achieve this through composition tuning rather than size.

Interest in optoelectronics based on QDs has been spurred primarily by (i) tunable optical bandgaps, (ii) tunable charge transport properties by manipulation of their surfaces and packing, (iii) high defect tolerance leading to relatively high photoluminescence quantum yields (PLQYs) despite their large surface area, (iv) low-cost manufactured single- and multijunction architectures, (v) confinement-induced phase and chemical stabilization, and (vi) the promise of multi-exciton generation (MEG) and utilization of hot-carriers that can potentially enable power conversion efficiencies (PCEs) beyond the present-day silicon (Si) single-junction solar cell technology.

Received: July 7, 2020
Accepted: August 26, 2020
Published: August 26, 2020

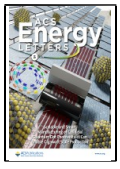

https://dx.doi.org/10.1021/acsenergylett.0c01453
ACS Energy Lett. 2020, 5, 3069–3100

Because ∼50% of the solar spectrum falls in the infrared (IR), which silicon (Si) solar cells, the mainstay of the commercial photovoltaic (PV) technology, cannot efficiently absorb, engineered QDs that harvest further into the IR than currently demonstrated can be used as bottom cells in tandem device architectures augmenting silicon PV and leading to enhancement of overall PCEs. Demonstrations of QDs tailored to absorb in the long-wavelength spectral region of 1100−2500 nm are promising recent developments toward this goal.[2−8] QDs also offer the unique prospect of MEG per absorbed high-energy photon.[9−11] MEG makes QDs exceptional among all the other PV materials and, in theory, allows exceeding the single-junction Shockley−Queisser (SQ) limit of *ca.* 33% PCE for a single-junction device by relaxing the constraint that each photon results in only a single photogenerated electron−hole pair.[12,13] These virtues have put QD solar cells on the roadmap of third-generation PV and have fueled intense research activity over the past two decades, though MEG itself has not yet been leveraged in PV or currently shown to substantially increase overall efficiency.

Initial demonstrations of solar cells based on inorganic nanocrystals involved a bulk heterojunction of CdSe nanorods with the conjugated polymer poly(3-hexylthiophene) (P3HT) as the absorber layer.[14] This era of initial exploration also produced solar cell architectures where QDs were used to sensitize mesoporous metal oxides in both liquid and solid states. CdS, CdSe, PbS, and InP QDs were used to sensitize mesoporous metal oxide layers, similar to the concept and design of dye-sensitized solar cells.[15−17] Lead chalcogenide (PbS and PbSe) QDs were the first class of solution-processed semiconductor nanocrystals to be utilized as standalone QD solid absorbers and semiconductor layers in thin-film PV cells without a polymer heterojunction or metal oxide scaffold. The success of these materials was ascribed to their large dielectric constants, which allow efficient delocalization of the photogenerated excitons resulting in high carrier mobilities and large diffusion lengths within the QD solid.[18,19] However, because QDs employ a large surface-to-volume ratio, many surface-related defect/trap states can form because of dangling bonds, atmosphere-induced surface species, and unsatisfied vacancies resulting in charge trapping. Therefore, a great deal of research effort has focused on developing strategies to properly address the surface ligand removal/replacement, all the while keeping QD solids as close-packed as possible to maximize charge carrier mobility and diffusion. Despite the large density of surface defects, the recent achievement of ∼14% PCEs and remarkable ambient stability and operational stability demonstrates that PbS-based QD solids can be highly tolerant to, and indeed overcome, many of these issues.[20−23]

Recently, colloidal metal halide perovskite QDs have emerged as another, perhaps most defect-tolerant material candidate for cost-effective and solution-processed solar cells, LEDs, and displays. In particular, inorganic perovskite QDs, the primary examples of which are cesium lead halides ($CsPbX_3$, X = I, Br, Cl), exhibit narrow emission line widths, strong optical absorption, excellent carrier mobility, and near-unity PLQYs, and because of QD processing protocols, they have lately been used to achieve 16−17% PCE solar cells with graded architectures that cannot easily be formed using bulk lead halide perovskite thin films.[24,25] The efficiency of these emerging materials is expected to increase well past 20% with more progress in chemistry, processing, and device optimization, and advances will need to leverage chemistry, structure, and size confinement to achieve thermodynamic and/or kinetic stability to surpass the stability of bulk lead halide perovskites.

Besides the obvious virtue of quantum size-confinement in the form of size-tunability of the optical absorption/emission spectrum, crystallographic phase stability/defect tolerance and environmental stability have been largely ignored or underappreciated in most discussions on QDs. This can be best acknowledged in the context of lead halide perovskite QDs. At room temperature, bulk $CsPbI_3$ has a nonperovskite orthorhombic (δ) preferential crystallographic phase which is optoelectronically incompatible as a solar cell active layer because of its large bandgap (>2.8 eV). However, with expanded lattice, i.e. after 300 °C postannealing, the structure undergoes transition into the optoelectronically desirable cubic (α) phase (bandgap ≈ 1.7 eV). The thermal budget involved, however, threatens to make the process unsuitable for low-cost and flexible PV applications. On the other hand, the surface termination of $CsPbI_3$ QDs causes tensile strain which stabilizes the perovskite phase at room-temperature, solving a crucial challenge. Importantly, $CsPbI_3$ QD solar cells have outperformed their bulk counterparts in terms of device performance (PCEs), further expanding the benefits portfolio of nanocrystal size effects. $CsPbBr_xI_{3-x}$ QD solids have also been employed very recently as interlayers to significantly boost the ambient stability of perovskite solar cells.[26]

Improved stability under ambient environment for nanometer-sized perovskites has been demonstrated through reduced dimensionality in the context of layered perovskites. For example, Ruddlesden−Popper and Dion−Jacobson perovskites have been shown to exhibit improved resilience against thermal stress, oxygen, and moisture compared to bulk phase perovskites.[27−30] Likewise, oxidation of bulk galena (PbS) in the presence of water has been well-known.[31] However, because of their size-dependent surface energy, PbS QDs can be made highly air-stable by controlling their crystallographic facets, resulting in highly stable QD solids. Smaller PbS QDs (diameter <4 nm) are mostly covered with Pb-rich (111) facets that bind strongly with surface ligands, increasing air stability of the QDs.[32] This improved stability of PbS QDs has allowed fabrication of highly stable and reliable QD solar cells, including a recent report where the PbS QD solar cells illustrated long-term (>1-year) shelf life in ambient conditions of high relative humidity (RH > 60%) and operational stability over 250 h of continuous illumination.[22]

In most discussions related to QDs to date, surface traps and related phenomena have taken center stage. Despite the well-acknowledged importance of surface traps, the not well-understood and managed surface traps have negatively impacted the performance of QD optoelectronic devices. However, the above-mentioned discussions clearly highlight the unexpectedly improved stability aspect related to dimensionality reduction of PV absorbers in general, and QDs in particular, despite their inherently large surface-to-volume ratio. We believe that better understanding of this key virtue will increasingly engage researchers in this community to pursue QDs as a viable path to stable, thin-film optoelectronics and photovoltaics.

Surface traps in QDs are a direct consequence of the crystal surface termination, and a better understanding of surfaces can potentially lead to efficient trap management strategies. An ideal chemical passivation strategy for QD surfaces will result in suppressed surface traps, reduced interdot spacing,

https://dx.doi.org/10.1021/acsenergylett.0c01453
ACS Energy Lett. 2020, 5, 3069−3100

improved charge transport, improved environmental stability, as well as facile and high-speed device processability.

This Review is focused on covering recent developments and challenges of visible and NIR-harvesting QD solids, including surface traps and successful attempts at alleviating them. Scalable fabrication of long-term stable QD solar cells forms another important focus of this Review. Key developments are highlighted where attempts to achieve trap-passivated QD inks and films have directly resulted in devices that can be scalably fabricated. Recent major advancements including solution-phase ligand exchange and the state-of-the-art *n-i-p* device architecture are discussed in detail, and the issue of moisture vulnerability of the *p*-layer is explored. The Review also highlights how a comprehensive understanding of the QD surface has paved the way to scalable fabrication of robust QD solar cells in realistic ambient environments of high humidity, solving a hurdle to commercialization. The emerging role that data science, machine learning, and artificial intelligence are beginning to play in accelerating the development of QD PV technologies and improving their manufacturing is also discussed. Finally, the Review discusses the prospects for end-to-end manufacturing of QD solar cells by combining smart in-flow synthesis with smart solution-phase solar cell manufacturing to enable low-cost distributed manufacturing of PV with grid-scale potential.

QD Synthesis. QDs offer the benefit of low-cost and facile solution-processability. Historically, hot-injection method in batch (flask-based) reactors has been the gold standard technique to synthesize colloidal QDs with high PLQY and high size monodispersity. However, batch synthesis techniques typically suffer from low manufacturing throughputs with difficulties in scale-up while preserving size dispersity, particularly for colloidal QDs with fast formation kinetics (e.g., organic/inorganic lead halide perovskite QDs). To address this issue and accelerate adoption of QDs in energy technologies, microfluidic synthesis techniques have recently been demonstrated with great success. These advances have enabled continuous production of high-quality QDs with significantly higher manufacturing throughputs without sacrificing their quality and size dispersity.

Hot-Injection Synthesis. The most commonly used synthesis method for lead chalcogenide and metal halide perovskite QDs is the so-called "hot-injection" method, which relies on a rapid injection of organometallic precursors into a high boiling point noncoordinating solvent (e.g., octadecene) in the presence of long-chain hydrocarbon surfactants maintained at an elevated temperature (Figure 1a,b). The hot-injection approach was first demonstrated by Murray and Bawendi for the synthesis of CdE (E = S, Se, Te) QDs from organometallic precursors.[33] Hot-injection leads to a rapid nucleation followed by a slow growth of the QDs, effectively decoupling the nucleation and growth stages of nanocrystals in order to avoid Ostwald ripening that is known to cause defocusing/polydispersity of the QD size.[34] Hot-injection method results in high size-monodispersity (5−10%) of the final product.[33,35,36] This was effectively implemented for PbS QD synthesis in 2003 by Hines and Scholes.[37] Oleic acid (OA) capped PbS QDs were precipitated by addition of a nonsolvent and finally redispersed in an organic solvent such as chloroform or toluene.

The reliance of hot-injection method, in some cases, on hazardous precursors such as bis(trimethylsilyl) sulfide has motivated research toward utilizing alternative, metal precursors.[41,42] A simplified, alternative non-hot-injection method

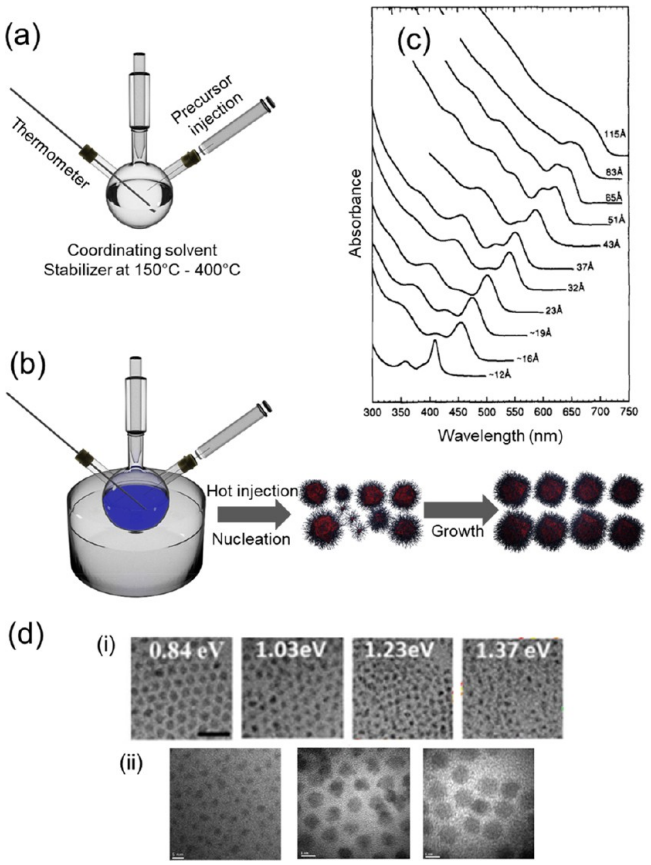

Figure 1. (a) Schematic representation of the hot-injection colloidal QD synthesis technique. (b) The reaction proceeds with a nucleation burst followed by a growth stage as the monomer concentration drops below supersaturation. Reprinted with permission from ref 38. Copyright 2007 Wiley. (c) Optical absorption spectra obtained at room temperature for CdSe QDs in hexane with diameters ranging from 1.2 to 11.5 nm synthesized by the hot-injection method. Adapted with permission from ref 33. Copyright 1993 American Chemical Society. (d) TEM images of PbS and PbSe QDs synthesized in various sizes relevant for optoelectronic applications (i) PbS QDs (scale bar = 20 nm) (Reprinted with permission from ref 39; Copyright 2016 American Chemical Society) and (ii) PbSe QDs (scale bar = 5 nm) (Reprinted with permission from ref 40; Copyright 2015 The Royal Society of Chemistry).

allows for lower temperature synthesis of QDs without compromising on the physical and chemical properties of the final product.[43] Furthermore, large-scale microfluidic synthesis of colloidal QDs has been demonstrated with minimum size dispersity using a numbered-up (parallel microchannels) strategy.[44,45]

A study by Jean et al. concluded that hot-injection is a highly capital-intensive method owing to low yields and, therefore, incompatible with industrial scale-up (Figure 2a).[46] A significant fraction of this high cost is the labor cost which can be attributed to the trial-and-error-based approach toward discovery, screening, and optimization of QDs and the lack of a continuous manufacturing technology for cost-efficient production of high-quality QDs. According to this Monte Carlo cost model, flow-based synthesis and heat-up synthesis can bring down the PbS QD PV module fabrication cost.[46] Further, the authors find that $CsPbI_3$ QD PV modules will cost significantly more than PbS QD PV modules because of the

https://dx.doi.org/10.1021/acsenergylett.0c01453
ACS Energy Lett. 2020, 5, 3069−3100

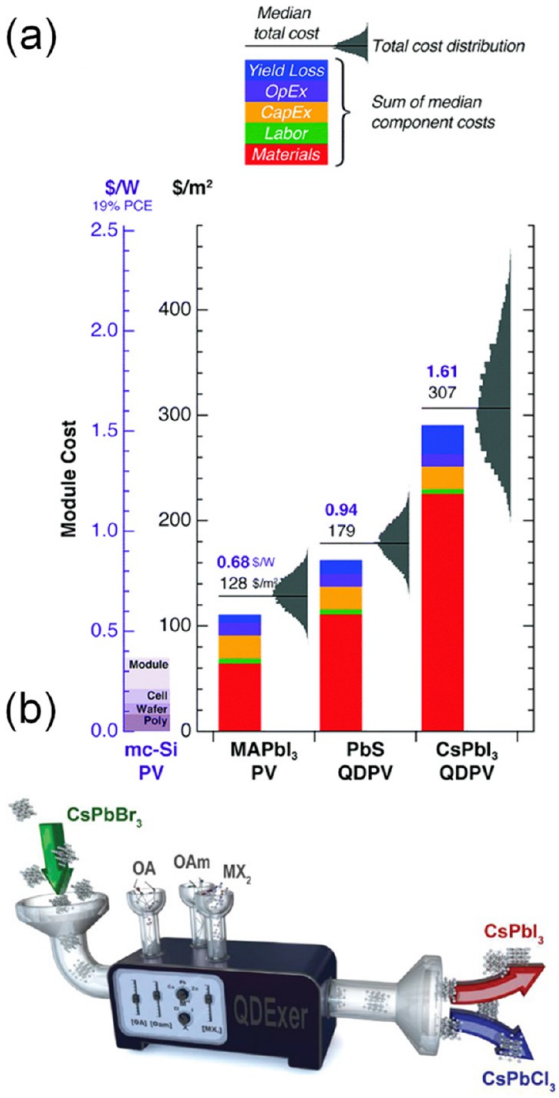

Figure 2. (a) Comparison of the module costs of $CsPbI_3$ and PbS QD PV as predicted by the Monte Carlo cost model. Reprinted with permission from ref 46, published by The Royal Society of Chemistry. (b) Schematic representation of the QDExer technology for automating the synthesis and exchange of QDs. Reprinted with permission from ref 58. Copyright 2019 Wiley.

isolation step involved in the synthesis of those QDs. Scale-up of $CsPbI_3$ QD synthesis is further compounded because of the fast reaction kinetics, which can lead to high size polydispersity.

Microfluidic Synthesis. The concept of microfluidic synthesis of colloidal QDs was first introduced in early 2000 by Mathies and Alivisatos,[47,48] as well as Jensen and Bawendi.[49,50] deMello was the first to demonstrate the potential of rapid synthesis optimization (black-box optimization) of QDs using a glass-based microfluidic reactor integrated with *in situ* spectroscopy.[51] Recently, microfluidic synthesis of QDs,[52−55] particularly lead halide perovskites,[56−59] has received significant attention, mainly because of the enhanced heat and mass-transfer rates as well as precise process control offered by microscale fluidic handling technologies.[60] Microfluidic synthesis of QDs offers the prospect of accelerated formulation screening, fundamental studies, and continuous manufacturing. In 2014, Lignos et al. reported a droplet-based microfluidic synthesis of PbS and PbSe QDs with narrow size distributions over a wide range of bandgaps with *in situ* PL monitoring. The QDs were found to have a noticeably higher PLQY compared to batch synthesis.[52] Lignos et al. recently demonstrated high-throughput screening of fully inorganic lead halide perovskite QDs using a heat-up synthesis approach in a droplet microfluidic platform.[56] The developed automated microfluidic platform enabled rapid parameter space mapping as well as kinetic studies of lead halide perovskite QDs. A recent report by Abdel-Latif et al. utilized a modular microfluidic platform to demonstrate computer-controlled bandgap tuning of $CsPbX_3$ QDs (X: Cl, Br, I), shown in Figure 2b.[58] Using the developed modular microfluidic synthesis technique, called "quantum dot exchanger" (or, QDExer), the QD size distribution, bandgap, and PLQY were simultaneously monitored in real-time using *in situ* UV−vis absorption and PL spectroscopy, during the automated synthesis/halide exchange of $CsPbX_3$ QDs.

It was asserted that a scaled-up continuous flow synthesis of QDs using computer-controlled microfluidic reactors would halve the predicted high labor costs involved in the current QD synthesis. To that end, the authors precisely mixed QD synthesis reagents using a train of monodispersed microdroplets flowing through a microreactor, achieving superior mass-transfer control compared to batch synthesis.[58] The technique can synthesize highly size-monodisperse, precisely bandgap engineered QDs at a production rate as high as 1 kg/day with minimal waste generation. Such modular, computer-controlled QD synthesis platforms integrated with *in situ* diagnostic probes provide an exciting opportunity to combine the wealth of real-time accessible materials informatics with rapidly emerging machine learning tools toward achieving autonomous QD development and manufacturing, as was recently demonstrated by Epps et al.[61]

Optical and Electronic Properties of QDs. The size-dependent bandgap tunability can perhaps be singled out as the distinguishing property of QDs that has been the motivating force behind research interest in the field. Lead chalcogenide QDs have high dielectric constants which allow efficient screening of charge carriers resulting in effective delocalization of carrier wave functions and hence high mobilities in QD solids. High dielectric constants also result in large Bohr radii of photogenerated excitons in these materials (18 nm for PbS).[62−64] QDs with diameters significantly smaller than the exciton radius harbor unique optical and electronic properties owing to quantum size confinement effects. Figure 3a shows the effect of size reduction on the first exciton energy of PbSe QDs. The bandgap of these QDs, and hence the absorption can be tuned simply by changing their size (Figure 3b,c). Thus, whereas bulk PbS exhibits a bandgap of 0.37 eV, PbS QDs of ∼3.2 nm size show a bandgap of ∼1.3 eV. Coupled with strong absorption, bandgap tunability makes QDs attractive for solar cell applications, allowing for more efficient harvest of the solar spectrum compared to conventional solar modules which are limited by single-bandgap absorption (1.1 eV for Si).

From Colloidal Inks to QD Solids. Surface ligands serve *three* crucial purposes during solution-phase synthesis: (i) controlling the growth, leading to enhanced crystallinity; (ii) sterically stabilizing the cores effectively avoiding aggregation; and (iii) electronically passivating the surface of the QDs.[67] The initial organic ligands used to impart colloidal stability to QDs in organic solvents are long-chain, insulating fatty acids (usually, oleic acid, OA) resulting in poor charge transport

https://dx.doi.org/10.1021/acsenergylett.0c01453
ACS Energy Lett. 2020, 5, 3069−3100

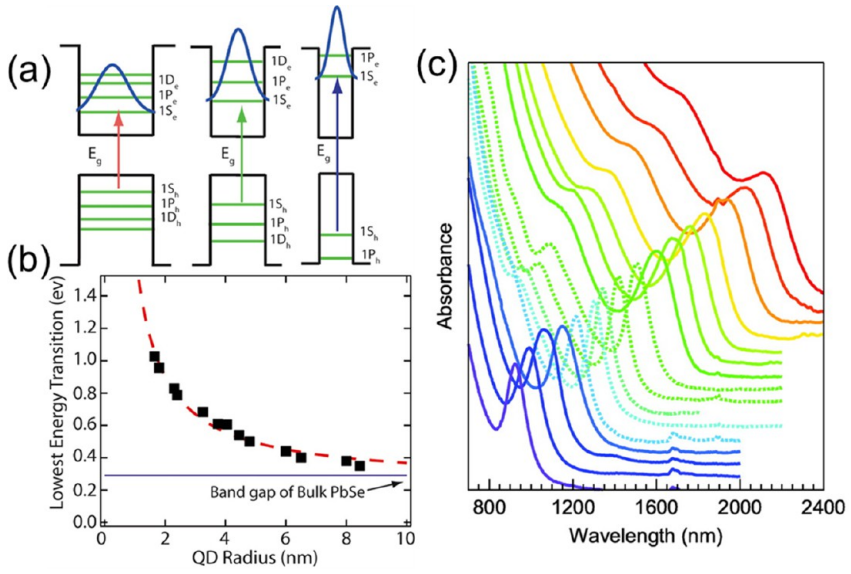

Figure 3. Quantum size effect. (a) Schematic demonstrating increase in quantum confinement with decreasing size of PbSe QDs. Reprinted with permission from ref 65. Copyright 2012 Elsevier. (b) Variation of the bandgap of PbSe QDs as a function of their size. Reprinted with permission from ref 65. Copyright 2012 Elsevier. (c) Absorbance spectra showing excitonic maxima of PbS QDs with sizes ranging from 3 to 10 nm. Spectra are found to red-shift with increasing size. Reprinted with permission from ref 66. Copyright 2011 American Chemical Society.

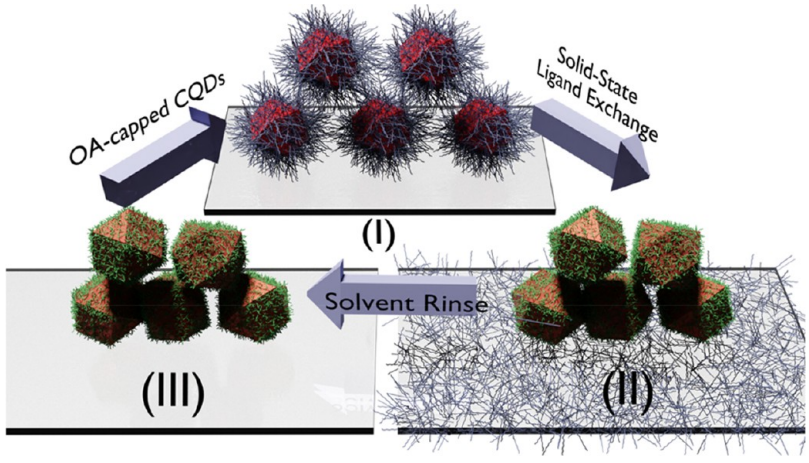

Figure 4. Solid-state ligand exchange. Schematic demonstrates the various steps involved in this exchange process. (I) QDs capped with the longer surfactant (in this case, OA) are cast into a thin solid film. (II) The film is then dipped for a short duration in the solution of a shorter ligand (thiol, halide, amine, etc.). The treatment leads to replacement of the longer ligands with the shorter ones (shown here with green chains capping the QD surfaces). (III) The exchanged thin film is rinsed with a process solvent to remove any traces of the clipped ligands. This process can be repeated several times to build the thickness of an electronically coupled QD active layer for solar cell applications.

through solids made from these QDs, making them the target of substitution with shorter ligands via solid-state or solution-phase ligand exchange.

The long-chain OA ligands, however, have been shown to impart significant order to the QD assembly, which can form long-range ordered superlattices. The transition of OA-PbS QDs from liquid phase to a solid state and appearance of mesoscale order has been studied in detail using grazing-incidence small-angle X-ray scattering (GISAXS).[68−71] Drying kinetics, QD size, and surface ligand type have been shown to impact the final superlattice configuration. In general, visible-NIR PV-relevant ∼1.3 eV bandgap OA-PbS QDs undergo an *fcc*−*bct*−*bcc* superlattice transition (Bain transition) during drying.[68,72] The potential optoelectronic benefits of QD superlattices have been discussed[73−76] but have not been directly translated to ligand-exchanged QD solids in PV applications.

Solid-State Ligand Exchange. The insulating OA−QD solids can be made electrically conductive via a ligand exchange process, wherein the insulating ligands are replaced by shorter, conducting ligands (thiols and halides). Removing the initial OA ligands exposes the QD surfaces to the neighboring environment and creates potentially nefarious surface trap states, which then need to be passivated by the shorter ligand shell. The *solid-state ligand exchange* (SSE) proceeds by briefly dipping the OA−QD solid in a solution of the shorter ligands, as shown in Figure 4.

It is crucial to supply an optimum number of shorter ligands to the OA-QD surface to enable efficient SSE. As the ligand concentration is tuned, the OA-QDs undergo a steep order−

https://dx.doi.org/10.1021/acsenergylett.0c01453
ACS Energy Lett. 2020, 5, 3069−3100

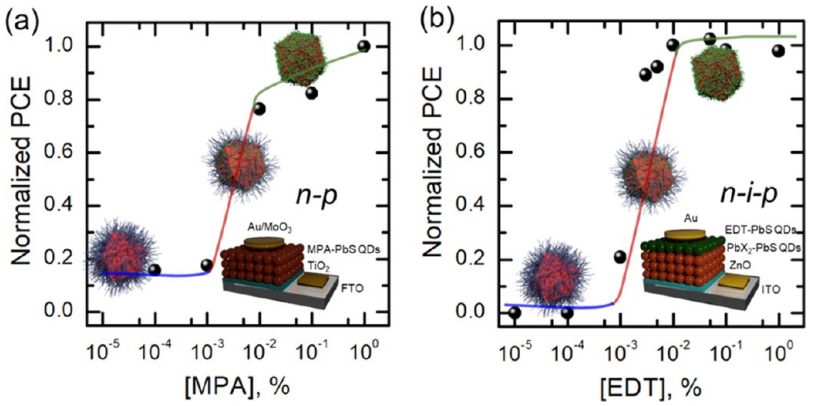

Figure 5. Optimizing solid-state ligand exchange. A sharp phase transition-like behavior in PCEs is observed when shorter ligand concentration (v:v%) during SSE is tuned. Reprinted with permission from ref 77. Copyright 2020 American Chemical Society. This is accompanied by a similar behavior observed for various physicochemical properties (interdot spacing, physical density, optical absorption, and carrier lifetimes) and happens because of an increased ligand−ligand cooperativity once a critical number of short ligands is supplied to the OA-QDs. The study explains why certain solid-state ligand concentrations, often optimized by trial-and-error, have traditionally resulted in the most efficient QD optoelectronics. Insets show the (a) *n-p* and (b) *n-i-p* device architectures and will be discussed in detail under *From QD Solids to Solar Cell Devices*. Also shown in the insets are QD cartoons highlighting the ligand shells getting tuned under the solvent- (blue), transition- (red) and shorter ligand- (green) dominated regimes. Lines are shown as a guide to the eye.

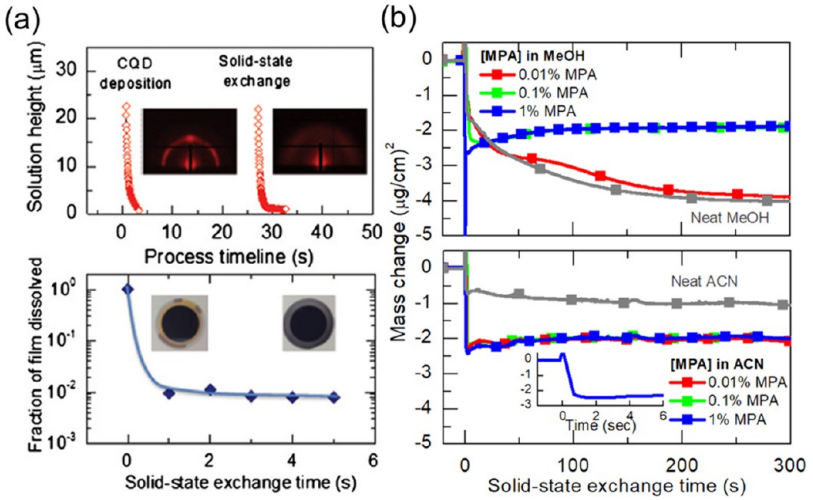

Figure 6. (a) Optical reflectometry and quartz crystal microbalance data demonstrating the rapid volume loss and fast kinetics of SSE. Reprinted with permission from ref 79. Copyright 2013 Cambridge University Press. Insets in top part of panel a are GISAXS patterns highlighting loss of long-range order in the QD solid upon completion of exchange. (b) Mass change of the QD solid during exchange is tracked as a function of exchange time using quartz crystal microbalance and suggests that exchange is complete within the first ∼1−3 s. Insights into exchange kinetics explain the loss of long-range order intrinsic to SSE. Reprinted with permission from ref 81. Copyright 2014 Wiley.

disorder transition, as the authors of this Review have recently found.[77] Below this optimized concentration, solvent effects dominate and the solid remains unexchanged. A sudden transition is then observed near the optimum, above which the various physical and chemical properties of the QD solid (interdot spacing, optical absorption, physical density, carrier lifetimes, PCEs) saturate in the case of PbS QDs, signaling completion of exchange (Figure 5). This likely happens because the interaction of shorter ligands with the OA ligand coronas is kinetically/sterically hindered, and an optimum concentration is required to initiate exchange because of ligand−ligand cooperativity.[77]

The exchange brings the QDs closer, enhancing charge-hopping rates besides ensuring that the QD surfaces remain efficiently passivated. The fast kinetics of the overall process (<1s) coupled to nearly 50% volume reduction, however, quickly destroy the initial long-range order (Figure 6), and all the reports to date have shown the exchanged QD solid to be disordered as the film exhibits only a weak nearest-neighbor coherence peak in GISAXS. The exchanged QD solid becomes insoluble, can be conveniently washed a few times with a process solvent to remove any loosely bound, unexchanged OA and excess shorter ligands without loss of QDs, and therefore allows additional material to be deposited on top without damaging the QD underlayers. This cycle is repeated around 10−12 times, in a layer-by-layer (LbL) process, to yield a *ca.* 300 nm thick film that can be used as the active layer in a solar cell.[78−80]

The first demonstration of SSE dates back to 2003 by Guyot-Sionnest and involved CdSe QDs capped with trioctylphosphine oxide (TOPO). The bulky organic ligands were replaced by dithiols and diamines enhancing charge

https://dx.doi.org/10.1021/acsenergylett.0c01453
ACS Energy Lett. 2020, 5, 3069−3100

transport.[82,83] The successful demonstration of a solution-processed PbS QD-based solar cell by Sargent in 2005 spurred interest in using these quantum materials for optoelectronic applications.[18] Replacing bulky, organic ligands with shorter ones, however, involves significant volume loss and leads to unwanted cracks and pinholes in the film (Figure 7a,b)[80]

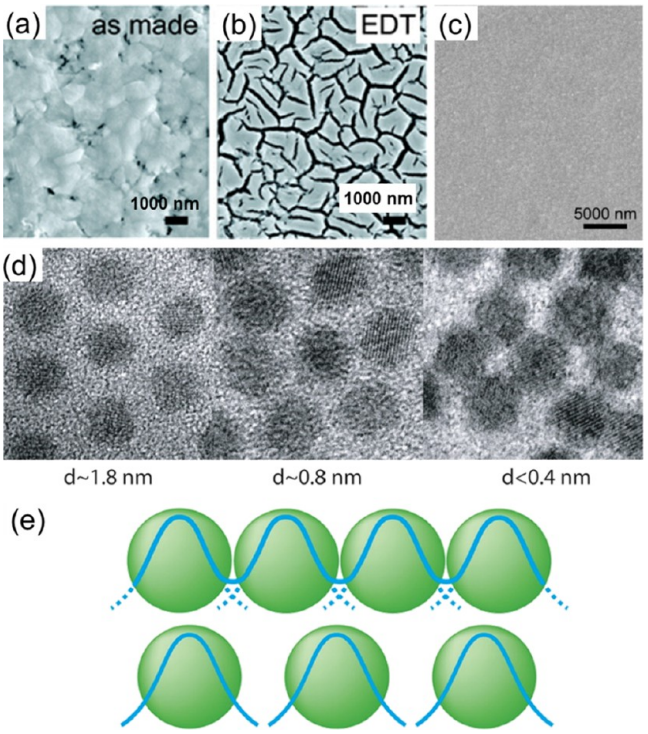

Figure 7. Optical images of spin-coated (a) OA-PbSe QD film and (b) the same film after EDT ligand exchange. Crack formation can be seen owing to the volume contraction upon exchange. (c) SEM image of an LbL film formed via dip-coating showing a smooth surface. Reprinted with permission from ref 80. Copyright 2008 American Chemical Society. (d) TEM images showing reduction in interdot distance when OA-PbSe QD solids are dipped in solutions of shorter ligands (aniline and ethylenediamine). Reprinted with permission from ref 84. Copyright 2006 American Chemical Society. (e) Reduced interdot distance is suggestive of QDs coming closer, leading to enhanced coupling and therefore a conductive solid. Reprinted with permission from ref 65. Copyright 2012 Elsevier.

An alternative was suggested by Luther et al. in the form of LbL SSE, in which several layers of exchanged QDs were deposited, in a repetitive process, leading to a crack-free, thick conductive solid (Figure 7c).[80] Conductive PbSe nanocrystal thin films made by LbL dip-coating and subsequent SSE were obtained using 1,2-ethanedithiol (EDT) as the surface passivant, effectively reducing the interdot distance and enhancing carrier transport.[80] This important work demonstrated LbL as a general method for fabricating QD solids for solar cell applications.

Figure 7d shows a series of TEM images wherein SSE was performed on an OA-PbSe QD solid.[84] The interdot distance decreased from 1.8 nm for OA ligands to 0.8 nm for aniline-capping. This further reduced to <0.4 nm for the case of ethylenediamine ligands. Reduced interdot distance leads to enhanced electronic coupling between adjacent QDs resulting in better wave function overlap and charge transport, as illustrated in Figure 7e. The importance of ligand exchange to transforming an ensemble of QDs into a semiconductor solid cannot be overstated and requires simultaneous passivation of surface trap states together with significant reduction of the interdot spacing while preserving QD integrity, i.e., quantum confinement, as well as thin-film integrity (i.e., no delamination, cracking, or pin holes).

The LbL process involving SSE is currently the standard protocol for transforming OA/oleylamine-capped $CsPbX_3$ QDs into coupled, conductive solids for optoelectronic applications.[24,85,86] While surface ligand exchange on perovskite QDs is far behind in terms of sophistication and diversity of ligands and protocols, some key concepts transfer over to the perovskite system showing generality. In $CsPbI_3$, the strong ionic nature of the compound makes this system incompatible with many polar solvents. It is critical to find a solvent to disperse the new ligands and which does not disperse the QDs with nonpolar organic ligands. Methyl acetate was found to accomplish this task well, promoting a moisture-sensitive displacement of native oleate ligands with short acetate molecules.[86,87] This process alone creates semiconducting films, but it was later found that oleylammonium ligands were not fully removed in the process. Perovskite QDs made this way are distinct in that there are both anionic (oleate) and cationic (oleylammonium) ligands which can be handled in separate steps. Sanehira et al. found that cationic ligands can be replaced with small, typical A-site perovskite cations such as formamidinium or methylammonium.[85] This more complete ligand exchange has two steps but greatly enhances the short-circuit photocurrent of perovskite QD devices and leads to tunability of the transport properties. Surface ligand engineering on $CsPbBr_3$ for efficient LEDs is understandably an important current topic.[88] The general use of shorter ammonium-based ligands such as quaternary ammonium bromides has been demonstrated.[89−91] Imran et al. reported simultaneous and complete cationic and anionic ligand exchange leading to a variety of advantageous features such as enhanced colloidal stability, thermal stability, and PLQY.[92] Lu et al. developed oleate-only ligated perovskite QDs and demonstrated X-type exchange with cinnamate ligands enabling enhanced tunability for photoredox reactions where the nanocrystals can be suspended in semipolar solvents.[93]

It is important to note that while solid-state ligand exchange has traditionally disrupted mesoscale order of the QD solid's superlattice, carrying out a very slow exchange on a long time scale has been shown to preserve the initial long-range *bcc* superlattice of the OA-QDs, resulting in significantly improved charge transport in the QD solid and highlighting the impact that preservation of long-range order can have on electrical properties of device-relevant QD films.[73] This result highlights the needs for more in-depth understanding of the complex ligand exchange process; a fundamental understanding of ligand exchange kinetics and thermodynamics and their relationship to the mesoscale ordering of the QD solid; and the development of structure−property relationships that govern QD self-assembly, ligand exchange, and transformation of electronically uncoupled OA-capped QD solids into a solid-state semiconductor film. Translation of this scientific knowledge of ligand exchange into successful engineering and manufacturing practices is therefore crucial for QD solids and QD-based thin-film PV.

Solution-Phase Ligand Exchange. Although the SSE process enhances charge transport tremendously, it requires repetitive

https://dx.doi.org/10.1021/acsenergylett.0c01453
ACS Energy Lett. 2020, 5, 3069−3100

Translation of the scientific knowledge of ligand exchange into successful engineering and manufacturing practices is crucial for QD solids and QD-based thin-film PV.

LbL deposition and processing, which are generally reliant on spin-coating, an easy-to-use but highly wasteful laboratory technique, making the processing incompatible with industrial scale-up. Dip-coating is more scalable to large areas and can be easily automated to meet industrial demands; however, the QD inks and solutions are likely to get contaminated during ligand exchange and may therefore require sophisticated and costly solvent recovery and purification. This expectation is based on an earlier demonstration of large-area scalable spray-coated PbS QD solar cells that required LbL build-up using SSE and consumed 155 g·m^{-2} PbS QDs compared to 58 g·m^{-2} for laboratory-based spin-coating.[94,95]

More recently, an alternate route to realizing exchange has been developed that employs a solution phase to carry out the exchange process. The *solution-phase ligand exchange*, or SolEx, yields an exchanged, *ready-to-coat* QD ink that helps realize single-step deposited active layers, moving away from the time- and materials-wasting LbL process.[96−98] SolEx, therefore, presents itself as a more economic and industrially viable route to high-performing QD PV scale-up. Indeed, this can be acknowledged from the fact that recent demonstrations of PbS QD solar cells using SolEx inks have utilized 25 g·m^{-2} (spin-coating), 6 g·m^{-2} (spray-coating), and 1 g·m^{-2} (blade-coating) PbS QDs, which are significantly smaller consumptions than SSE with spin-coating.[22,96,99]

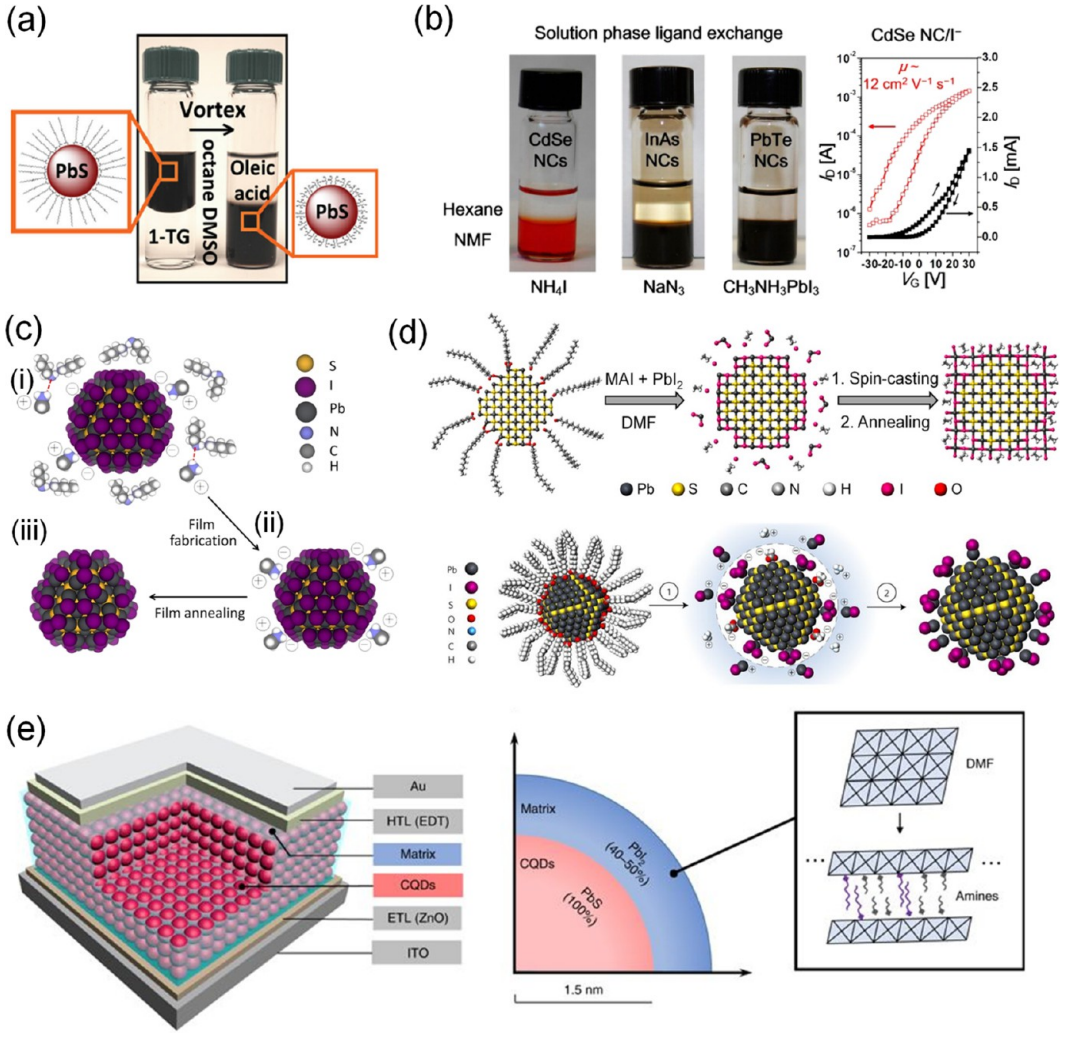

Figure 8. Solution-phase ligand exchange. (a) OA-PbS QDs in octane (left) are mixed in solution phase with TG. The QDs become soluble in a polar solvent such as DMSO following the exchange (right). Reprinted with permission from ref 106. Copyright 2013 Wiley. (b) Halide-, pseudohalide-, and halometallate-capped QDs obtained via solution-exchange exhibiting excellent charge transport properties. The exchanged QDs are soluble in *N*-methylformamide (NMF). Reprinted with permission from ref 107. Copyright 2014 American Chemical Society. (c) Iodide-capped QDs obtained using MAI as the precursor. Reprinted with permission from ref 108. Copyright 2014 American Chemical Society. (d) Perovskite-shelling of QDs (upper panel) (Reprinted with permission from ref 97. Copyright 2015 American Chemical Society) and PbX_2-QDs employing ammonium acetate as a colloidal stabilizer (lower panel). Reprinted with permission from ref 96. (e) Two-dimensionally confined PbI_2 matrix shells on QDs for improved carrier diffusion lengths. Reprinted with permission from ref 109.

https://dx.doi.org/10.1021/acsenergylett.0c01453
ACS Energy Lett. 2020, 5, 3069−3100

An efficient SolEx process was demonstrated by Talapin and co-workers that involved replacing the long-chain, organic insulating ligands on CdSe QDs with inorganic molecular metal chalcogenides (MCC) in solution phase, yielding field-effect electron mobilities (FET) as high as 38 $cm^2 V^{-1} s^{-1}$.[100−102] These demonstrations illustrate the remarkable ability of SolEx to passivate surface traps and electronically couple QDs to form a QD solid. The electronic coupling has been shown to result in coherent excitons which can exist over multiple nanocrystals before dephasing.[103]

The first attempts at employing SolEx for PV applications goes back to 2005 when Gur et al. used pyridine molecules to replace the initial, insulating ligands on rod-shaped CdSe and CdTe nanocrystals. These exchanged nanorods were used as absorber layers in a bilayer structure for solar cells reaching 3.0% PCEs.[104] In the context of PbS QDs, one of the first demonstrations of the SolEx came in the form of a 1.8% PCE Schottky solar cell that employed *n*-butylamine (BTA) ligand to replace the OA capping layer in solution phase.[105]

The previous attempts (noted above) employed more than one layer to achieve the desired absorber thickness. However, the promise of SolEx lies in the possibility of a single-step deposited absorber layer that can do away with the menial and wasteful LbL protocol. The first such attempt involved replacing the initial OA ligands with shorter, conducting thioglycerol (TG) molecules in solution phase (Figure 8a).[106] The exchanged QDs were redispersed in a polar solvent, dimethyl sulfoxide (DMSO), and were drop-cast to make the absorber layer. Drop-casting was necessary because DMSO is a high boiling point solvent (189 °C), and therefore, film formation requires a longer time (~5 h). The QDs, however, suffered from poor surface coverage leading to low PCEs (~2%). Also, charge transport was found to be limited by the morphological inhomogeneity of the film, including pinhole formation in the drop-cast film, which was reflected by the low fill factor (FF) of 35% in PV devices. The procedure nonetheless opened routes toward achieving directly deposited conductive active layers of PbS QDs in a single-step, avoiding the rigor and materials wastage involved in the standard SSE process.[79,106]

The *solution-phase ligand exchange*, or SolEx, yields an exchanged, *ready-to-coat* QD ink that helps realize single-step deposited active layers, moving away from the time- and materials-wasting LbL process.

Recently, metal halides and hybrid perovskites have been explored as the shorter ligands in the latest brand of solution-exchanged QD inks.[6,96−98,107,108,110,111] Halide-, pseudohalide- and halometallate-capped QD inks with excellent optical and electronic properties were obtained, ushering in a new class of robust inks that could be deposited, in a single-step, as active layers for solar cells.[98,107,110] In one such report, iodide-capped CdSe QD films were found to have field-effect mobilities as high as 12 $cm^2 V^{-1}s^{-1}$ (Figure 8b).[107]

One of the first demonstrations of high-efficiency solar cells based on these robust, solution-exchanged QD inks came in 2014 when Ning et al. demonstrated a solar cell featuring a single-step deposited QD active layer.[108] The QDs were capped with iodide ligands obtained via solution-exchange. The solar cell exhibited a PCE of ~6%, an encouraging device performance given that no solid-state LbL treatment was needed. The steps involved in the exchange process and film fabrication are shown in Figure 8c. A solution of methylammonium iodide (MAI) precursor in dimethylformamide (DMF) was mixed with an octane-based colloid of OA-PbS QDs. Vigorous mixing of the two phases led to ligand exchange in the solution phase observed as a phase separation. These exchanged QDs were then separated, centrifuged, and redispersed in BTA. The advantage of using the lower boiling point solvent BTA (77−79 °C), as compared to the previous attempt which employed DMSO, was that it enabled a faster solution drying and solidification of the QD film, allowing moving away from drop-casting to spin-coating to achieve sufficiently thick photoactive layers in a single step. The BTA-based QD ink was spin-coated to form a single-step deposited, uniform, and continuous active layer. The final film was mildly annealed to remove the organic methylammonium counter-cations, leaving behind a completely inorganic QD solid.

This demonstration was followed by a report where the authors employed a mixture of MAI and lead iodide (PbI_2) as precursors in the solution-exchange step.[97] This resulted in replacement of the OA ligands and formation of methylammonium lead triiodide ($MAPbI_3$), a hybrid perovskite, on the surface of the QDs, upon mild annealing (Figure 8d, upper panel). These $MAPbI_3$−PbS QD solar cells exhibited high PCEs approaching 9%, which was remarkable for a single-step deposited device.

A novel precursor mixture was recently reported wherein the authors aimed to maximize the halide ligand coverage of the QD surfaces (Figure 8d, lower panel).[96] A mixture of PbX_2 (X = I and Br) and ammonium acetate (AA) dissolved in DMF was used as the precursor solution. AA was found to facilitate the exchange process and was removed from the final QD solid during precipitation. The exchanged QDs were redispersed in BTA and spin-coated to form the absorbing layer. As a result of the high halide surface coverage, these QD solids featured significantly suppressed band tails leading to gains in device performance, compared to all the previous SolEx-based QD solar cells. With PCEs as high as 11.3%, this recipe, for the first time, also outperformed solid-state LbL-deposited QD solar cells. Until this point, the absorber layers had to be limited to *ca.* 300 nm in thickness, owing to their moderate photocarrier diffusion lengths. This resulted in a trade-off between optical absorption (short-circuit current, J_{SC}) and carrier extraction (FF). The gain in J_{SC} for thicker absorbers was compromised by a decrease in FF. It was later found by Xu et al. that redispersing these SolEx PbS QDs in an amine solvent mixture (BTA, amylamine, and hexylamine in a 7:2:1 volumetric ratio) led to the growth of a two-dimensional inorganic passivating matrix around the QD surface leading to improved photocarrier diffusion length (Figure 8e).[109] Formation of solvent−PbX_2 complexes was also found to increase solution viscosity, resulting in thicker active layer deposition by spin-coating. This allowed for *ca.* 500 nm thick absorbers with simultaneous boosts in J_{SC} and FF and resulted in 12.5% PCE solar cells.

These latest solar cell advances suggest halide-ligands to be unique surface passivants. This choice makes sense in view of recent insights gleaned from inelastic neutron scattering and *ab initio* molecular dynamics simulations highlighting the role of QD surfaces in charge trapping.[112] Wood and co-workers have demonstrated that phonon modes on mechanically "soft" QD

https://dx.doi.org/10.1021/acsenergylett.0c01453
ACS Energy Lett. 2020, 5, 3069−3100

surfaces couple strongly with electronic transitions leading to carrier trapping. This study highlights the necessity of employing surface ligands that exhibit low vibrational modes, such as halides. Halide surface passivation results in "rigid" QD surfaces, suppressing the electron−phonon coupling and leading to reduced carrier recombination.[113]

One of the promises of SolEx QD inks is to enable long-range order via self-assembly in resulting solids by avoiding the disruptive SSE process and thus allow improved carrier mobilities and, potentially, band-like transport.[74,114,115] However, all of the reports on SolEx PbS QDs, to date, indicate the presence of only the nearest-neighbor coherence peak in GISAXS similar to solid-state exchanged QDs and a complete absence of long-range order. Long-range order has been associated with size dispersity of the initial OA-PbS QDs prior to exchange, and therefore, further improvements in size dispersity, for instance, by employing microfluidic synthesis, can likely result in long-range order via SolEx. The biggest culprit by far, however, is likely to be the nonequilibrium solution-processing methods, whereby solidification of the solute has been shown, through extensive *in situ* characterization, to occur in the very last second(s) of the solution drying process.[116] This is known to occur in spin-cast molecular,[117−119] polymeric,[116,120] and metal halide perovskite materials,[121−123] as well as in QD films.[79,109] In a rapidly drying solution, the solidification process involves complex phase transformation which is initiated by heterogeneous nucleation and growth at first, but quickly transitions to bulk precipitation as the solution becomes highly supersaturated,[124] with the remaining solute becoming quenched into a disordered phase. The upside of rapid drying in solution processing is that it forms uniform films which tend to be pinhole-free, a major requirement for solar cell devices to work. However, this compromise between mesoscopic order and macroscopic imperfections points to significant opportunities in leveraging innovations in ligand chemistry, self-assembly, formulation science, and processing to make major improvements to QD solid-state semiconductor engineering. Controlling the temporal and spatial onsets and mechanism of solidification should alter the quality of QD solids, analogous to how it has impacted other solution-processed semiconductors, such as conjugated organic materials and bulk metal halide perovskites, with direct impact on their solid-state semiconductor properties and PV device performance.

The compromise between mesoscopic order and macroscopic imperfections points to significant opportunities in leveraging innovations in ligand chemistry, self-assembly, formulation science, and thin-film processing to make major improvements to QD solid-state semiconductor engineering.

In this regard, the recent success of metal halide passivation is worth a closer look, because metalate−solvent complexes are known to form and can dominate the solution processing of these materials via formation of a *sol* which can dramatically slow the effective drying kinetics by retaining the solvent in the as-cast film through a sol−gel process.[121,125] The estimation of solvent retention varies from ca. 50% to 70% by volume in as-cast hybrid perovskite films.[121,123] It has also been demonstrated that the metal halide formulation can extend the normal drying time of a solvent mixture from <20 s to >3 min without altering processing conditions.[123] The observation of enhanced solvent retention has been made in the latest generation of QDs cosolubilized with metal halides by *in situ* measurements of the solution thinning kinetics during spin-coating,[109] which pointed to a sol−gel-like film formation mechanism in contrast to traditional QD solids, requiring thermal annealing to remove the trapped solvent. This constitutes among the first examples of a passivation strategy which can also alter the ink viscosity and film thickness, solidification kinetics, and mechanism of QD solid formation with direct implication on their optoelectronic properties.

Atomic-Ligand and Hybrid Passivation. A few other surface passivation schemes that were the state-of-the-art recently are worth mentioning here. Most of these have now been outperformed by the novel, halide-based SolEx schemes (discussed above). They may offer lessons and inspiration for the lead halide perovskite QD solar cells to adopt. These schemes employed a combination of an initial solution-phase and a solid-state exchange, and at the time, led to high-performing solar cells. These attempts (Figure 9) highlighted the importance of halide passivation and, therefore, guided the research front toward the now-established halide-SolEx.

One of these schemes, the "atomic-ligand passivation", employed an initial solution-phase step where the OA-PbS QDs were first treated with a mixture of cadmium chloride ($CdCl_2$), tetradecylphosphonic acid (TDPA), and oleylamine (OLA).[126] The resulting cadmium−tetradecylphosphonic acid (Cd−TDPA) complex passivated the surface dangling bonds. The QD solid obtained from this ink was then made to undergo an SSE with cetyltrimethylammonium bromide (CTAB) dissolved in methanol (MeOH). This second step ensured that the final solid was left with purely inorganic atomic passivants on the QD surfaces, resulting in LbL-deposited devices with PCEs of ∼6%, a QD PV record at the time.

Another similar scheme developed *n*-type PbS QDs by first partially exchanging a few of the surface OA ligands with iodide atomic ligands.[111] Tetrabutylammonium iodide (TBAI) precursor was employed. This was then followed by an SSE with TBAI solution in MeOH. This "sol−hal" approach resulted in an *n*-type QD solid which was exploited in a quantum-junction QD solar cell (*n-p* homojunction architecture; to be discussed in detail later) with a PCE of 6.6%, besides the demonstration of a record electron FET mobility at the time (for a QD solid with a bandgap >1.2 eV) of 0.24 $cm^2 V^{-1} s^{-1}$.

In 2012, Ip and Thon showed that a ligand exchange strategy designed to deliver inorganic ligands in solution phase followed by organic thiol molecules in solid state can lead to improved trap passivation and closer packing of the QD solids.[127] This strategy, called the hybrid ligand exchange, translated into high-performing solar cells with a certified record PCE of 7%. The strategy involved supplying $CdCl_2$ to the as-synthesized OA-PbS QDs in solution phase. Binding of the metal cations as well as the halide atoms to the surface atoms was confirmed spectroscopically. The halides and cations successfully tied to the surface sites that were otherwise not easily accessible because of steric hindrance of the bulky OA molecules. These pretreated QDs were then subjected to

https://dx.doi.org/10.1021/acsenergylett.0c01453
ACS Energy Lett. 2020, 5, 3069−3100

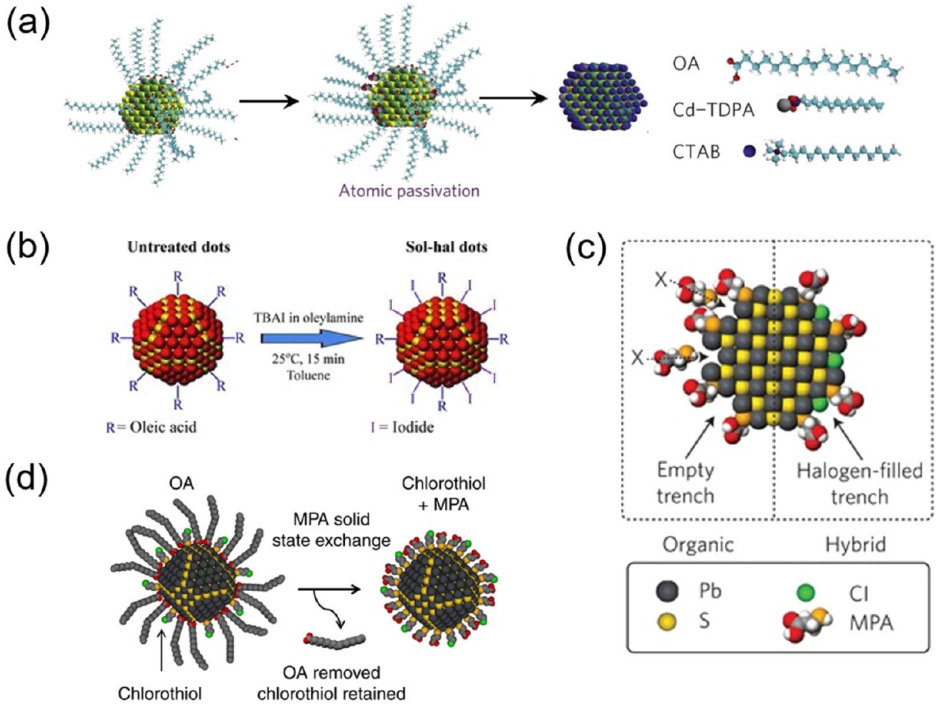

Figure 9. Schematics summarizing ligand exchange strategies that involved an initial solution-phase treatment followed by an SSE step. (a) Atomic ligand passivation scheme involving the removal of OA with Br atoms. Cetyltrymethylammonium bromide (CTAB) is used to carry the Br atoms to the surface. A solution-phase treatment of the OA-PbS QDs with a mixture of $CdCl_2$, TDPA, and OLA aimed at passivating the surface dangling bonds precedes the SSE. Reprinted with permission from ref 126. Copyright 2011 Springer Nature. (b) The sol-hal approach involves an initial solution-phase halide passivation that removes some of the weakly bound OA and replaces them with halogen atoms. Iodine is delivered via TBAI salt dissolved in MeOH. Reprinted with permission from ref 111. Copyright 2012 Wiley. This is followed by a TBAI-based SSE, resulting in an n-type QD solid. (c) Schematic explaining the concept of hybrid passivation. SSE with organic ligands (MPA) leads to empty trenches on the QD surface owing to steric interaction between the organic molecules (left). These unpassivated trenches can behave as carrier traps. An initial solution-phase treatment employing atomic passivants (for example, halides) can avoid this scenario (right). Reprinted with permission from ref 127. Copyright 2012 Springer Nature. (d) This strategy involves a solution-phase ligand exchange step in which chlorothiols and $CdCl_2$ are introduced to the QD surface. This is followed by the usual SSE with MPA. Reprinted with permission from ref 128. Copyright 2014 Springer Nature.

an SSE with MPA, leading to efficiently coupled PV solids. The hybrid-passivated QD solids exhibited significantly suppressed trap states owing to enhanced surface passivation, as proved by ultraviolet and inverse photoemission spectroscopies (UPS and IPES) that allow direct measurements of the band tail states.[129] The concept of metal halide passivation can be used to tune a variety of the properties of PbX QD arrays through judicious choice of salts.[130]

> The currently achievable manufacturing throughput for perovskite QDs with a low-cost single-channel microfluidic reactor is ∼100 g/day, which is clearly aligned with industrial adoption and can be easily scaled-up to 1−10 kg/day using a numbered-up strategy.

Nonetheless, it is highly likely that the harsh and rough nature of the SSE step might leach off some of the surface passivation imparted to the QDs during the solution-exchange step, resulting in trap formation.[81] To overcome this, a modification to the hybrid passivation scheme was developed with introduction of chlorothiols along with $CdCl_2$ in the solution-exchange step.[128] The strongly binding thiols remain attached to the QD surface during the harsh SSE step resulting in better-than-ever surface passivation. This resulted in enhanced carrier diffusion lengths driven by a suppression of recombination centers leading to PCEs of 8.5%.

While atomic and hybrid passivation approaches have been surpassed in the PbS QD literature, we take the view that opportunities exist for such strategies in perovskite QDs, where ligand passivation is comparatively rudimentary but an active topic of research.[93]

QD Doping. Doping of the QD solid is crucial, just as doping of any other semiconductor, as it allows for tailoring the transport properties by changing carrier concentration. This is the basis of semiconductor heterojunctions and is foundational for numerous applications, such as photodetectors, solar cells, and transistors.[19,100,131−140] Substantial effort has, consequently, focused on realizing efficient doping of QDs. However, initial attempts which involved mixing of dopants with the QD precursors in solution phase during synthesis were less successful.[141]

The striking observation by Guyot-Sionnest and co-workers that sodium biphenyl leads to $1S_e-1P_e$ intraband absorption in CdSe QDs via remote charge transfer opened the door to realizing successful doping schemes in QDs.[142] Significant increase in film conductivity was observed for CdSe QDs when potassium was used as the dopant.[83] Impressive enhancements in mobilities of PbSe QD solids were found upon hydrazine

https://dx.doi.org/10.1021/acsenergylett.0c01453
ACS Energy Lett. 2020, 5, 3069−3100

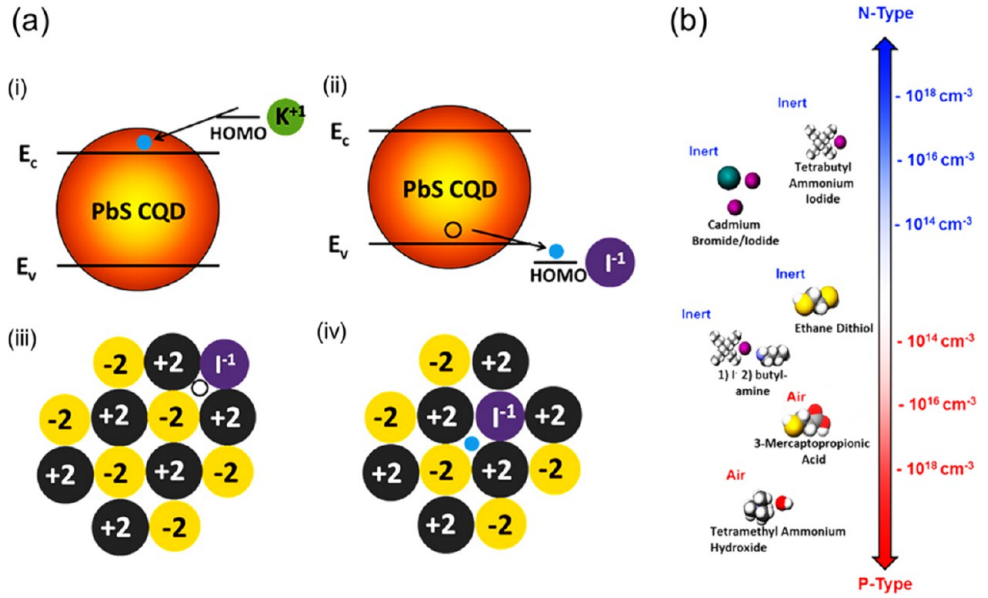

Figure 10. (a) Remote doping by the ligands can be explained from the alignment of energy levels at the interface of the QD and the ligand. A remote cation (potassium) with a shallow HOMO level (lying above the conduction band minima (CBM) of the QD) will behave as a donor, leading to *n*-doping (i). On the other hand, a remote anion (iodide) with HOMO deeper than the valence band maxima (VBM) of the QD will result in *p*-doping (ii). Parts iii and iv represent remote and substitutional doping scenarios by iodide ligands, respectively. The type of doping can be discerned simply by counting the total number of excess electrons in the system for each case. Reprinted with permission from ref 144. Copyright 2012 American Chemical Society. (b) Effect of various ligand treatments on the doping density of PbS QDs obtained from FET measurements. Reprinted with permission from ref 144. Copyright 2012 American Chemical Society.

treatment suggestive of charge-transfer doping.[19] Substitutional doping, which requires the dopant to replace an atom from the QD, forms the second important category of doping in QDs.[143]

Ligands as Remote Dopants. Besides enhancing electronic coupling between QDs, ligands can also be chemically and electronically designed to alter and tune the QD carrier concentration and can therefore act as remote dopants.[142] A charge−orbital balance picture has been suggested to predict the doping phenomenon in QDs based on the overall stoichiometry.[144] Under this premise (Figure 10a), the nature of doping (*n*- or *p*-type) can be determined simply by calculating the total number of excess electrons available to the QD. For the case of iodide ligands on PbS QDs, remote charge transfer results in an extra hole and, therefore, *p*-dopes the solid. Substitution of a sulfur atom with an iodide, on the other hand, results in an extra electron, *n*-doping the solid. Given the vast library of available ligands, the carrier concentration and doping of QDs can be tuned over a wide window (Figure 10b).

High carrier mobilities have been achieved for PbS QDs capped with iodide ligands.[111,144−147] Employing iodide ligands, *n*-type PbS QDs were realized leading to high-efficiency quantum junction and inverted solar cells.[148,149] The Konstantatos group has demonstrated remote trap passivation by employing zinc oxide (ZnO) nanocrystals which were shown to remotely transfer electrons into the in-gap states of PbS QDs leading to suppression of trap-assisted carrier recombination.[150]

From the above discussion, it is clear that the secondary function of ligands as remote and substitutional dopants has significantly helped QD PV. Employing ligands for doping, nonetheless, involves modification of the QD surfaces. A key challenge of this approach is that ligands must fulfill several important and occasionally competing tasks, such as effective trap state passivation, reduction of interdot spacing, and *p*- or *n*-doping, simultaneously. To further enhance the doping level and carrier concentration of the QD solids, a facile method that is not limited by the lack of binding sites (surface coverage) on the ligand-passivated QD surfaces can be employed. Electrochemical doping is an interesting avenue; however, it is not compatible with practical applications because it necessitates an externally applied bias.[3,83] There have been encouraging demonstrations of using molecules of cobaltocene, decamethylferrocene, and decamethylferrocenium as remote dopants for EDT-PbSe and PbS QD solids;[151,152] however, these reports lacked any demonstration of molecular remote doping directly leading to solar cell applications.

Remote Molecular Doping. Although ligands can be used to affect doping in QDs, they chemically bind to the QD surfaces. Any further control over doping for charge transport improvement and/or trap state passivation, therefore, has to be performed via physisorption, i.e. by a route independent of the chemical docking sites available on the surface. This can be achieved by using molecules that can penetrate the nanoporous QD film and affect charge transfer without necessarily chemically binding to the QD surface. Engel et al. demonstrated 2 orders of magnitude improvement in hole concentration after *p*-doping EDT-PbSe QD films with decamethylferrocene and decamethylferrocenium via reversible charge transfer from solution.[152] Remarkably, Koh et al. efficiently converted the insulating OA-PbS and OA-PbSe QD films into *n*-doped solids via electron transfer from cobaltocene. This was realized via a postfabrication single-step dipping.[151] Similarly, benzyl viologen has been used to induce heavy *n*-doping in exchanged PbS QD solids by a simple dipping process, resulting in an electron mobility of 0.64 $cm^2 V^{-1} s^{-1}$ with a SiO_2 gate dielectric.[153]

https://dx.doi.org/10.1021/acsenergylett.0c01453
ACS Energy Lett. 2020, 5, 3069−3100

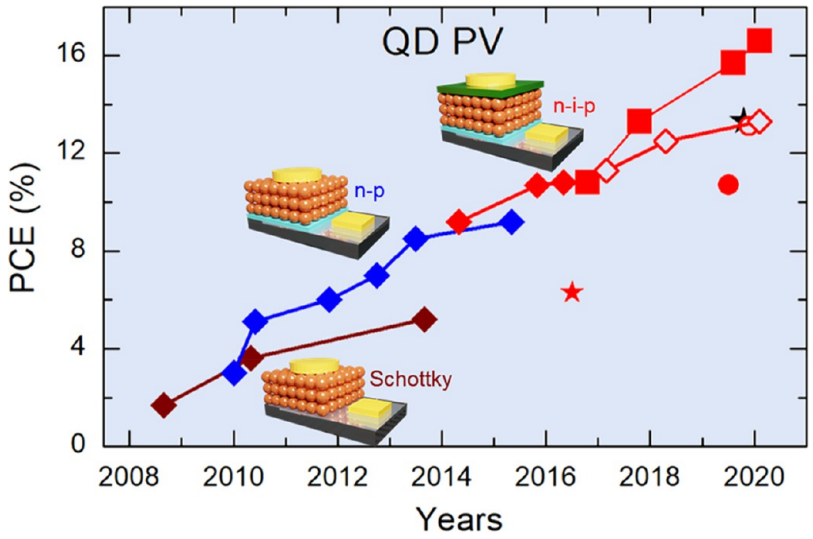

Figure 11. PCEs for QD PV over the years. The PCE growth can be ascribed, largely, to the introduction of three main QD solar cell architectures over time, Schottky (brown), DHJ (blue), and *n-i-p* (red). These device engineering breakthroughs have been further augmented along the way with robust surface passivation recipes and the deployment of SSE, and later, SPE. Data points shown in the graph are mentioned here in chronological order along with their references. All of the data points represented with solid symbols have employed SSE, while the open symbols represent SPE, with the exception of black-star that represents QD-sensitized solar cell. (brown ◆) Schottky PbS QD PV: 1.7%,[163] 3.6%,[164] 5.2%;[165] (blue ◆) *n-p* PbS QD PV: 3.0% (certified),[166] 5.1%,[167] 6.0%,[126] 7.0% (certified),[127] 8.5%,[168] 9.2%;[169] (red ◆) *n-i-p* PbS QD PV: 9.2%,[170] 10.7%,[171] 10.8%;[95] (red ◇) *n-i-p* PbS QD PV (SPE): 11.3% (certified),[96] 12.5%,[109] 13.3%;[20] (red ■) *n-i-p* Perovskite QD PV: 10.8%,[86] 13.4% (certified),[85] 15.7% (certified),[24] 16.6% (certified);[25] (black ★) QD-sensitized PV: 13.3%;[172] (red ★)*n-i-p* $AgBiS_2$ QD PV: 6.3% (certified);[173] (red ○) PbS QD/organic hybrid (SPE): 13.1%;[21] (red ●) *n-i-p* PbSe QD PV: 10.7%.[174]

Given these encouraging demonstrations, the authors of this Review pursued the goal of enabling molecular remote doping in the context of QD solar cells to controllably shift the position of the Fermi level (E_F) inside the QD bandgap without having to alter the coating process of the QD solid or its ligand chemistry.[154,155] It was realized that the MPA-PbS QDs used as absorbers in *n-p* heterojunction solar cells were marginally *n*-type, in accordance with earlier reports.[156,157] This means *p*-doping these absorbers will increase the quasi-E_F separation of ETL and the absorbers, boosting V_{OC}. Excessive *p*-doping, however, is likely to considerably reduce depletion width in the absorber resulting in reduced J_{SC} and FF. To this end, *p*-doping of the MPA-PbS QD solids with an ACN solution of a metal−organic complex, molybdenum tris(1-(trifluoroacetyl)-2-(trifluoromethyl)ethane-1,2-dithiolene), $Mo(tfd\text{-}COCF_3)_3$, was attempted. The choice of ACN was done in accordance with our previous finding that it does not interact and modify the QD surface.[81] The doping was carried out as a postfabrication step by dipping the device in the dopant solution for an optimized time (several minutes) before electrode deposition. Band structure of the doped QD solids was probed with UPS, which clearly showed migration of the E_F toward the middle of the bandgap, suggesting *p*-doping. For higher dopant concentrations, significant shifts in the band structure were observed. From this it was concluded that for these high dopant concentrations, dopant molecules around the QDs formed dipoles, significantly shifting the VBM to large values. As expected, device performance degraded in this dopant concentration regime. For the optimized dopant concentration, device performance increased from PCE of 6.3% via concomitant improvements in the J_{SC}, V_{OC}, and FF, leading to a highest PCE of 7.8%.

The idea of molecular remote doping was next extended to *n-i-p* architecture solar cells that utilized SolEx absorbers. Specifically, *p*-doping the EDT-PbS QD HTL for solar cells based on $MAPbI_3$−PbS QD and PbX_2-PbS QD absorbers was targeted. The idea was inspired by the general observation in silicon PV where a heavily *n*-doped Si layer is used to fully deplete the Si absorber layer. EDT-PbS QD solids are known to be weakly *p*-doped,[158,159] and further gains in hole concentration are required in order to extend depletion in the absorber. Besides, both these absorber layers are intrinsically *n*-doped, meaning that the ETL needs to be degenerately doped in order to maintain band bending at the maximum power point (MPP) during device operation. This inherent *n*-type nature of the absorbers and the difficulty in achieving degenerate *n*-type doping in the ETL further necessitate efficient designs to enable *p*-doping in the HTL. Importantly, the *n-i-p* architecture differs from the *n-p* architecture in that *p*-doping of the HTL can potentially increase depletion width in the absorber benefiting charge collection while increasing V_{OC}.[160]

With this target in mind, *p*-doping of the EDT-PbS QD solids was optimized, resorting to the metal−organic complex, $Mo(tfd\text{-}COCF_3)_3$. Interestingly, the authors again found two distinct dopant concentration regimes: the lower concentrations successfully tuned the E_F, while the higher concentrations also led to surface dipoles and pushed down the entire band structure. A notable challenge in doping the HTL in this architecture was to selectively dope the HTL (thickness, ∼30−50 nm), which is on top of the light-harvesting QD layer in *n-i-p* devices. This was achieved by briefly soaking the HTL upon device fabrication in the optimized dopant concentration in a single step for ∼30s. This led to improvement in the interfacial band bending at the absorber:HTL interface and extended depletion in the absorber, resulting in improvements in J_{SC} and FF and leading to overall increase in PCEs (best-performing device = 9.5%

https://dx.doi.org/10.1021/acsenergylett.0c01453
ACS Energy Lett. 2020, 5, 3069−3100

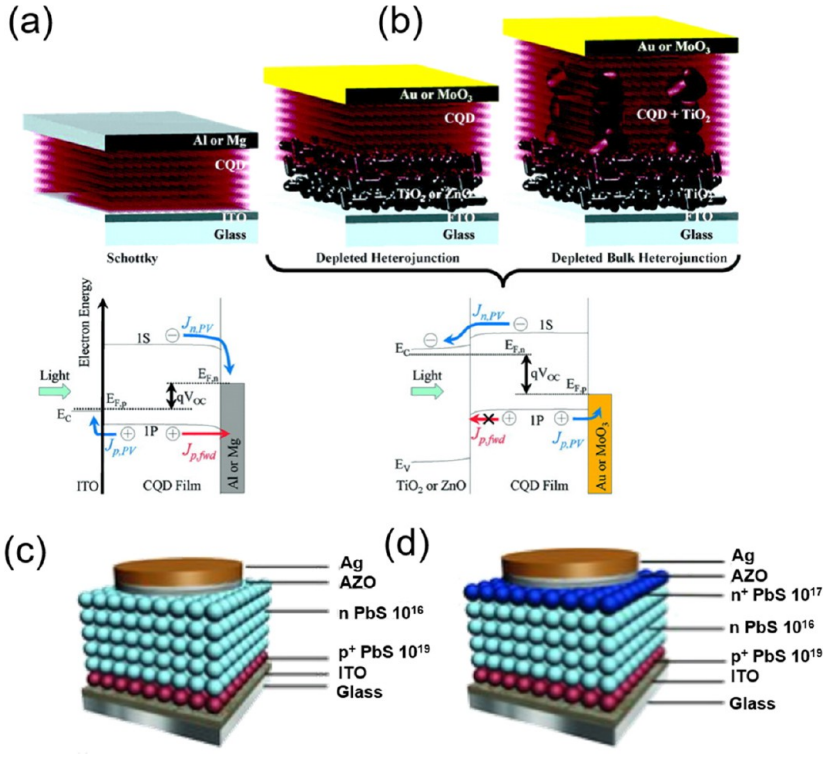

Figure 12. (a) Schottky device architecture. Reprinted with permission from ref 177. Copyright 2011 American Chemical Society. (b) DHJ (left) and DBJ (right) architectures. Reprinted with permission from ref 177. Copyright 2011 American Chemical Society. (c) Quantum homojunction device architecture. Reprinted with permission from ref 178. Copyright 2013 Wiley. (d) Graded doped device architecture. Reprinted with permission from ref 178. Copyright 2013 Wiley.

PCE). External quantum efficiency (EQE) measurements done at MPP confirmed that the optimally doped device was able to maintain better band bending at MPP, in accordance with extended depletion of the absorber.

Remote doping such as this is also very effective in perovskite QD systems such as $CsPbI_3$ QDs using 2,3,5,6-tetrafluoro-7,7,8,8-tetracyanoquinodimethane (F_4TCNQ) as the *p*-dopant or benzyl viologen as the *n*-dopant.[161] Here, the modification of the QD array with remote dopants leads to a dramatic increase in the mobility of charges and was used for efficient phototransistors.

From QD Solids to Solar Cell Devices. Thermalization of hot carriers to band edges accounts in 33% loss for a single-junction 1.1 eV bandgap solar cell. Besides this, the bandgap sets a lower limit on the wavelengths that can be absorbed by the PV device. Subtracting the losses incurred because of extraction of charges leaves 33% of the available solar power that can be harnessed by the solar cell, a number also called the SQ limit.[12] QD solar cells, however, are capable of breaching the SQ limit because of the possibility of harvesting hot carriers and MEG.[10,11] In addition, through the engineering of intermediate bands in QDs, it is possible to absorb the below-gap IR photons that are otherwise wasted.[162] Although these features have not been explicitly exploited yet in QD PV, they make this technology one of the most promising thin-film PV technologies in the long run to break the SQ limit and have been among the guiding forces behind the intense research in this area over the past decade. Below, we chronicle the development of QD PV device architectures.

PbS QD PV efficiencies have risen dramatically over the past decade. The PCE growth is summarized in Figure 11 and can be categorized into three main eras: Schottky architecture era (brown), depleted heterojunction (DHJ) architecture era (blue), and *n-i-p* architecture era (red). In each of these eras, modifications to ligand exchange, control over doping type and amplitude, and improvements in device architecture have combined to push the PCEs up. Major QD solar cell architectures are briefly discussed below.

Schottky Architecture. Schottky solar cells employ a fairly simple architecture with a thin QD absorber layer sandwiched between the top (a low-work function metal) and bottom Ohmic-contact transparent (ITO) electrodes (Figure 12a). The QD absorber forms a Schottky contact with the metal electrode which effectively separates excitons photogenerated in the absorber. The Schottky device architecture primarily suffers from two major issues: (i) Because the junction is formed at the back side (far-end) and transport in QDs is limited owing to small minority carrier diffusion lengths, thickness of the absorber and hence absorption are limited, leading to ineffective collection of charges generated at the back end of the cell. (ii) A second disadvantage of this architecture is the E_F-pinning limiting the open-circuit voltage (V_{OC}) which cannot exceed half the QD bandgap. Schottky architecture was, in fact, the first to be studied in QD solar cells. The first demonstration employed SSE with EDT ligands and led to PCEs of 1.8%.[163] Improvement was demonstrated when a combination of SolEx and SSE was employed.[164] SSE with 1,4-benzenedithiol (BDT) has recently taken these cells to 5.2%;[165] however, interest in Schottky architecture has waned since the advent of the better-performing DHJ and *n-i-p* architectures. The growth of QD PV employing the Schottky architecture is represented by the brown thread in Figure 11.

Depleted Heterojunction Architecture. One of the first demonstrations of the DHJ architecture employed PbSe QDs

https://dx.doi.org/10.1021/acsenergylett.0c01453
ACS Energy Lett. 2020, 5, 3069−3100

in contact with a ZnO layer and resulted in 1.6% PCE.[175] This architecture was adopted by the PbS QD community[166,167] and was an immediate success resulting, simultaneously, in higher J_{SC} and V_{OC} and therefore higher PCEs. These solar cells carry the obvious distinction of a *n-p* heterojunction between the *p*-type QD and the *n*-type wider bandgap metal oxide layers (Figure 12b). Importantly, the depleted heterojunction is situated closer to the transparent front contact, overcoming the charge extraction bottleneck associated with the Schottky architecture, leading to high FFs in excess of 55%. Because the excitons generated at the back end had to rely on diffusion for extraction, robust passivation schemes were developed to suppress traps and enhance diffusion lengths in the solids. Atomic-ligand and hybrid passivation strategies made impacts and led to record PCEs at the time.[126,127] These strategies employed a pretreatment of SolEx passivation of QDs, followed by an SSE of the films, to ensure better overall surface passivation.

Because the DHJ architecture had to rely on diffusion-limited charge transport beyond the depleted QD solid, it was argued that enhancing the depletion region would benefit charge extraction, similar to the effect of increasing carrier diffusion lengths. This led to the concept of the "donor-supply electrode".[168,176] The electron-accepting metal oxide was placed in contact with a shallow work function front electrode. This effectively enhanced the electron density in the oxide layer via charge-transfer doping. The *n*-type oxide with an increased free carrier density pushed forward the depletion region in the QD solid, resulting in better charge collection. The concept led to 8.5% PCE DHJ solar cells.[168] These devices employed hybrid passivated PbS QDs.

The hybrid passivation scheme, as mentioned earlier, involved a $CdCl_2$ surface treatment of the QDs in the solution-phase, besides the usual solid-state treatment (with MPA) of the solid. It was found that replacing $CdCl_2$ with amines in the SolEx induced partial fusion of the QDs leading to self-passivation of the surfaces.[169] This modified hybrid passivation approach effectively reduced the overall QD surface area leading to reduced surface traps.

Future research should explore developing efficient ligand exchange, improving charge transport and extraction, and suppressing size dispersity in wide bandgap (∼1.5−2 eV) and NIR (∼0.6−0.8 eV) PbS QDs to meet the demand and promise of hybrid tandem PV.

These robust QDs featured record-high diffusion lengths in excess of 200 nm, allowing fabrication of 600 nm thick absorber layers resulting in J_{SC} as high as 29.5 mA cm^{-2}. This strategy took the DHJ solar cells to 9.2%.

An interesting modification of the DHJ architecture targeted enhancement of charge extraction from the absorber by employing nanostructured electron acceptors. The idea is similar to the scheme well-known in organic PV where the electron-donating phase (donor) and electron-accepting phase (acceptor) are mixed together forming nanodomains that improve charge extraction, circumventing the short carrier diffusion lengths in those materials.[116] This architecture was called the depleted bulk-heterojunction (DBJ) and aimed to break the photon absorption−carrier extraction compromise in the DHJ solar cells (Figure 12b). Usually, nanopillars, nanowires, or larger nanoparticles of the electron acceptor were employed into which QDs were deposited.[179−182] This allowed deposition of thicker PV solids and lent a three-dimensional spatial extent to the *n-p* junction, compensating for the short diffusion lengths of minority carriers in these solids.[183,184] PCEs with the bulk heterojunction architecture have very recently approached 10% by carefully controlling the growth orientation of the ZnO nanowires and by enabling capillary attractive interactions between the nanowires and PbS QDs that led to denser packing and increased infiltration of the QDs.[185]

Quantum Homojunction. The slight offset between the bands of the electron acceptor and the QD solid in the DHJs leads to an unfavorable "spike" at the interfacial band structure, which hurts either the V_{OC} or the J_{SC}, depending on its direction. This necessitates the concept of a homojunction which can guarantee a smooth band bending at the interface. This requirement fueled the demonstration of the first quantum homojunction QD solar cell.[149] It had an added advantage of photon absorption by both the *n*- and *p*-sides of the junction, enhancing light harvesting. The architecture is shown in Figure 12c and employs a thick *n*-type QD solid atop a thin *p*-type QD layer. A highest performing device of 5.4% PCE was achieved. Importantly, this was one of the first demonstrations of a PV device employing *n*-type QDs.

The *n*-type solids employed in this architecture had low doping. Increasing the doping of these layers can lead to a higher V_{OC}; however, this will decrease the depletion region width. To solve this, a graded doping approach was developed (Figure 12d).[178] A highly *n*-doped QD solid was placed atop the *n*-type QD layer aiding carrier extraction and also the overall V_{OC}. This adjustment led to a 7.4% PCE quantum junction solar cell.

n-i-p Architecture. In 2014, Chuang et al. noticed that it was possible to affect energy level shifts in the QD band structures by varying the surface ligands (Figure 13a).[156] Whereas halide ligands were found to push the band structures deep (large electron affinities), thiols would render the QD band structures shallow (small electron affinities). It was suggested that the overall changes to the band structures were due to a combination of the QD−ligand interface dipole and the interface dipole moment of the ligand.

This understanding led to the development of a novel device architecture wherein a thin film of EDT-PbS QDs with a shallow CBM was placed atop the absorber layer (Figure 13b, c).[170] This additional layer prohibited backflow of photogenerated electrons into the hole-collecting electrode while aiding hole-extraction and depleting the mildly *n*-type TBAI-PbS QD active layer. It is important to mention that TBAI-PbS QD solids were earlier used as absorbers; however, employing an EDT-PbS QD hole-transporting layer (HTL) helped increase the PCEs significantly in addition to enhancing air stability.[170] Recent findings suggest that it is this absorber:HTL junction in these devices that is the dominant rectifying junction, as the TBAI-PbS QD absorber layer is *n*-type.[186] The architecture is, therefore, essentially n^+-*n-p* and requires the HTL to be strongly *p*-doped. TBAI ligands are known to leave organic residues that can likely hurt device performance. Crisp et al. later demonstrated a path to organic-

https://dx.doi.org/10.1021/acsenergylett.0c01453
ACS Energy Lett. 2020, 5, 3069−3100

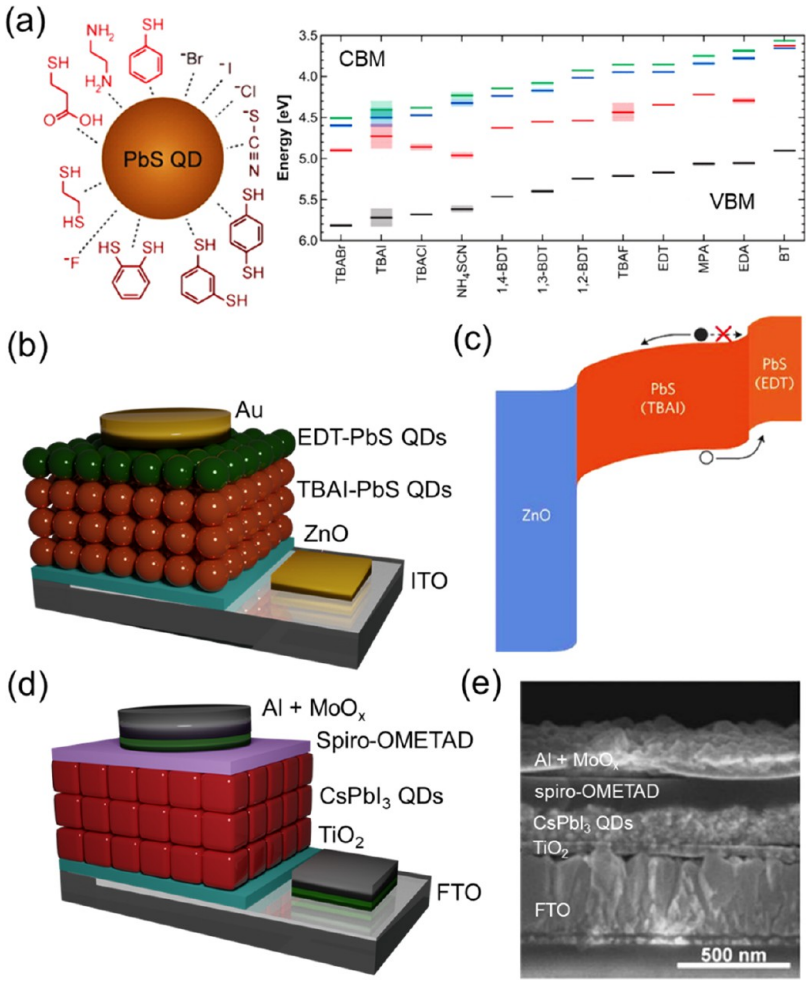

Figure 13. (a) The *n-i-p* architecture is based on the concept of ligand engineering of QD band structures. UPS was used to track the changes to the vacuum level for a variety of ligands. Reprinted with permission from ref 156. Copyright 2014 American Chemical Society. (b) With this information, suitably chosen ligands were employed to form the *n-i-p* device architecture, where (c) EDT-PbS QDs were used as the HTL reducing back-flow of photogenerated electrons. Reprinted with permission from ref 170. Copyright 2014 Springer Nature. (d) $CsPbI_3$ QD solar cells also employ *n-i-p* architecture. (e) Cross-sectional SEM image of a $CsPbI_3$ QD solar cell. Reprinted with permission from ref 86. Copyright 2016 AAAS.

free exchanged PbS QD solids by developing an SSE that involved post-treatment with PbI_2 with appreciable device performance.[187]

This new device architecture has opened routes to further improvements and catalyzed the steep growth in QD PV over the past couple of years, as Figure 11 (red thread) suggests. Soon after this demonstration, a QD absorber exchanged with a combination of SolEx and SSE with halide ligands (iodide) led to 10.2% PCEs, benefiting from enhanced passivation.[188] This was followed by a vacuum level modulation of the electron-transporting layer (ETL) by self-assembled monolayers resulting in a high V_{OC} of 0.66 V with PCEs reaching 10.7%.[97] Modification of the electron transporter with EDT has also been recently reported.[189]

As discussed in the previous section, SolEx has been utilized to yield single-step deposited QD absorbers, taking the QD PV technology a step closer to scalable fabrication. These solar cells have also employed a top EDT-PbS QD HTL in an *n-i-p* configuration. Hybrid perovskites and lead halide ligands have been used to cap the QD surfaces in solution phase, resulting in highly efficient QD inks which have recently led to the realization of 12.5% PCE *n-i-p* solar cells.[96−98,109] Although these solar cells did not require LbL buildup of the active layer, spin-coating was still used to fabricate the absorber. The HTL, however, still requires SSE via LbL deposition (2 layers).

The *n-i-p* architecture has also been found to benefit tandem solar cells fabricated from QDs.[190] Two subcells of equally sized QDs featuring TBAI-QDs as the absorber and EDT-QDs as the HTL were connected via an ultrathin Au layer which acted as the inorganic recombination layer. The overall device performance of the tandem device approached 9.0%, which is almost twice the previous best all-QD tandem solar cell.[191]

Nonetheless, there has been growing evidence that the *n-i-p* architecture suffers from inherent doping issues with the HTL that directly hinder charge transport, ambient manufacturability, and stability of the *n-i-p* devices. It was found by Speirs et al. that the EDT-PbS QD HTL is unoptimally *p*-doped, and a postdeposition treatment with sodium hydrosulfide (NaHS) was found to effectively increase the hole concentration, further depleting the TBAI-PbS QD active layer and improving J_{SC} and FF in TBAI/EDT *n-i-p* architecture solar cells.[159] Further, the authors found that the HTL needed to have an order of magnitude higher doping concentration compared to the active layer, in order to fully deplete the active layer.[159] A

https://dx.doi.org/10.1021/acsenergylett.0c01453
ACS Energy Lett. 2020, 5, 3069−3100

similar observation was made by us recently in the context of *n-i-p* solar cells that employed SolEx $MAPbI_3$−PbS QDs and PbX_2-PbS QDs as the active layers and an EDT-PbS QD HTL. The large electron-affinity (EA) metal−organic complex, $Mo(tfd\text{-}COCF_3)_3$, was used as the *p*-dopant to tune the E_F of the HTL, improving J_{SC} and FF. This HTL doping strategy was also found to work for perovskite solar cells, as demonstrated recently.[192]

The suboptimal doping of the HTL has also been found to be a severe concern when PbS QD solar cells are fabricated in high RH ambient conditions, proving to be a major bottleneck to ambient manufacturability of these devices.[22,193]

It is important to note that this is currently the standard device architecture for $CsPbI_3$ QD solar cells (Figure 13d,e). A QD absorber layer is deposited using the SSE LbL process via spin-coating. The as-cast QD film is soaked in methyl acetate (MeOAc) to enable ligand removal/exchange.[87] The architecture employs spiro-OMETAD as the HTL. Very recently, it was shown that forming the absorber layer by layering $CsPbI_3$ QDs atop $Cs_{0.25}FA_{0.75}PbI_3$QDs results in a charge-separating interface within the absorber.[24] This modified architecture resulted in certified ∼17% PCE solar cells.[24]

QD-Sensitized Solar Cells. QD-sensitized solar cells have been pursued since the 1980s, and competitive PCEs of >13% have been recently reported.[16,17,172] An important distinction with the other QD device architectures is that these solar cells are not based on QD solids but use QDs to sensitize a mesoporous metal oxide photoanode and are similar in design and operation to dye-sensitized solar cells. Electrons photogenerated in the QDs upon light absorption are injected into the metal oxide, while an electrolyte regenerates the oxidized QDs.[194]

However, the appreciable carrier diffusion lengths in QDs enable planar device architectures to perform equally efficiently in extracting photogenerated charge carriers. Further, QD-sensitized solar cells require extra care in QD loading on the mesoporous photoanodes making the process time-consuming. For higher PCEs, the architecture can also require liquid electrolytes that limit device stability and can constrain handling and packaging, presenting a scalability challenge.

Challenges, Opportunities, and Future Directions. Despite the significant inroads made over the past few years in improving surface passivation and charge extraction, considerable further progress is required to improve PCEs beyond 20% in a scalable fashion and/or possibly warrant their integration into hybrid tandem solar cells with other PV materials. Fundamental developments in materials and surface chemistry, self-assembly and thin-film processing, and device engineering, together with breakthroughs in precision synthesis, as well as the stability of QD solar cells and their scalable and ambient manufacturability have recently received attention and will help delineate the path forward for QD solar cells.

Improvements in Charge Extraction and Collection. The optimum QD absorber layer thickness required to absorb all the incident light is *ca.* 1 μm; however, current device architectures employ significantly thinner absorbers (ca. 500 nm). Improved surface passivation schemes have helped increase carrier diffusion lengths which are, however, still generally limited to 100 nm,[109] holding back the achievable absorber thicknesses and therefore the J_{SC}. Improvements in QD passivation and mesoscale arrangement and ordering of closely packed QD solids via improved passivation and remote doping strategies, as well as precise solution processing of QD thin films, are expected to yield increases in the carrier diffusion length in QD solids. An alternative or complementary approach to this problem can be to search for highly *p*-doped HTLs, which can ensure full depletion of thick absorbers. This should potentially also increase the V_{OC}, another important parameter that needs attention, and which is governed by the split in the quasi-E_F of the *n*-type ETL and *p*-type HTL in *n-i-p* architecture devices. A third route can be development of highly efficient BHJs, which rely on nanostructured ETLs that penetrate into the absorber layer alleviating the problem of short diffusion lengths. Blending *p*- and *n*-type QDs into carefully assembled and bicontinuous nanodomains might also allow thicker absorbers without compromising charge collection, compared to the current layered device structures.[195]

The ETL plays a crucial role in the *n-i-p* architecture, in general, by depleting the absorber and extracting electrons while blocking hole backflow. This is still important in the context of the latest QD solar cells despite the fact that the absorber:ETL interface is not the dominant rectifying junction. ZnO nanoparticles have traditionally been used as the ETL in *n-i-p* QD solar cells. Although charge transport in ZnO ETLs is better compared to titania (TiO_x), exploring alternative ETLs with even higher electron mobilities and weaker optical absorption will be helpful. Besides, given the *n*-type nature of the generally used QD absorbers (TBAI-PbS and PbX_2-PbS), having strong *n*-doping in ETLs is desirable. Indium oxide (In_2O_3) has a wider bandgap (∼3.8 eV) and a high electron density due to oxygen vacancies. In principle, it should allow better harvesting of the UV-photons which are otherwise absorbed by ZnO. Further *n*-doping of ETLs should increase absorber layer depletion. The higher-energy UV-photons should help increase J_{SC} further, besides aiding MEG by making high-energy photons available for harvesting. Optical transparency to UV photons can also have implications on improving various stabilities of the CQD solar cells. In fact, the authors of this Review have recently found that replacing the standard, thick ZnO ETL in *n-i-p* CQD solar cells with an ultrathin bilayer In_2O_3/ZnO ETL leads to noticeably improved UV-stability, shelf life, and *I*−*V* hysteresis, while allowing 11% PCE.[196]

Improvements in V_{OC}. In general, V_{OC} has been less than half the PbS QD bandgap. Even though PCEs have significantly improved from Schottky architectures to the current best-performing *n-i-p* PbS QD solar cells, V_{OC} has only increased from 0.50 to 0.65 V, a comparatively less impressive ascent which needs attention. Band tails arising out of disorder in the PbS QD solid and sub-bandgap traps have been suggested to be the possible origin of the observed low V_{OC}.[96,160] An exciting report on bulk nanoheterojunction device architecture employed a combination of MPA and zinc iodide (ZnI_2) as ligands suppressing sub-bandgap traps, and led to a record high V_{OC} of 0.8 V.[197] This advanced device architecture involves incorporation of ZnO nanocrystals into the PbS QD matrix which trap passivate the QD traps via remote charge transfer.[150,198] Although the overall optical absorption is lowered, hurting the J_{SC}, it is likely that with further optimization of this architecture and systematic passivation of subgap and tail states, concomitant improvements in V_{OC} and J_{SC} should be within reach. Size polydispersity is a well-known cause of V_{OC} deficit as it creates inclusions inside the bandgap.[199] Controlling size polydispersity arising from QD

https://dx.doi.org/10.1021/acsenergylett.0c01453
ACS Energy Lett. 2020, 5, 3069−3100

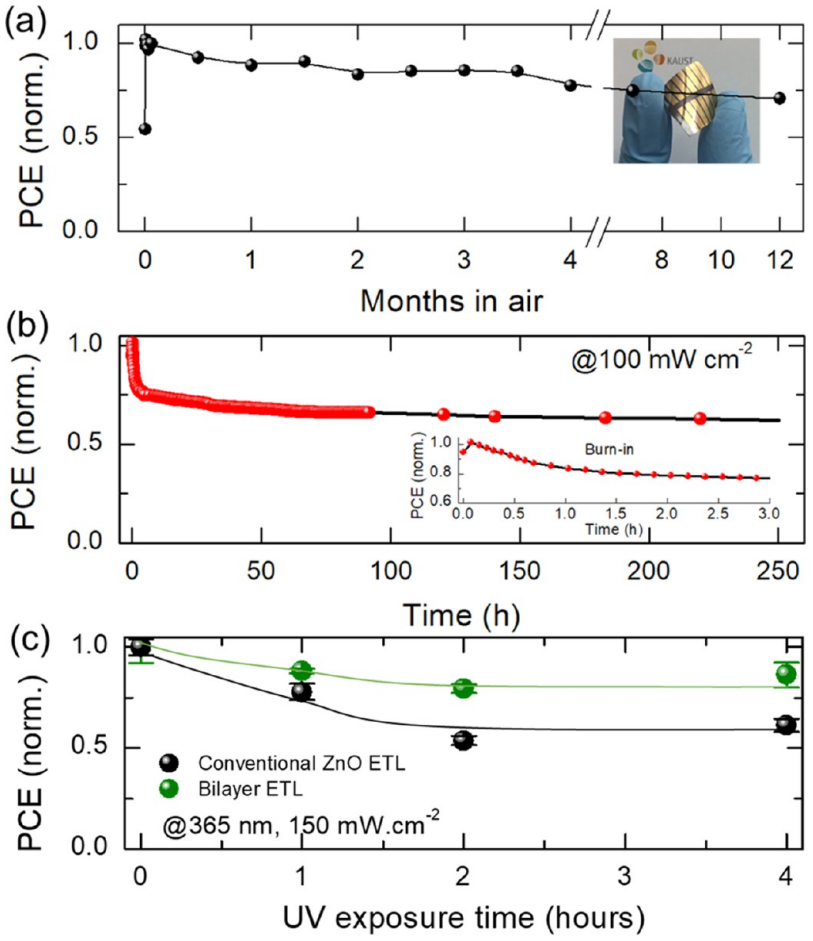

Figure 14. (a) Stability of unencapsulated devices over several months of storage in high-RH (50−60%) ambient air. Inset shows a flexible device on plastic ITO substrate.[22] (b) Photostability of unencapsulated devices over several hours of continuous light irradiation. Inset shows the initial burn-in, after which the PCE saturates. Reprinted with permission from ref 22. Copyright 2018 Wiley. (c) Improved UV-resilience when ultrathin In_2O_3/ZnO bilayer is used as ETL (green data points). Lines are drawn as a guide to the eye. Reprinted with permission from ref 196. Copyright 2020 American Chemical Society.

fusion during the exchange process can yield V_{OC} improvements, as Jo et al. have recently shown.[200]

Improvements in charge transport in QD solids, unfortunately, come at the cost of the long-range order that the long, insulating ligands impart. Bringing the QDs closer by ligand exchange increases the charge tunneling rate, improving charge transport. However, the exchange process removes any signs of the initially existing mesoscale order, creating a disordered arrangement of QDs within the solid and resulting in increased band tails, which are a source of the large V_{OC}-deficit QD PV currently suffers from.[74,96] We have reason to believe further gains in charge transport can be obtained if this disorder can be suppressed. There have been recent key advances where exchanged QD superlattices have been used to fabricate electronic devices with record carrier mobilities (24 $cm^2 V^{-1} s^{-1}$).[73,146,201] Promoting improved self-assembly via precision-controlled solidification processes should help improve the quality of QD solids and eliminate a source of energetic disorder. Suppressing size polydispersity, for instance, with the help of more fundamental and quantitative understanding of nucleation and growth mechanisms of colloidal nanomaterials, together with a transition to in-flow reaction synthesis and with process automation and machine-learning-guided experimentation, will enable improved QD quality, defect mitigation, self-assembly, and marked improvements in V_{OC} and charge extraction by suppressing bandgap inclusions and enabling band-like transport.[74] Together, these steps will accelerate the pathway to bringing >20% PCEs within reach in the coming few years.

Ligand exchange is also known to introduce nonradiative trap states in PbS QD solids leading to a significant decrease in PLQY upon exchange.[202] It is known that every order-of-magnitude reduction in PLQY corresponds to a 60 mV drop in V_{OC}.[203] For 1.3 eV bandgap PbS QDs, maximum achievable V_{OC} limited by SQ limit is 1.03 V, and implies that the latest solar cells with a V_{OC} of 0.65 V possibly have PLQY in the range of 10^{-5}%,[202] highlighting the need for further improvements. There have been recent reports on using quasi-Fermi level splitting (QFLS) to understand V_{OC}-loss mechanisms in perovskite solar cells.[204,205] Light intensity-dependent QFLS measurements have helped decouple the impacts of perovskite absorber and charge extraction layers on overall device performance.[204] Such studies do not currently exist for PbS QD solar cells and are urgently needed to understand carrier loss mechanisms for suppressing the significant V_{OC} losses and improve PCEs.

Tandem QD PV. Another key area which needs dedicated research focus is development of tandem and hybrid tandem solar cells that integrate QD PV as the back cell to harvest the NIR component of the solar spectrum. There have been

https://dx.doi.org/10.1021/acsenergylett.0c01453
ACS Energy Lett. 2020, 5, 3069−3100

encouraging demonstrations of such device architectures over the past few years where 1.3 eV solid-state exchanged PbS QDs have been employed.[206−208]

PCEs nearing 13% have lately been achieved for a hybrid QD:organic tandem solar cell design that uses an organic bulk heterojunction as the back cell.[209] Importantly, these solar cells demonstrated appreciable long-term shelf life. Similarly, a four-terminal tandem solar cell utilizing dye-sensitized and QD subcells recently reached 12% PCE.[210] PbS QDs have also been explored as rear subcells in tandem with CdTe QDs resulting in impressive voltages in excess of 1.1 V.[211]

A major advantage of QDs is their ability to absorb in the NIR spectral range. Fresh insights in large-sized NIR QD PV solids have successfully pushed the >1100 nm wavelength EQEs to ∼80%, resulting in massive gains in J_{SC} and significantly improved harvest of NIR photons[7,8,212−214] that currently the most-efficient PV technologies including commercial Si, perovskites, and organic tandem cells fail to harness.[215,216] SolEx has enabled scalable fabrication of stable and high-performing PbS QD solids, and integrating the larger-sized SolEx NIR PbS QDs as back cells with the best single-junction organic solar cells (>18% PCE) should lead to further improvements thanks to the spectral complementarity of the two semiconductor materials.[217,218] This looks more likely with the recent developments in $CsPbI_3$ QD PV where >16% PCE single-junction solar cells have been reported. With nonfullerene acceptors (NFAs) now leading organic solar cells to >18% PCEs, an organic-QD hybrid tandem solar cell can potentially be optimized to achieve PCE >20% in the near term. For this to happen, efficient recombination layers and solvent compatibility between the QD and organic subcells need to be realized, which requires development of new ink formulations as well as robust recombination layers, as was recently demonstrated.[206] In this regard, SolEx can be helpful as a ready-to-coat QD ink minimizing solvent exposure, but ink developments in general need to avoid damage to other soluble or mechanically fragile layers used in the multilayer device stack.

Long-Term Stability of QD PV. Foremost attention to date has focused on perfecting the QD surfaces and PV device architectures, resulting in steady gains in charge transport and device performance. However, attention must now begin to focus on making QD solar cells an inherently stable technology. This concern has recently been highlighted by Tan et al., who mentioned three types of stabilities as crucial and timely requirements for further progress of QD PV: long-term device stability, QD ink stability, and ambient manufacturability.[219]

Solar cells with PCE > 10% were shown to exhibit ambient shelf life of >1 year without encapsulation (Figure 14a).[22] More impressive still, they exhibited operational stability with 250 h of continuous operation under 100 $mW{\cdot}cm^{-2}$ illumination in inert atmosphere. The devices exhibited an initial burn-in which saturated after 3 h of operation, beyond which the PCEs were remarkably stable.[22] It is clear from Figure 14b that the QD solar cells undergo negligible degradation after the burn-in, suggesting a lifetime significantly longer than 250 h. Similarly, UV-resilience of the solar cells increased when the conventional thick ZnO ETL was replaced with ultrathin In_2O_3/ZnO bilayers (Figure 14c), owing to enhanced optical transmittance and reduced carrier recombination in these bilayer ETLs.[196] These results point toward the intrinsic stability and promise of QD PV for long-term applications. Further efforts must target an understanding of burn-in and ways of overcoming this initial performance degradation. It is important to translate these early demonstrations to QD solar cell modules and subsequent field testing under various environmental stressors, such as moisture, oxygen, heat, and UV-light. Because the year-long ambient stability discussed above was obtained for unencapsulated devices, encapsulated modules are expected to show longer lifetimes given the extra layer of protection from moisture and oxygen attack. Still, the stabilities discussed above for PbS QD PV are far lower than what are needed under realistic conditions (>25 years), and further efforts are required to meet this goal. It is also crucial to explore the performance and stability of QD solar cells upon irradiation with high-energy radiation, such as α and β particles, γ ray photons, protons, and neutrons. Such tests will determine the feasibility of QDs as light-weight thin-film PV for installation in low-earth orbit satellites with exposure to ionizing radiation.

Dimensionality reduction has played a defining role in crystallographically and chemically stabilizing all-inorganic perovskites at room temperature and resulted in high-performing $CsPbI_3$ QD solar cells.[24,86] However, it is unclear at this time if these devices can demonstrate long-term shelf life and operational stability. Given the ionic nature of $CsPbI_3$, these QDs are expected to suffer from degradation under moisture. Demonstration of effective passivation layers, such as 2D perovskites in the context of bulk perovskite PV,[28] should therefore be a key step toward establishing $CsPbI_3$ QD PV as a promising technology.

Scalable Fabrication of QD PV. Solvent Engineering. In the legacy LbL protocol for absorber layer fabrication via SSE, 10−12 repeats of the *coating−exchanging−rinsing* cycle are carried out. This makes the overall process highly time- and material-consuming even if it is automated. It is important to understand the need behind such a rigorous, time-consuming, and materials-wasting process. Limited carrier diffusion lengths in QDs constrain the optimum absorber layer thickness, which is usually ∼300 nm for MPA- and TBAI-PbS QDs. In principle, a compact ∼300 nm absorber can be achieved by (i) starting with a thick OA-PbS QD film and soaking it with MPA or TBAI solutions for a long time (∼several minutes) or (ii) starting with an initially thin OA-PbS QD film, soaking it with MPA or TBAI solutions for a shorter time (∼few sec), and repeating the process several times. In the nascent stages of QD PV, it was realized that choice i would not be successful because the exchange resulted in a significant volume loss, leading to observable cracks in the film which can act as barrier to charge flow during device operation. Choice ii was therefore accepted as the standard protocol. In this process, the as-cast layer of OA-PbS QDs is usually ∼80 nm thick and requires a ∼3s soaking in the MPA ligand solution in MeOH (MPA/MeOH) to be fully exchanged without causing harm to the film. The resulting cracks in the exchanged and rinsed film are filled by a subsequent OA-PbS QD layer coated directly on top, which is then similarly exchanged and rinsed. Because the films require spin-coating, the process entails significant materials wastage, is time-consuming, and is definitely not scalable.

With an aim of remedying this issue, a modified LbL scheme was sought which involved a far fewer number of cycles.[81] The strategy involved fabricating the ∼300 nm absorber in 3 cycles of 100 nm per exchanged layer. Accordingly, each ∼250 nm thick OA-PbS QD layer was exchanged for ∼60s in MPA/

https://dx.doi.org/10.1021/acsenergylett.0c01453
ACS Energy Lett. 2020, 5, 3069−3100

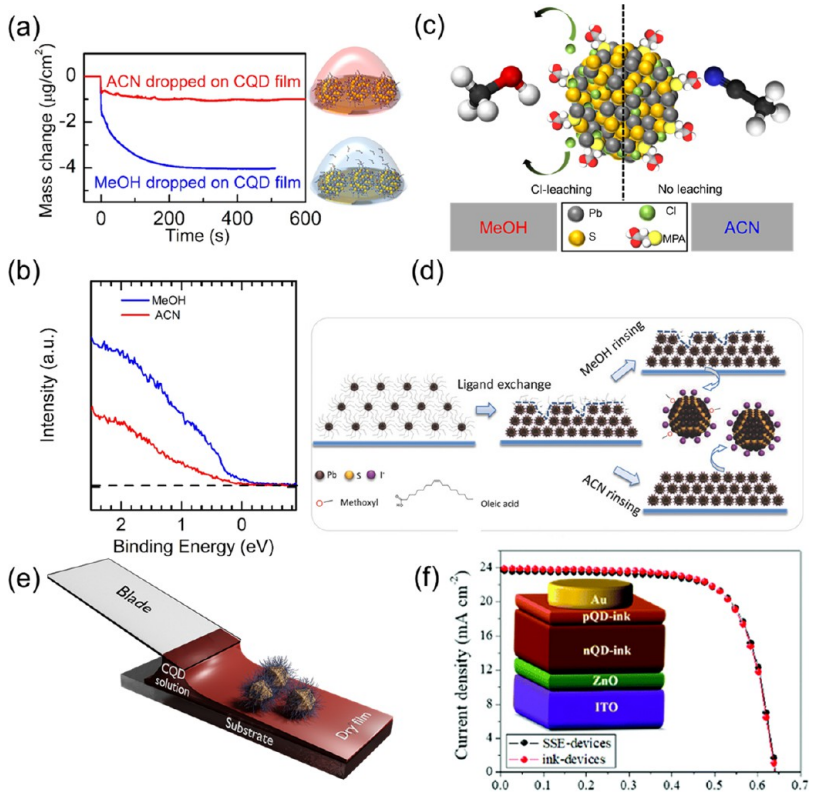

Figure 15. (a) Quantifying interaction of QD surface with MeOH and ACN using QCM in terms of OA ligand removal. Reprinted with permission from ref 81. Copyright 2014 Wiley. (b) Near-Fermi level density of states of the QD absorbers soaked for a long time in MeOH and ACN. Band tails are observed for the MeOH treated absorber. Reprinted with permission from ref 81. Copyright 2014 Wiley. (c) Schematic depicting the halide leaching effect of MeOH from the QD surface. Reprinted with permission from ref 81. Copyright 2014 Wiley. (d) "Solvent-curing" of the *n-i-p* devices using ACN as the rinsing solvent. Reprinted with permission from ref 221. Copyright 2018 Wiley. (e) Blade-coating of QD absorbers. (f) *J*−*V* curve (red) of a fully bladed QD solar cell that uses SolEx for both the absorber and the HTL. Also included is the *J*−*V* curve for the corresponding device made by SSE (black). Reprinted with permission from ref 223. Copyright 2018 The Royal Society of Chemistry.

MeOH, resulting in a ∼100 nm exchanged MPA-PbS QD layer; however, the overall device performance was significantly poorer compared to the 10−12 LbL solar cells. It has been reported that protic solvents such as MeOH desorb carboxylate ligands from the surface of QDs.[220] An investigation into solvent-QD interactions in real time via a quartz crystal microbalance (QCM) detected mass loss by the OA-PbS QD film in contact with MeOH (Figure 15a) suggesting that MeOH had a role in the observed performance loss. This solvent interaction was found to leach-off the surface halide passivant (chloride), resulting in surface traps which were directly measured using UPS (Figure 15b). Confirming the negative impact of a long exposure of MeOH on device performance, a completely contrasting and aprotic solvent, acetonitrile (ACN), was deployed as the processing solvent. ACN turned out to be a very benign solvent without any halide leach-off. In a modification of the ligand exchange process, QD absorbers were fabricated using MPA/ACN solution in 3 LbL steps, resulting in solar cells that performed on par with the 10−12 LbL controls using the legacy MPA/MeOH. The demonstration highlighted that surface trap mitigation, ligand chemistry, and process scalability are often indirectly coupled.

Lu et al. recently extended the idea of solvent engineering in the context of the *n-i-p* architecture QD solar cells (TBAI/EDT).[221] These solar cells, in general, require a TBAI/MeOH ligand exchange to build up the absorber layer via a 10-step LbL process and an EDT/ACN ligand exchange to build up the HTL via a 2-step LbL process. Each step involves a few seconds of MeOH (absorber layer) or ACN (HTL) rinse to remove the unbound OA and excess TBAI or EDT ligands, respectively. The authors posited that replacing the MeOH rinses with ACN for the absorber layer build-up would reduce surface traps and morphological damage to the films (Figure 15d).[222] Doing so also allowed for reducing the number of steps in the LbL build-up with an impressive PCE of 10.6% achieved with as little as 2 LbL steps for the absorber layer, significantly curbing materials wastage. The strict requirement of a protic carrier solvent (MeOH) for enabling the TBAI-exchange with OA-PbS QDs has,[146] thus far, stymied any attempts at deploying an aprotic solvent (ACN) for this exchange; nonetheless, being able to do so successfully should, in principle, further reduce the surface trap density and boost the performance. This anticipation stems from the fact that the TBAI/MeOH soak during the absorber layer build-up takes ∼30 s, allowing ample time for MeOH to interact and undesirably modify the QD surface.[170,221]

Meniscus-Guided Scalable Coating. Despite highlighting the underlying link between surface trap mitigation and process scalability, the above studies have relied on spin-coating. In 2018, scalable fabrication of PbS QD solar cells with >10% PCEs was reported using blade-coating, a meniscus-guided coating technique. Blade-coating is a low-cost, roll-to-roll compatible solution printing technique and is an established prototyping technique for the industrially compatible slot-die

https://dx.doi.org/10.1021/acsenergylett.0c01453
ACS Energy Lett. 2020, 5, 3069−3100

coating (Figure 15e). SolEx PbX_2-PbS QD absorber and EDT-PbS QD HTL were blade-coated in a single step at industrially compatible coating speeds of ∼18 $m \cdot min^{-1}$ in high-RH ambient conditions.[22] Importantly, these devices required ∼25 times less QD material compared to the best spin-coated QD solar cell to date.[109] This report also included demonstration of a 1.1 cm^2 active area device with >9% PCE, highlighting the large-area compatibility of QD PV. These high coating speeds enabled by blade-coating are directly compatible with industrial requirements of roll-to-roll fabrication.[224] Around the same time, Aqoma et al. reported a blade-coated QD solar cell with 10% PCE where both the absorber and HTL employed SolEx.[223] This design had the advantage of completely avoiding SSE that the EDT-PbS QD HTL requires (Figure 15f).

Scalable fabrication of PbS QD solids and devices needs to be next demonstrated using slot-die coating, which is an industrially compatible coating technique with large-area, high-throughput, and continuous manufacturing capabilities. A recent *in situ* X-ray scattering study exploring fundamental aspects of OA-PbS QD self-assembly during slot-die coating is therefore a welcome advance.[225] It is also crucial to realize that ready-to-coat SolEx HTLs merit focused research attention, as do other device layers, including the ETL and conducting electrodes. However, the latter two are less specific to QD PV and benefit from material and technology transfer from other areas of thin-film PV. An alternate HTL can be the utilization of polymeric HTLs that do not rely on a post-treatment. In this regard, the demonstration of ∼12% PCE PbS QD solar cells using organic π-conjugated polymer-based HTLs deposited in a single-step atop the SolEx PbS QD absorber is a promising step.[223,226−228]

The majority of the reports on $CsPbX_3$ QD solar cells have relied on spin-coating. This is expected because these QDs employ SSE which is more compatible with spin-coating or dip-coating, and no SolEx recipe is yet available. Attention should therefore be given to enabling exchange in solution phase, which should allow for single-step deposition of the QD inks via sheet-to-sheet and roll-to-roll compatible coating techniques.

Ambient Air Coating of QD Solids. The majority of the high-performing QD solar cells reported to date have been fabricated in low-RH controlled environments using spin coating.[229] Although efficient at the laboratory-scale for demonstration of proof-of-concepts, this fabrication route is unscalable because of the involved materials wastage and large costs involved due to moisture control. There have been encouraging developments with the demonstration of ambient-fabricated devices using blade-coating, although PCEs have remained low.[164,230,231] There have also been demonstrations of spray-coated QD solar cells, although LbL spray-coating consumed ∼3 times more QD material ($g \cdot m^{-2}$) compared to LbL spin-coating, as discussed above.[94,232] In general, ambient processing and fabrication of QD solids are expected to face hurdles given the possibility of QD surface interaction with ambient moisture and oxygen. To test this proposition, SolEx and subsequent *n-i-p* solar cell fabrication were recently carried out in a highly humid ambient environment (RH > 60%).[22] The as-prepared devices performed poorly, with an average of 4.5% PCE.[22] These devices were also highly unstable in ambient and lost ∼85% of the initial PCEs after 1 month of storage. A detailed atomic analysis of the various layers in the stack gave us evidence that the EDT-PbS QD HTL was, in fact, the manufacturability bottleneck. EDT-PbS QDs have an affinity to partially oxidize forming $(SO_4)^{2-}$ and $(SO_3)^{2-}$ surface species, which scales with QD size.[80,233] In the process, some of the bound EDT ligands are lost. This oxidation results in a slight shift of the E_F closer to the VBM (*p*-doping).[22] In a high-RH ambient, however, moisture attacks the surface of these QDs, blocking ingress of oxygen and leading to an unoptimally *p*-doped HTL. As-prepared devices, therefore, behave poorly because of charge extraction issues arising from an unfavorable "spike" at the absorber:HTL interfacial band structure. It was found that storing these devices in an oxygen-rich dry-air environment for a few hours led to a significant PCE boost, largely stemming from increases in V_{OC} and FF. These efforts helped realize QD solar cells with >10% PCE (best-performing device = 11.0% PCE) processed and fabricated under high-RH ambient environment, on relatively twice the active areas (0.1 cm^2) compared to what are usually reported. In fact, a slight improvement in PCEs was observed earlier upon ambient air storage of the fully prepared devices.[170,182]

Nontoxic QDs through Green Chemistry. A green approach to QD PV would ideally involve green QDs, chemistry and solvents—components that are nontoxic, require small amounts of energy to manufacture, and have limited carbon footprint.

There is growing epidemiological evidence that Pb can possibly cause cancer and other health-related issues by inducing DNA and genetic damage both in humans and animals.[234] The International Agency on Research on Cancer (IARC) *Monographs on the Evaluation of Carcinogenic Risks to Humans* (Vol 87, 2006) classified inorganic Pb compounds under Group 2B ("probably carcinogenic to humans"). The impact of organic Pb compounds on health is inconclusive. This necessitates the search for Pb-free QD systems that can be transformed into an efficient and health-friendly PV technology. It is important to note that PbS is not deliquescent because of the strong Pb−S bond. Inorganic perovskite QDs, however, currently rely on Pb as the B-site metal cation, highlighting the need for a nontoxic alternative. The demonstration of a 6.3% PCE solar cell based on $AgBiS_2$ QDs as the absorber is an important step in the right direction.[173] This impressive performance was achieved with only a 35 nm thick absorber layer, which highlights the room for improvement of these materials as light-harvesting QDs for PV applications.

A recent demonstration of on-device Pb-sequestration in high-performing bulk perovskite solar cells holds significant promise with regard to Pb toxicity.[76] The solar cell was coated with an optically transparent, Pb-absorbing, organic film that effectively sequestered ∼96% Pb when the damaged (intentionally shattered) device was soaked in water, remarkably containing Pb from leakage to the environment. Similar studies are required to demonstrate the robustness and safety with PbS and $CsPbI_3$ QD solar cells.

Similarly, it is crucial to explore alternatives to the currently used toxic precursors and solvents for the synthesis of QDs and device fabrication. Synthesis of PbS QDs requires bis-(trimethylsilyl) sulfide as a precursor, which is considered toxic. To the best of our knowledge, all of the reports on SolEx PbS QDs have used DMF as the polar solvent during the exchange step. DMF is readily absorbed through the skin and can potentially cause damage to the liver. BTA, a toxic and highly flammable solvent, is commonly used to solubilize SolEx

https://dx.doi.org/10.1021/acsenergylett.0c01453
ACS Energy Lett. 2020, 5, 3069−3100

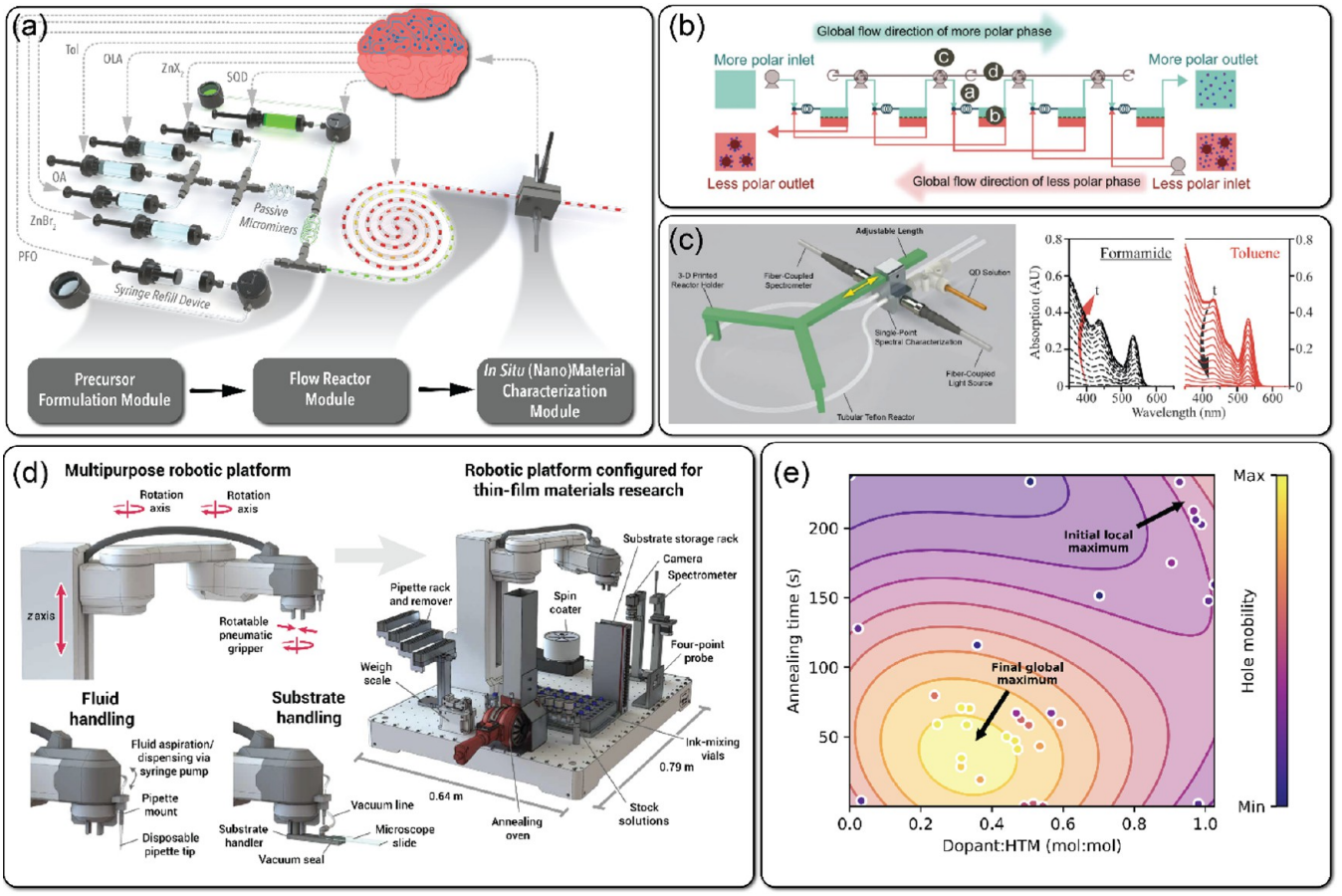

Figure 16. (a) Schematic of the recently developed "artificial chemist" platform for autonomous synthesis of colloidal QDs. Reprinted with permission from ref 61. Copyright 2020 Wiley. (b) Microfluidic purification. Reprinted with permission from ref 240. Copyright 2017 The Royal Society of Chemistry. (c) Suface engineering of QDs. Reprinted with permission from ref 241. Copyright 2017 Wiley. (d) Schematic of a self-driving robotic platform for accelerated studies of thin-film coating. Reprinted with permission from ref 242. (e) Rapid identification of the desired processing conditions using the self-driving robotic platform shown in panel d. Data points correspond to the experimental conditions (annealing time and dopant ratio) sampled by the algorithm during the experimental run for optimizing hole mobility of an organic semiconductor. The algorithm-driven robot makes a fast transition from the local to the global maximum in hole mobility, without the need to study the full parameter space, cutting down the time and materials required. Reprinted with permission from ref 242.

PbS QDs. QD solids spin- and blade-coated out of BTA result in highly-quality, smooth, and shiny films and high-performing solar cells, given the low boiling point of the solvent and its adequate viscosity.[22,96,109] In fact, prior attempts at using DMSO as the solvent for SolEx PbS QDs were less successful because of its high boiling point, which hurts film quality and device performance.[106] Further studies should therefore be targeted toward exploring the considerable green solvent space which other semiconductors, such as organic polymers and bulk hybrid perovskites,[235−237] have started exploiting.

Compared to the case of SolEx, PbS QD solar cells fabricated using SSE currently present a greener route as the exchange process requires the relatively greener solvent MeOH.[238,239] Although ACN, a toxic solvent, has also been used in *n-p* architecture devices and is the standard solvent for delivering EDT ligands for HTL fabrication in *n-i-p* solar cells,[81,109] the overall amount of the solvent needed is significantly low, alleviating the risk to an extent.

In terms of green solvents, $CsPbI_3$ QDs appear to have a significant advantage over PbS QDs. Most of the solvents required for synthesis of these QDs and fabrication of solar cells are considerably less toxic (methyl acetate, octadecene, and hexane).

With the chemistry and physics of Pb-based QDs understood at a fundamental level, PCE soon to surpass 20%, and industry-compatible manufacturing being demonstrated, it will soon be time to look for and translate this rich understanding to efficient nontoxic, Earth-abundant, greener alternatives so that low-cost QD optoelectronics becomes a reality to meet the projected spiraling energy demand of society this century.

Perspectives on Next-Generation Advanced Manufacturing of QD PV. Next-generation QD PV manufacturing would require advances on both accelerated R&D as well as integration of upstream QD ink synthesis and downstream roll-to-roll module fabrication. The recent advancements in autonomous (i) QD development and surface engineering and (ii) thin-film coating, shown in Figure 16, can revolutionize the current paradigm of QD PV development. We briefly discuss below the state-of-the-art on these fronts and suggest future guidelines.

Continuous Manufacturing of QD Inks. As discussed previously in the Microfluidic Synthesis section, microfluidic synthesis of QDs integrated with *in situ* diagnostic probes can enable low-cost, highly efficient manufacturing of QDs with

https://dx.doi.org/10.1021/acsenergylett.0c01453
ACS Energy Lett. 2020, 5, 3069−3100

desired optoelectronic properties for downstream applications in PV devices. To achieve a true end-to-end continuous manufacturing scheme of QDs utilizing modular process units, new technological advancements beyond continuous precursor formulation and flow synthesis modules (Figure 16a) are needed. Specifically, robust continuous purification and surface engineering of QDs will be crucial steps within an end-to-end QD manufacturing platform to achieve high-quality purification of as-synthesized QDs as well as application-guided surface engineering of the purified QDs. Automated QD purification strategies utilizing liquid−liquid extraction (Figure 16b) or column-based separation approaches have been demonstrated to be promising techniques for facile integration with flow synthesis.[240,243] In addition to the formulation, synthesis, purification, and surface engineering modules (Figure 16c), advanced process controllers connected to live-streamed *in situ* diagnostic probes are needed to ensure high-quality manufacturing of QDs with the desired figures of merit for the downstream processing.

Data-Driven Optimization of QD Synthesis. In a recent study, Li et al. developed an automated microfluidic platform for rapid screening of the effect of surface ligand structure on the optical properties of $CsPbBr_3$ QDs utilizing *in situ* PL monitoring.[244] Expedited parameter screening using automation can be beneficial to the industry for rapid, data-driven optimization of the final product without the need for laborious experimentation, driving down labor and materials costs.[46] Bezinge et al. demonstrated targeted synthesis of multinary perovskite nanocrystals using a droplet-based microfluidic reactor informed by a self-optimizing algorithm.[245] It was demonstrated that when the self-optimizing microfluidic platform is utilized, multinary perovskite nanocrystals could be synthesized on-demand for a predefined peak emission wavelength. The system was further demonstrated to make intelligent predictions about certain spectral properties of the nanocrystals.[245] Recently, Epps et al. developed a self-driving modular flow reactor, called *Artificial Chemist*, for simultaneous hands-free optimization of PLQY and FWHM of metal halide perovskite QDs at any desired peak emission energy (Figure 16a).[61] Utilizing an artificial intelligence-based decision-making strategy combined with prior information from in-house generated QD synthesis data, the artificial chemist was able to synthesize optimal (i.e., maximum PLQY with minimum FWHM) metal halide perovskite QDs for any emission color in less than 15 min. Furthermore, the authors demonstrated an autonomous reconfigurability of the artificial chemist from the accelerated R&D mode to continuous QD manufacturing mode for scaled-up production of the in-flow optimized QDs. There has also been recent progress on improving size dispersity in PbS QDs guided by machine learning algorithms. Voznyy et al. developed a model using Bayesian neural networks to optimize PbS QD synthesis.[246] The model led to key insights into the role of OLA in controlling size dispersity, enabling synthesis of wide bandgap (∼2 eV) PbS QDs with a half-width at half-maximum (HWHM) of 145 meV and smaller bandgaps (∼0.83 eV) with HWHM of only 24 meV.[246] Several higher-energy transitions were readily observed in the absorption spectra, an indication of improved size dispersity. Wide bandgap QDs are exciting for hybrid tandem PV applications to reduce spectral overlap between subcells; however, V_{OC} losses typically increase for larger bandgaps likely because of increased polydispersity.[209] Therefore, demonstration of ∼2 eV PbS QDs with low FWHM is an encouraging development.

Manufacturing throughput is another important factor that needs to be considered when developing end-to-end QD manufacturing platforms. The key factors controlling manufacturing throughput are the QD formation kinetics, reaction yield, microfluidic reactor geometry, and maximum initial precursor concentrations without causing fouling and reactor clogging. For example, the fast formation kinetics of fully inorganic lead halide perovskite QDs[56] can be leveraged to achieve manufacturing throughputs up to 0.1 kg/day QD solids in a single-channel microfluidic reactor. The manufacturing throughput can be further increased by utilizing parallel microfluidic reactors (i.e., scaling-out) connected to the same source of precursors and operated through a fluidic distribution module.[44,45]

End-to-End Manufacturing of QD PV. Finally, we believe that automation has a substantial role to play in industrial adoption of QD PV. Smart fabrication of QD PV appears increasingly likely in the near term given the focused attention on using machine-learning-guided automation to optimize QD synthesis by several research groups, as discussed above, as well as renewed focus on downstream processing such as machine-learning-guided coating of thin films.[242]

Considering a stabilized module PCE of 15%, we project >1.4 GW of annual electrical power production capacity for each of these distributed QD PV manufacturing sites.

Considering the above-mentioned developments in continuous manufacturing and processing of colloidal QDs, a fully automated manufacturing scheme can be envisioned for end-to-end manufacturing of QD PV modules with high-quality QDs and minimum batch-to-batch variation. In this proposed design based on recent advancements noted in Figure 16, a modular flow reactor integrated with an *in situ* diagnostic probe will continuously manufacture QDs with bespoke properties (composition, size, ligands, concentration, and throughput) at an industrially relevant throughput (10−50 kg/day). The modular microfluidic QD manufacturing platform will include continuous in-series precursor formulation, flow reactor, purification, and surface engineering modules. The continuously manufactured optimized colloidal QD ink will then be automatically transferred to the downstream roll-to-roll device fabrication module for large-scale fabrication of QD PV cells.

Assuming that (i) the coating speeds of 1080 $m \cdot hr^{-1}$ we recently demonstrated for small-area PbS QD solar cells are scalable to a 1 m-wide continuous roll-to-roll manufacturing line and (ii) under optimized absorber thickness conditions 1 g of QDs is required to coat 1 m^2 of the roll, we estimate a daily QD requirement of ∼26 kg. As discussed above, this requirement can be met using scaled-out microfluidic reactors. These coating speeds correspond to a total annual coated area of 9.5 million m^2. Considering a stabilized module PCE of 15%, we project >1.4 GW of annual electrical power production capacity for each of these distributed QD PV manufacturing sites.

https://dx.doi.org/10.1021/acsenergylett.0c01453
ACS Energy Lett. 2020, 5, 3069−3100

It has been recently suggested that synthesis costs dictate the overall cost per watt for QD PV, and the current standards for QD ink synthesis have been projected to fail in enabling feasible production costs of 0.20 $/W, making this technology currently less viable for industrial scale-up.[46] The QD synthesis throughput considered in the study in question, after surveying the available synthesis protocols, are in the range of 12 g for $CsPbI_3$ QDs and 250 g for PbS QDs. The results suggest that improving the synthesis throughput can potentially drive down the cost per watt by reducing the required materials and labor costs.[46] Solvent recycling can also likely reduce the production costs. We believe the future directions we have pointed out above are key to improving the economic feasibility of this promising technology. The currently achievable manufacturing throughput for perovskite QDs with a low-cost single-channel microfluidic reactor is ∼100 g/day, which is clearly aligned with industrial adoption and can be easily scaled-up to 1−10 kg/day using a numbered-up strategy.[44,56−58,61] We suggest that life-cycle assessment and techno-economic feasibility analysis of QD PV considering high throughput and large-scale module performance should be conducted in future work to access viability.

Conclusions and Outlook. QD PV is one of the fastest growing fields in thin-film optoelectronics and offers benefits beyond the reach of contemporary PV technologies. PCEs have risen sharply to >16% in 2020 after recent breakthroughs in perovskite QDs. We have chronicled the development of this PV technology over recent years with detailed discussion on the various chemical passivation schemes and device designs that have combined to play a central role in its rapid ascent. Solution-phase ligand exchange and the *n-i-p* device architecture have been the major milestones in the young history of this nascent field. Scalable fabrication and ambient manufacturability of efficient QD solar cells, along with demonstrations of machine learning-guided automated flow reactor synthesis of QDs with high throughput are important recent demonstrations that highlight their potential for market entry in the short term.

We have suggested a few key areas that should be the focus of research going forward to push the PCEs above 20%. This includes improving extraction of photogenerated charge carriers (FF) and suppressing size polydispersity that can potentially enhance V_{OC} and charge transport in PbS QDs. Hybrid tandem solar cell designs are suggested as the fastest route to >20% PCE, although single-junction devices should be considerably simpler and cheaper to produce. Focusing on efficient recombination layers and solvent compatibility between organic and QD subcells should lead to major advances. To this end, both wide bandgap and NIR QDs appear promising, as front and rear subcells, respectively. Most of the chemical approaches to date have been developed for visible-to-NIR QDs with 1.3 eV bandgap. Future research should explore developing efficient ligand exchange, improving charge transport and extraction, and suppressing size dispersity in wide bandgap (∼1.5−2 eV) and NIR (∼0.6−0.8 eV) PbS QDs to meet the demand and promise of hybrid tandem PV.

There has been considerably less attention given to nontoxic alternatives to QD PV. With growing evidence of health-related issues associated with inorganic Pb salts, this topic should see increased research activity. In this regard, $AgBiS_2$ QD solar cells have been a promising development. Similarly, it is important to screen the various precursors and solvents used for QD synthesis for toxicity and cost. Greener and sustainable alternatives will help in scale-up of this technology and drive down the materials cost involved. Of great importance is the search for an on-device Pb sequestration technology that suppresses Pb leach-off upon damage to QD PV modules without compromising device performance. A similar demonstration for bulk perovskite solar cells is a highly encouraging step in this direction and suggests that the present unavailability of a robust Pb-free QD PV should not be an impediment to industrial scale-up provided this demonstration of Pb sequestration is transferable to QD solar cells.

Overall, these demonstrations of ambient manufacturability and scalable fabrication of QD PV, along with recent interest in automated and autonomous flow-synthesis of QDs on demand, are promising signs for this nascent field.

Overall, these demonstrations of ambient manufacturability and scalable fabrication of QD PV,[22,223] along with recent interest in automated and autonomous flow-synthesis of QDs on demand,[58] are promising signs for this nascent field.[247−249] Combined, these latest developments can bring down the materials and labor costs involved which have been projected as the main contributors to the total manufacturing cost for QD PV modules,[46] smoothing their journey to the manufacturing line and enabling annual gigawatt power production.

AUTHOR INFORMATION

Corresponding Authors

Ahmad R. Kirmani − *Chemical and Nanoscience Center, National Renewable Energy Laboratory (NREL), Golden, Colorado 80215, United States;* orcid.org/0000-0002-8351-3762; Email: ahmad.kirmani@nrel.gov

Aram Amassian − *Materials Science and Engineering, Organic and Carbon Electronic Laboratories (ORaCEL), North Carolina State University (NCSU), Raleigh, North Carolina 27695, United States;* orcid.org/0000-0002-5734-1194; Email: aamassi@ncsu.edu

Authors

Joseph M. Luther − *Chemical and Nanoscience Center, National Renewable Energy Laboratory (NREL), Golden, Colorado 80215, United States;* orcid.org/0000-0002-4054-8244

Milad Abolhasani − *Chemical and Biomolecular Engineering, North Carolina State University (NCSU), Raleigh, North Carolina 27695, United States;* orcid.org/0000-0002-8863-3085

Complete contact information is available at: https://pubs.acs.org/10.1021/acsenergylett.0c01453

Notes

The authors declare no competing financial interest.

Biographies

Ahmad R. Kirmani is a postdoctoral researcher at the Chemical & Nanoscience Center, National Renewable Energy Laboratory (NREL). He has a Ph.D. degree (2017) in materials science from the King Abdullah University of Science & Technology (KAUST) and was a guest researcher at the National Institute of Standards and

https://dx.doi.org/10.1021/acsenergylett.0c01453
ACS Energy Lett. 2020, 5, 3069−3100

Technology (NIST) prior to joining NREL. His research interests include roll-to-roll compatible coating and characterization of inorganic semiconductor inks, such as colloidal quantum dots, hybrid perovskites, and metal oxides.

Joseph M. Luther has been a senior research scientist at the National Renewable Energy Laboratory since 2009. His group's research focuses on developing optoelectronic technologies utilizing solution-processed nanomaterials such as colloidal semiconducting quantum dots and halide perovskite materials.

Milad Abolhasani is an Assistant Professor in the Department of Chemical and Biomolecular Engineering at North Carolina State University. He received his Ph.D. degree (2014) from the Department of Mechanical and Industrial Engineering in collaboration with the Department of Chemistry at the University of Toronto. Prior to joining NC State University in 2016, he was an NSERC postdoctoral fellow in the Department of Chemical Engineering at Massachusetts Institute of Technology. Dr. Abolhasani leads a diverse research group that studies flow chemistry strategies tailored towards accelerated development and manufacturing of solution-processed materials using autonomous robotic experimentation in flow.

Aram Amassian is an Associate Professor of Materials Science and Engineering and a member of the Carbon Electronics Cluster. He received his Ph.D. degree (2006) in Engineering Physics from Ecole Polytechnique in Montreal, Canada. Prior to joining NC State University (2018), he was an NSERC postdoctoral fellow in Materials Science and Engineering at Cornell University (2006−2009) and was subsequently founding faculty at the King Abdullah University of Science and Technology (KAUST), 2009−2018, where he held the Career Development SABIC Chair (2013−2016). Dr. Amassian's research is focused on solution-processed hybrid semiconductors, particularly for (opto)electronic and photovoltaic applications, where he has developed *in situ* characterization strategies for thin-film deposition in lab-scale and fab-scale processes.

■ ACKNOWLEDGMENTS

This work was authored in part by the Alliance for Sustainable Energy, Limited Liability Company, the manager and operator of the National Renewable Energy Laboratory under Contract No. DE-AC36-08GO28308. The views expressed in the article do not necessarily represent the views of the Department of Energy or the U.S. Government. NREL authors were funded through a technical service agreement with Equinor. A.A. and M.A. acknowledge financial support from the UNC Research Opportunities Initiative (UNC-ROI) grant and the North Carolina State University.

■ REFERENCES

(1) Aldakov, D.; Reiss, P. Safer-by-Design Fluorescent Nanocrystals: Metal Halide Perovskites vs Semiconductor Quantum Dots. *J. Phys. Chem. C* **2019**, *123* (20), 12527−12541.
(2) Wang, C.; Shim, M.; Guyot-Sionnest, P. Electrochromic nanocrystal quantum dots. *Science* **2001**, *291* (5512), 2390−2.
(3) Liu, H.; Keuleyan, S.; Guyot-Sionnest, P. n- and p-Type HgTe Quantum Dot Films. *J. Phys. Chem. C* **2012**, *116* (1), 1344−1349.
(4) Deng, Z.; Guyot-Sionnest, P. Intraband Luminescence from HgSe/CdS Core/Shell Quantum Dots. *ACS Nano* **2016**, *10* (2), 2121−7.
(5) Shen, G.; Guyot-Sionnest, P. HgS and HgS/CdS Colloidal Quantum Dots with Infrared Intraband Transitions and Emergence of a Surface Plasmon. *J. Phys. Chem. C* **2016**, *120* (21), 11744−11753.
(6) Kiani, A.; Sutherland, B. R.; Kim, Y.; Ouellette, O.; Levina, L.; Walters, G.; Dinh, C.-T.; Liu, M.; Voznyy, O.; Lan, X.; Labelle, A. J.; Ip, A. H.; Proppe, A.; Ahmed, G. H.; Mohammed, O. F.; Hoogland, S.; Sargent, E. H. Single-step colloidal quantum dot films for infrared solar harvesting. *Appl. Phys. Lett.* **2016**, *109* (18), 183105.
(7) Bi, Y.; Bertran, A.; Gupta, S.; Ramiro, I.; Pradhan, S.; Christodoulou, S.; Majji, S.-N.; Akgul, M. Z.; Konstantatos, G. Solution processed infrared- and thermo-photovoltaics based on 0.7 eV bandgap PbS colloidal quantum dots. *Nanoscale* **2019**, *11* (3), 838−843.
(8) Bi, Y.; Pradhan, S.; Gupta, S.; Akgul, M. Z.; Stavrinadis, A.; Konstantatos, G. Infrared Solution-Processed Quantum Dot Solar Cells Reaching External Quantum Efficiency of 80% at 1.35 μm and Jsc in Excess of 34 mA cm-2. *Adv. Mater.* **2018**, *30* (7), 1704928.
(9) Nozik, A. J. Quantum dot solar cells. *Phys. E* **2002**, *14* (1), 115−120.
(10) Semonin, O. E.; Luther, J. M.; Choi, S.; Chen, H. Y.; Gao, J.; Nozik, A. J.; Beard, M. C. Peak external photocurrent quantum efficiency exceeding 100% via MEG in a quantum dot solar cell. *Science* **2011**, *334* (6062), 1530−3.
(11) Schaller, R. D.; Klimov, V. I. High Efficiency Carrier Multiplication in PbSe Nanocrystals: Implications for Solar Energy Conversion. *Phys. Rev. Lett.* **2004**, *92* (18), 186601.
(12) Shockley, W.; Queisser, H. J. Detailed Balance Limit of Efficiency of p-n Junction Solar Cells. *J. Appl. Phys.* **1961**, *32* (3), 510−519.
(13) Nozik, A. J. Spectroscopy and hot electron relaxation dynamics in semiconductor quantum wells and quantum dots. *Annu. Rev. Phys. Chem.* **2001**, *52* (1), 193−231.
(14) Huynh, W. U.; Dittmer, J. J.; Alivisatos, A. P. Hybrid Nanorod-Polymer Solar Cells. *Science* **2002**, *295* (5564), 2425−2427.
(15) Vogel, R.; Pohl, K.; Weller, H. Sensitization of highly porous, polycrystalline TiO2 electrodes by quantum sized CdS. *Chem. Phys. Lett.* **1990**, *174* (3), 241−246.
(16) Zaban, A.; Mićić, O. I.; Gregg, B. A.; Nozik, A. J. Photosensitization of Nanoporous TiO2 Electrodes with InP Quantum Dots. *Langmuir* **1998**, *14* (12), 3153−3156.
(17) Plass, R.; Pelet, S.; Krueger, J.; Grätzel, M.; Bach, U. Quantum Dot Sensitization of Organic-Inorganic Hybrid Solar Cells. *J. Phys. Chem. B* **2002**, *106* (31), 7578−7580.
(18) McDonald, S. A.; Konstantatos, G.; Zhang, S.; Cyr, P. W.; Klem, E. J. D.; Levina, L.; Sargent, E. H. Solution-processed PbS quantum dot infrared photodetectors and photovoltaics. *Nat. Mater.* **2005**, *4* (2), 138−142.
(19) Talapin, D. V.; Murray, C. B. PbSe nanocrystal solids for n- and p-channel thin film field-effect transistors. *Science* **2005**, *310* (5745), 86−9.
(20) Choi, M.-J.; García de Arquer, F. P.; Proppe, A. H.; Seifitokaldani, A.; Choi, J.; Kim, J.; Baek, S.-W.; Liu, M.; Sun, B.; Biondi, M.; Scheffel, B.; Walters, G.; Nam, D.-H.; Jo, J. W.; Ouellette, O.; Voznyy, O.; Hoogland, S.; Kelley, S. O.; Jung, Y. S.; Sargent, E. H. Cascade surface modification of colloidal quantum dot inks enables efficient bulk homojunction photovoltaics. *Nat. Commun.* **2020**, *11* (1), 103.
(21) Baek, S.-W.; Jun, S.; Kim, B.; Proppe, A. H.; Ouellette, O.; Voznyy, O.; Kim, C.; Kim, J.; Walters, G.; Song, J. H.; Jeong, S.; Byun, H. R.; Jeong, M. S.; Hoogland, S.; García de Arquer, F. P.; Kelley, S. O.; Lee, J.-Y.; Sargent, E. H. Efficient hybrid colloidal quantum dot/organic solar cells mediated by near-infrared sensitizing small molecules. *Nature Energy* **2019**, *4* (11), 969−976.
(22) Kirmani, A. R.; Sheikh, A. D.; Niazi, M. R.; Haque, M. A.; Liu, M.; de Arquer, F. P. G.; Xu, J.; Sun, B.; Voznyy, O.; Gasparini, N.; Baran, D.; Wu, T.; Sargent, E. H.; Amassian, A. Overcoming the Ambient Manufacturability-Scalability-Performance Bottleneck in Colloidal Quantum Dot Photovoltaics. *Adv. Mater.* **2018**, *30* (35), No. 1801661.
(23) Sun, B.; Johnston, A.; Xu, C.; Wei, M.; Huang, Z.; Jiang, Z.; Zhou, H.; Gao, Y.; Dong, Y.; Ouellette, O.; Zheng, X.; Liu, J.; Choi, M.-J.; Gao, Y.; Baek, S.-W.; Laquai, F.; Bakr, O. M.; Ban, D.; Voznyy, O.; García de Arquer, F. P.; Sargent, E. H. Monolayer Perovskite Bridges Enable Strong Quantum Dot Coupling for Efficient Solar Cells. *Joule* **2020**, *4* (7), 1542−1556.

https://dx.doi.org/10.1021/acsenergylett.0c01453
ACS Energy Lett. 2020, 5, 3069−3100

(24) Zhao, Q.; Hazarika, A.; Chen, X.; Harvey, S. P.; Larson, B. W.; Teeter, G. R.; Liu, J.; Song, T.; Xiao, C.; Shaw, L.; Zhang, M.; Li, G.; Beard, M. C.; Luther, J. M. High efficiency perovskite quantum dot solar cells with charge separating heterostructure. *Nat. Commun.* **2019**, *10* (1), 2842.
(25) Hao, M.; Bai, Y.; Zeiske, S.; Ren, L.; Liu, J.; Yuan, Y.; Zarrabi, N.; Cheng, N.; Ghasemi, M.; Chen, P.; Lyu, M.; He, D.; Yun, J.-H.; Du, Y.; Wang, Y.; Ding, S.; Armin, A.; Meredith, P.; Liu, G.; Cheng, H.-M.; Wang, L. Ligand-assisted cation-exchange engineering for high-efficiency colloidal Cs1-xFAxPbI3 quantum dot solar cells with reduced phase segregation. *Nature Energy* **2020**, *5* (1), 79−88.
(26) Akin, S.; Altintas, Y.; Mutlugun, E.; Sonmezoglu, S. Cesium lead based inorganic perovskite quantum-dots as interfacial layer for highly stable perovskite solar cells with exceeding 21% efficiency. *Nano Energy* **2019**, *60*, 557−566.
(27) Cen, Y.-l.; Shi, J.-j.; Zhang, M.; Wu, M.; Du, J.; Guo, W.-h.; Liu, S.-m.; Han, S.-p.; Zhu, Y.-h. Design of Lead-Free and Stable Two-Dimensional Dion-Jacobson-Type Chalcogenide Perovskite A′La2B3S10 (A′ = Ba/Sr/Ca; B = Hf/Zr) with Optimal Band Gap, Strong Optical Absorption, and High Efficiency for Photovoltaics. *Chem. Mater.* **2020**, *32* (6), 2450−2460.
(28) Grancini, G.; Roldán-Carmona, C.; Zimmermann, I.; Mosconi, E.; Lee, X.; Martineau, D.; Narbey, S.; Oswald, F.; De Angelis, F.; Graetzel, M.; Nazeeruddin, M. K. One-Year stable perovskite solar cells by 2D/3D interface engineering. *Nat. Commun.* **2017**, *8* (1), 15684.
(29) Yusoff, A. R. b. M.; Nazeeruddin, M. K. Low-Dimensional Perovskites: From Synthesis to Stability in Perovskite Solar Cells. *Adv. Energy Mater.* **2018**, *8* (26), 1702073.
(30) Huang, P.; Kazim, S.; Wang, M.; Ahmad, S. Toward Phase Stability: Dion-Jacobson Layered Perovskite for Solar Cells. *ACS Energy Letters* **2019**, *4* (12), 2960−2974.
(31) Eadington, P.; Prosser, A. P. Oxidation of Lead Sulfide in Aqueous Suspensions. *Trans. Inst. Min. Metall.* **1969**, *78*, 74−82.
(32) Choi, H.; Ko, J.-H.; Kim, Y.-H.; Jeong, S. Steric-Hindrance-Driven Shape Transition in PbS Quantum Dots: Understanding Size-Dependent Stability. *J. Am. Chem. Soc.* **2013**, *135* (14), 5278−5281.
(33) Murray, C. B.; Norris, D. J.; Bawendi, M. G. Synthesis and characterization of nearly monodisperse CdE (E = sulfur, selenium, tellurium) semiconductor nanocrystallites. *J. Am. Chem. Soc.* **1993**, *115* (19), 8706−8715.
(34) Peng, X.; Wickham, J.; Alivisatos, A. P. Kinetics of II-VI and III-V Colloidal Semiconductor Nanocrystal Growth: "Focusing" of Size Distributions. *J. Am. Chem. Soc.* **1998**, *120* (21), 5343−5344.
(35) Murray, C. B.; Kagan, C. R.; Bawendi, M. G. Synthesis and Characterization of Monodisperse Nanocrystals and Close-Packed Nanocrystal Assemblies. *Annu. Rev. Mater. Sci.* **2000**, *30* (1), 545−610.
(36) Kim, J. Y.; Voznyy, O.; Zhitomirsky, D.; Sargent, E. H. 25th Anniversary Article: Colloidal Quantum Dot Materials and Devices: A Quarter-Century of Advances. *Adv. Mater.* **2013**, *25* (36), 4986−5010.
(37) Hines, M. A.; Scholes, G. D. Colloidal PbS Nanocrystals with Size-Tunable Near-Infrared Emission: Observation of Post-Synthesis Self-Narrowing of the Particle Size Distribution. *Adv. Mater.* **2003**, *15* (21), 1844−1849.
(38) Park, J.; Joo, J.; Kwon, S. G.; Jang, Y.; Hyeon, T. Synthesis of Monodisperse Spherical Nanocrystals. *Angew. Chem., Int. Ed.* **2007**, *46* (25), 4630−4660.
(39) Hou, B.; Cho, Y.; Kim, B. S.; Hong, J.; Park, J. B.; Ahn, S. J.; Sohn, J. I.; Cha, S.; Kim, J. M. Highly Monodispersed PbS Quantum Dots for Outstanding Cascaded-Junction Solar Cells. *ACS Energy Letters* **2016**, *1* (4), 834−839.
(40) Čapek, R. K.; Yanover, D.; Lifshitz, E. Size control by rate control in colloidal PbSe quantum dot synthesis. *Nanoscale* **2015**, *7* (12), 5299−5310.
(41) Peng, Z. A.; Peng, X. Formation of High-Quality CdTe, CdSe, and CdS Nanocrystals Using CdO as Precursor. *J. Am. Chem. Soc.* **2001**, *123* (1), 183−184.
(42) Qu, L.; Peng, Z. A.; Peng, X. Alternative Routes toward High Quality CdSe Nanocrystals. *Nano Lett.* **2001**, *1* (6), 333−337.
(43) Pradhan, N.; Reifsnyder, D.; Xie, R.; Aldana, J.; Peng, X. Surface Ligand Dynamics in Growth of Nanocrystals. *J. Am. Chem. Soc.* **2007**, *129* (30), 9500−9509.
(44) Nightingale, A. M.; Bannock, J. H.; Krishnadasan, S. H.; O'Mahony, F. T. F.; Haque, S. A.; Sloan, J.; Drury, C.; McIntyre, R.; deMello, J. C. Large-scale synthesis of nanocrystals in a multichannel droplet reactor. *J. Mater. Chem. A* **2013**, *1* (12), 4067.
(45) Wang, L.; Karadaghi, L. R.; Brutchey, R. L.; Malmstadt, N. Self-optimizing parallel millifluidic reactor for scaling nanoparticle synthesis. *Chem. Commun.* **2020**, *56* (26), 3745−3748.
(46) Jean, J.; Xiao, J.; Nick, R.; Moody, N.; Nasilowski, M.; Bawendi, M.; Bulović, V. Synthesis cost dictates the commercial viability of lead sulfide and perovskite quantum dot photovoltaics. *Energy Environ. Sci.* **2018**, *11* (9), 2295−2305.
(47) Chan, E. M.; Mathies, R. A.; Alivisatos, A. P. Size-Controlled Growth of CdSe Nanocrystals in Microfluidic Reactors. *Nano Lett.* **2003**, *3* (2), 199−201.
(48) Chan, E. M.; Alivisatos, A. P.; Mathies, R. A. High-Temperature Microfluidic Synthesis of CdSe Nanocrystals in Nanoliter Droplets. *J. Am. Chem. Soc.* **2005**, *127* (40), 13854−13861.
(49) Yen, B. K. H.; Stott, N. E.; Jensen, K. F.; Bawendi, M. G. A Continuous-Flow Microcapillary Reactor for the Preparation of a Size Series of CdSe Nanocrystals. *Adv. Mater.* **2003**, *15* (21), 1858−1862.
(50) Yen, B. K. H.; Günther, A.; Schmidt, M. A.; Jensen, K. F.; Bawendi, M. G. A Microfabricated Gas-Liquid Segmented Flow Reactor for High-Temperature Synthesis: The Case of CdSe Quantum Dots. *Angew. Chem., Int. Ed.* **2005**, *44* (34), 5447−5451.
(51) Krishnadasan, S.; Brown, R. J.; deMello, A. J.; deMello, J. C. Intelligent routes to the controlled synthesis of nanoparticles. *Lab Chip* **2007**, *7* (11), 1434−41.
(52) Lignos, I.; Protesescu, L.; Stavrakis, S.; Piveteau, L.; Speirs, M. J.; Loi, M. A.; Kovalenko, M. V.; deMello, A. J. Facile Droplet-based Microfluidic Synthesis of Monodisperse IV-VI Semiconductor Nanocrystals with Coupled In-Line NIR Fluorescence Detection. *Chem. Mater.* **2014**, *26* (9), 2975−2982.
(53) Kubendhiran, S.; Bao, Z.; Dave, K.; Liu, R.-S. Microfluidic Synthesis of Semiconducting Colloidal Quantum Dots and Their Applications. *ACS Applied Nano Materials* **2019**, *2* (4), 1773−1790.
(54) Li, S.; Hsiao, J. C.; Howes, P. D.; deMello, A. J. Microfluidic Tools for the Synthesis of Bespoke Quantum Dots. *Nanotechnology and Microfluidics* **2020**, 109−148.
(55) Abolhasani, M.; Coley, C. W.; Xie, L.; Chen, O.; Bawendi, M. G.; Jensen, K. F. Oscillatory Microprocessor for Growth and in Situ Characterization of Semiconductor Nanocrystals. *Chem. Mater.* **2015**, *27* (17), 6131−6138.
(56) Lignos, I.; Stavrakis, S.; Nedelcu, G.; Protesescu, L.; deMello, A. J.; Kovalenko, M. V. Synthesis of Cesium Lead Halide Perovskite Nanocrystals in a Droplet-Based Microfluidic Platform: Fast Parametric Space Mapping. *Nano Lett.* **2016**, *16* (3), 1869−77.
(57) Epps, R. W.; Felton, K. C.; Coley, C. W.; Abolhasani, M. Automated microfluidic platform for systematic studies of colloidal perovskite nanocrystals: towards continuous nano-manufacturing. *Lab Chip* **2017**, *17* (23), 4040−4047.
(58) Abdel-Latif, K.; Epps, R. W.; Kerr, C. B.; Papa, C. M.; Castellano, F. N.; Abolhasani, M. Facile Room-Temperature Anion Exchange Reactions of Inorganic Perovskite Quantum Dots Enabled by a Modular Microfluidic Platform. *Adv. Funct. Mater.* **2019**, *29* (23), 1900712.
(59) Lignos, I.; Morad, V.; Shynkarenko, Y.; Bernasconi, C.; Maceiczyk, R. M.; Protesescu, L.; Bertolotti, F.; Kumar, S.; Ochsenbein, S. T.; Masciocchi, N.; Guagliardi, A.; Shih, C. J.; Bodnarchuk, M. I.; deMello, A. J.; Kovalenko, M. V. Exploration of Near-Infrared-Emissive Colloidal Multinary Lead Halide Perovskite Nanocrystals Using an Automated Microfluidic Platform. *ACS Nano* **2018**, *12* (6), 5504−5517.

(60) Kerr, C. B.; Epps, R. W.; Abolhasani, M. A low-cost, non-invasive phase velocity and length meter and controller for multiphase lab-in-a-tube devices. *Lab Chip* **2019**, *19* (12), 2107−2113.
(61) Epps, R. W.; Bowen, M. S.; Volk, A. A.; Abdel-Latif, K.; Han, S.; Reyes, K. G.; Amassian, A.; Abolhasani, M. Artificial Chemist: An Autonomous Quantum Dot Synthesis Bot. *Adv. Mater.* **2020**, *32* (30), No. 2001626.
(62) Stolle, C. J.; Harvey, T. B.; Korgel, B. A. Nanocrystal photovoltaics: a review of recent progress. *Curr. Opin. Chem. Eng.* **2013**, *2* (2), 160−167.
(63) Fu, H.; Tsang, S.-W. Infrared colloidal lead chalcogenide nanocrystals: Synthesis, properties, and photovoltaic applications. *Nanoscale* **2012**, *4* (7), 2187−2201.
(64) Hillhouse, H. W.; Beard, M. C. Solar cells from colloidal nanocrystals: Fundamentals, materials, devices, and economics. *Curr. Opin. Colloid Interface Sci.* **2009**, *14* (4), 245−259.
(65) Semonin, O. E.; Luther, J. M.; Beard, M. C. Quantum dots for next-generation photovoltaics. *Mater. Today* **2012**, *15* (11), 508−515.
(66) Moreels, I.; Justo, Y.; De Geyter, B.; Haustraete, K.; Martins, J. C.; Hens, Z. Size-Tunable, Bright, and Stable PbS Quantum Dots: A Surface Chemistry Study. *ACS Nano* **2011**, *5* (3), 2004−2012.
(67) Vanmaekelbergh, D.; Liljeroth, P. Electron-conducting quantum dot solids: novel materials based on colloidal semiconductor nanocrystals. *Chem. Soc. Rev.* **2005**, *34* (4), 299−312.
(68) Weidman, M. C.; Smilgies, D.-M.; Tisdale, W. A. Kinetics of the self-assembly of nanocrystal superlattices measured by real-time in situ X-ray scattering. *Nat. Mater.* **2016**, *15*, 775.
(69) Maiti, S.; André, A.; Banerjee, R.; Hagenlocher, J.; Konovalov, O.; Schreiber, F.; Scheele, M. Monitoring Self-Assembly and Ligand Exchange of PbS Nanocrystal Superlattices at the Liquid/Air Interface in Real Time. *J. Phys. Chem. Lett.* **2018**, *9* (4), 739−744.
(70) Choi, J. J.; Bealing, C. R.; Bian, K.; Hughes, K. J.; Zhang, W.; Smilgies, D.-M.; Hennig, R. G.; Engstrom, J. R.; Hanrath, T. Controlling Nanocrystal Superlattice Symmetry and Shape-Anisotropic Interactions through Variable Ligand Surface Coverage. *J. Am. Chem. Soc.* **2011**, *133* (9), 3131−3138.
(71) Hanrath, T.; Choi, J. J.; Smilgies, D.-M. Structure/Processing Relationships of Highly Ordered Lead Salt Nanocrystal Superlattices. *ACS Nano* **2009**, *3* (10), 2975−2988.
(72) Bian, K.; Choi, J. J.; Kaushik, A.; Clancy, P.; Smilgies, D.-M.; Hanrath, T. Shape-Anisotropy Driven Symmetry Transformations in Nanocrystal Superlattice Polymorphs. *ACS Nano* **2011**, *5* (4), 2815−2823.
(73) Balazs, D. M.; Matysiak, B. M.; Momand, J.; Shulga, A. G.; Ibanez, M.; Kovalenko, M. V.; Kooi, B. J.; Loi, M. A. Electron Mobility of 24 cm(2) V(−1) s(−1) in PbSe Colloidal-Quantum-Dot Superlattices. *Adv. Mater.* **2018**, *30* (38), No. 1802265.
(74) Guyot-Sionnest, P. Electrical Transport in Colloidal Quantum Dot Films. *J. Phys. Chem. Lett.* **2012**, *3* (9), 1169−75.
(75) Kagan, C. R.; Murray, C. B. Charge transport in strongly coupled quantum dot solids. *Nat. Nanotechnol.* **2015**, *10* (12), 1013−26.
(76) Septianto, R. D.; Liu, L.; Iskandar, F.; Matsushita, N.; Iwasa, Y.; Bisri, S. Z. On-demand tuning of charge accumulation and carrier mobility in quantum dot solids for electron transport and energy storage devices. *NPG Asia Mater.* **2020**, *12* (1), 33.
(77) Kirmani, A. R.; Walters, G.; Kim, T.; Sargent, E. H.; Amassian, A. Optimizing Solid-State Ligand Exchange for Colloidal Quantum Dot Optoelectronics: How Much Is Enough? *ACS Applied Energy Materials* **2020**, *3* (6), 5385−5392.
(78) Carey, G. H.; Abdelhady, A. L.; Ning, Z.; Thon, S. M.; Bakr, O. M.; Sargent, E. H. Colloidal Quantum Dot Solar Cells. *Chem. Rev.* **2015**, *115* (23), 12732−12763.
(79) Carey, G. H.; Chou, K. W.; Yan, B.; Kirmani, A. R.; Amassian, A.; Sargent, E. H. Materials processing strategies for colloidal quantum dot solar cells: advances, present-day limitations, and pathways to improvement. *MRS Commun.* **2013**, *3* (2), 83−90.
(80) Luther, J. M.; Law, M.; Song, Q.; Perkins, C. L.; Beard, M. C.; Nozik, A. J. Structural, optical, and electrical properties of self-assembled films of PbSe nanocrystals treated with 1,2-ethanedithiol. *ACS Nano* **2008**, *2* (2), 271−80.
(81) Kirmani, A. R.; Carey, G. H.; Abdelsamie, M.; Yan, B.; Cha, D.; Rollny, L. R.; Cui, X.; Sargent, E. H.; Amassian, A. Effect of solvent environment on colloidal-quantum-dot solar-cell manufacturability and performance. *Adv. Mater.* **2014**, *26* (27), 4717−23.
(82) Guyot-Sionnest, P.; Wang, C. Fast Voltammetric and Electrochromic Response of Semiconductor Nanocrystal Thin Films†. *J. Phys. Chem. B* **2003**, *107* (30), 7355−7359.
(83) Yu, D.; Wang, C.; Guyot-Sionnest, P. n-Type conducting CdSe nanocrystal solids. *Science* **2003**, *300* (5623), 1277−80.
(84) Murphy, J. E.; Beard, M. C.; Nozik, A. J. Time-Resolved Photoconductivity of PbSe Nanocrystal Arrays. *J. Phys. Chem. B* **2006**, *110* (50), 25455−25461.
(85) Sanehira, E. M.; Marshall, A. R.; Christians, J. A.; Harvey, S. P.; Ciesielski, P. N.; Wheeler, L. M.; Schulz, P.; Lin, L. Y.; Beard, M. C.; Luther, J. M. Enhanced mobility $CsPbI_3$ quantum dot arrays for record-efficiency, high-voltage photovoltaic cells. *Sci. Adv.* **2017**, *3* (10), No. eaao4204.
(86) Swarnkar, A.; Marshall, A. R.; Sanehira, E. M.; Chernomordik, B. D.; Moore, D. T.; Christians, J. A.; Chakrabarti, T.; Luther, J. M. Quantum dot-induced phase stabilization of alpha-CsPbI3 perovskite for high-efficiency photovoltaics. *Science* **2016**, *354* (6308), 92−95.
(87) Wheeler, L. M.; Sanehira, E. M.; Marshall, A. R.; Schulz, P.; Suri, M.; Anderson, N. C.; Christians, J. A.; Nordlund, D.; Sokaras, D.; Kroll, T.; Harvey, S. P.; Berry, J. J.; Lin, L. Y.; Luther, J. M. Targeted Ligand-Exchange Chemistry on Cesium Lead Halide Perovskite Quantum Dots for High-Efficiency Photovoltaics. *J. Am. Chem. Soc.* **2018**, *140* (33), 10504−10513.
(88) Grisorio, R.; Di Clemente, M. E.; Fanizza, E.; Allegretta, I.; Altamura, D.; Striccoli, M.; Terzano, R.; Giannini, C.; Irimia-Vladu, M.; Suranna, G. P. Exploring the surface chemistry of cesium lead halide perovskite nanocrystals. *Nanoscale* **2019**, *11* (3), 986−999.
(89) Park, J. H.; Lee, A.-y.; Yu, J. C.; Nam, Y. S.; Choi, Y.; Park, J.; Song, M. H. Surface Ligand Engineering for Efficient Perovskite Nanocrystal-Based Light-Emitting Diodes. *ACS Appl. Mater. Interfaces* **2019**, *11* (8), 8428−8435.
(90) Wu, H.; Zhang, Y.; Lu, M.; Zhang, X.; Sun, C.; Zhang, T.; Colvin, V. L.; Yu, W. W. Surface ligand modification of cesium lead bromide nanocrystals for improved light-emitting performance. *Nanoscale* **2018**, *10* (9), 4173−4178.
(91) Zheng, W.; Li, Z.; Zhang, C.; Wang, B.; Zhang, Q.; Wan, Q.; Kong, L.; Li, L. Stabilizing perovskite nanocrystals by controlling protective surface ligands density. *Nano Res.* **2019**, *12* (6), 1461−1465.
(92) Imran, M.; Ijaz, P.; Goldoni, L.; Maggioni, D.; Petralanda, U.; Prato, M.; Almeida, G.; Infante, I.; Manna, L. Simultaneous Cationic and Anionic Ligand Exchange For Colloidally Stable CsPbBr3 Nanocrystals. *ACS Energy Letters* **2019**, *4* (4), 819−824.
(93) Lu, H.; Zhu, X.; Miller, C.; Martin, J. S.; Chen, X.; Miller, E. M.; Yan, Y.; Beard, M. C. Enhanced photoredox activity of CsPbBr3 nanocrystals by quantitative colloidal ligand exchange. *J. Chem. Phys.* **2019**, *151* (20), 204305.
(94) Kramer, I. J.; Minor, J. C.; Moreno-Bautista, G.; Rollny, L.; Kanjanaboos, P.; Kopilovic, D.; Thon, S. M.; Carey, G. H.; Chou, K. W.; Zhitomirsky, D.; Amassian, A.; Sargent, E. H. Efficient Spray-Coated Colloidal Quantum Dot Solar Cells. *Adv. Mater.* **2015**, *27* (1), 116−121.
(95) Liu, M.; de Arquer, F. P.; Li, Y.; Lan, X.; Kim, G. H.; Voznyy, O.; Jagadamma, L. K.; Abbas, A. S.; Hoogland, S.; Lu, Z.; Kim, J. Y.; Amassian, A.; Sargent, E. H. Double-Sided Junctions Enable High-Performance Colloidal-Quantum-Dot Photovoltaics. *Adv. Mater.* **2016**, *28* (21), 4142−8.
(96) Liu, M.; Voznyy, O.; Sabatini, R.; Garcia de Arquer, F. P.; Munir, R.; Balawi, A. H.; Lan, X.; Fan, F.; Walters, G.; Kirmani, A. R.; Hoogland, S.; Laquai, F.; Amassian, A.; Sargent, E. H. Hybrid organic-inorganic inks flatten the energy landscape in colloidal quantum dot solids. *Nat. Mater.* **2017**, *16* (2), 258−263.

https://dx.doi.org/10.1021/acsenergylett.0c01453
ACS Energy Lett. 2020, 5, 3069−3100

(97) Yang, Z.; Janmohamed, A.; Lan, X.; García de Arquer, F. P.; Voznyy, O.; Yassitepe, E.; Kim, G.-H.; Ning, Z.; Gong, X.; Comin, R.; Sargent, E. H. Colloidal Quantum Dot Photovoltaics Enhanced by Perovskite Shelling. *Nano Lett.* **2015**, *15* (11), 7539−7543.
(98) Aqoma, H.; Al Mubarok, M.; Hadmojo, W. T.; Lee, E.-H.; Kim, T.-W.; Ahn, T. K.; Oh, S.-H.; Jang, S.-Y. High-Efficiency Photovoltaic Devices using Trap-Controlled Quantum-Dot Ink prepared via Phase-Transfer Exchange. *Adv. Mater.* **2017**, *29* (19), 1605756.
(99) Choi, H.; Lee, J.-G.; Mai, X. D.; Beard, M. C.; Yoon, S. S.; Jeong, S. Supersonically Spray-Coated Colloidal Quantum Dot Ink Solar Cells. *Sci. Rep.* **2017**, *7* (1), 622.
(100) Kovalenko, M. V.; Scheele, M.; Talapin, D. V. Colloidal Nanocrystals with Molecular Metal Chalcogenide Surface Ligands. *Science* **2009**, *324* (5933), 1417−1420.
(101) Chung, D. S.; Lee, J.-S.; Huang, J.; Nag, A.; Ithurria, S.; Talapin, D. V. Low Voltage, Hysteresis Free, and High Mobility Transistors from All-Inorganic Colloidal Nanocrystals. *Nano Lett.* **2012**, *12* (4), 1813−1820.
(102) Lee, J.-S.; Kovalenko, M. V.; Huang, J.; Chung, D. S.; Talapin, D. V. Band-like transport, high electron mobility and high photoconductivity in all-inorganic nanocrystal arrays. *Nat. Nanotechnol.* **2011**, *6* (6), 348−352.
(103) Crisp, R. W.; Schrauben, J. N.; Beard, M. C.; Luther, J. M.; Johnson, J. C. Coherent exciton delocalization in strongly coupled quantum dot arrays. *Nano Lett.* **2013**, *13* (10), 4862−9.
(104) Gur, I.; Fromer, N. A.; Geier, M. L.; Alivisatos, A. P. Air-Stable All-Inorganic Nanocrystal Solar Cells Processed from Solution. *Science* **2005**, *310* (5747), 462−465.
(105) Johnston, K. W.; Pattantyus-Abraham, A. G.; Clifford, J. P.; Myrskog, S. H.; MacNeil, D. D.; Levina, L.; Sargent, E. H. Schottky-quantum dot photovoltaics for efficient infrared power conversion. *Appl. Phys. Lett.* **2008**, *92* (15), 151115.
(106) Fischer, A.; Rollny, L.; Pan, J.; Carey, G. H.; Thon, S. M.; Hoogland, S.; Voznyy, O.; Zhitomirsky, D.; Kim, J. Y.; Bakr, O. M.; Sargent, E. H. Directly Deposited Quantum Dot Solids Using a Colloidally Stable Nanoparticle Ink. *Adv. Mater.* **2013**, *25* (40), 5742−5749.
(107) Zhang, H.; Jang, J.; Liu, W.; Talapin, D. V. Colloidal Nanocrystals with Inorganic Halide, Pseudohalide, and Halometallate Ligands. *ACS Nano* **2014**, *8* (7), 7359−7369.
(108) Ning, Z.; Dong, H.; Zhang, Q.; Voznyy, O.; Sargent, E. H. Solar Cells Based on Inks of n-Type Colloidal Quantum Dots. *ACS Nano* **2014**, *8* (10), 10321−10327.
(109) Xu, J.; Voznyy, O.; Liu, M.; Kirmani, A. R.; Walters, G.; Munir, R.; Abdelsamie, M.; Proppe, A. H.; Sarkar, A.; Garcia de Arquer, F. P.; Wei, M.; Sun, B.; Liu, M.; Ouellette, O.; Quintero-Bermudez, R.; Li, J.; Fan, J.; Quan, L.; Todorovic, P.; Tan, H.; Hoogland, S.; Kelley, S. O.; Stefik, M.; Amassian, A.; Sargent, E. H. 2D matrix engineering for homogeneous quantum dot coupling in photovoltaic solids. *Nat. Nanotechnol.* **2018**, *13* (6), 456−462.
(110) Dirin, D. N.; Dreyfuss, S.; Bodnarchuk, M. I.; Nedelcu, G.; Papagiorgis, P.; Itskos, G.; Kovalenko, M. V. Lead Halide Perovskites and Other Metal Halide Complexes As Inorganic Capping Ligands for Colloidal Nanocrystals. *J. Am. Chem. Soc.* **2014**, *136* (18), 6550−6553.
(111) Ning, Z.; Ren, Y.; Hoogland, S.; Voznyy, O.; Levina, L.; Stadler, P.; Lan, X.; Zhitomirsky, D.; Sargent, E. H. All-Inorganic Colloidal Quantum Dot Photovoltaics Employing Solution-Phase Halide Passivation. *Adv. Mater.* **2012**, *24* (47), 6295−6299.
(112) Bozyigit, D.; Yazdani, N.; Yarema, M.; Yarema, O.; Lin, W. M. M.; Volk, S.; Vuttivorakulchai, K.; Luisier, M.; Juranyi, F.; Wood, V. Soft surfaces of nanomaterials enable strong phonon interactions. *Nature* **2016**, *531* (7596), 618−622.
(113) Yazdani, N.; Bozyigit, D.; Vuttivorakulchai, J.; Luisier, M.; Wood, V. Influence of the Surface of a Nanocrystal on its Electronic and Phononic Properties. *arXiv* **2016**, 1611.09930.
(114) Talapin, D. V.; Lee, J.-S.; Kovalenko, M. V.; Shevchenko, E. V. Prospects of Colloidal Nanocrystals for Electronic and Optoelectronic Applications. *Chem. Rev.* **2010**, *110* (1), 389−458.
(115) Boles, M. A.; Engel, M.; Talapin, D. V. Self-Assembly of Colloidal Nanocrystals: From Intricate Structures to Functional Materials. *Chem. Rev.* **2016**, *116* (18), 11220−11289.
(116) Richter, L. J.; DeLongchamp, D. M.; Amassian, A. Morphology Development in Solution-Processed Functional Organic Blend Films: An In Situ Viewpoint. *Chem. Rev.* **2017**, *117* (9), 6332−6366.
(117) Wei Chou, K.; Ullah Khan, H.; Niazi, M. R.; Yan, B.; Li, R.; Payne, M. M.; Anthony, J. E.; Smilgies, D.-M.; Amassian, A. Late stage crystallization and healing during spin-coating enhance carrier transport in small-molecule organic semiconductors. *J. Mater. Chem. C* **2014**, *2* (28), 5681−5689.
(118) Smilgies, D.-M.; Li, R.; Giri, G.; Chou, K. W.; Diao, Y.; Bao, Z.; Amassian, A. Look fast: Crystallization of conjugated molecules during solution shearing probed in-situ and in real time by X-ray scattering. *Phys. Status Solidi RRL* **2013**, *7* (3), 177−179.
(119) Giri, G.; Li, R.; Smilgies, D.-M.; Li, E. Q.; Diao, Y.; Lenn, K. M.; Chiu, M.; Lin, D. W.; Allen, R.; Reinspach, J.; Mannsfeld, S. C. B.; Thoroddsen, S. T.; Clancy, P.; Bao, Z.; Amassian, A. One-dimensional self-confinement promotes polymorph selection in large-area organic semiconductor thin films. *Nat. Commun.* **2014**, *5* (1), 3573.
(120) Chou, K. W.; Yan, B.; Li, R.; Li, E. Q.; Zhao, K.; Anjum, D. H.; Alvarez, S.; Gassaway, R.; Biocca, A.; Thoroddsen, S. T.; Hexemer, A.; Amassian, A. Spin-Cast Bulk Heterojunction Solar Cells: A Dynamical Investigation. *Adv. Mater.* **2013**, *25* (13), 1923−1929.
(121) Munir, R.; Sheikh, A. D.; Abdelsamie, M.; Hu, H.; Yu, L.; Zhao, K.; Kim, T.; Tall, O. E.; Li, R.; Smilgies, D.-M.; Amassian, A. Hybrid Perovskite Thin-Film Photovoltaics: In Situ Diagnostics and Importance of the Precursor Solvate Phases. *Adv. Mater.* **2017**, *29* (2), 1604113.
(122) Tang, M.-C.; Barrit, D.; Munir, R.; Li, R.; Barbé, J. M.; Smilgies, D.-M.; Del Gobbo, S.; Anthopoulos, T. D.; Amassian, A. Bismuth-Based Perovskite-Inspired Solar Cells: In Situ Diagnostics Reveal Similarities and Differences in the Film Formation of Bismuth- and Lead-Based Films. *Solar RRL* **2019**, *3* (7), 1800305.
(123) Wang, K.; Tang, M.-C.; Dang, H. X.; Munir, R.; Barrit, D.; De Bastiani, M.; Aydin, E.; Smilgies, D.-M.; De Wolf, S.; Amassian, A. Kinetic Stabilization of the Sol-Gel State in Perovskites Enables Facile Processing of High-Efficiency Solar Cells. *Adv. Mater.* **2019**, *31* (32), 1808357.
(124) Li, R.; Khan, H. U.; Payne, M. M.; Smilgies, D.-M.; Anthony, J. E.; Amassian, A. Heterogeneous Nucleation Promotes Carrier Transport in Solution-Processed Organic Field-Effect Transistors. *Adv. Funct. Mater.* **2013**, *23* (3), 291−297.
(125) Barrit, D.; Cheng, P.; Tang, M.-C.; Wang, K.; Dang, H.; Smilgies, D.-M.; Liu, S.; Anthopoulos, T. D.; Zhao, K.; Amassian, A. Impact of the Solvation State of Lead Iodide on Its Two-Step Conversion to MAPbI3: An In Situ Investigation. *Adv. Funct. Mater.* **2019**, *29* (47), 1807544.
(126) Tang, J.; Kemp, K. W.; Hoogland, S.; Jeong, K. S.; Liu, H.; Levina, L.; Furukawa, M.; Wang, X.; Debnath, R.; Cha, D.; Chou, K. W.; Fischer, A.; Amassian, A.; Asbury, J. B.; Sargent, E. H. Colloidal-quantum-dot photovoltaics using atomic-ligand passivation. *Nat. Mater.* **2011**, *10* (10), 765−771.
(127) Ip, A. H.; Thon, S. M.; Hoogland, S.; Voznyy, O.; Zhitomirsky, D.; Debnath, R.; Levina, L.; Rollny, L. R.; Carey, G. H.; Fischer, A.; Kemp, K. W.; Kramer, I. J.; Ning, Z.; Labelle, A. J.; Chou, K. W.; Amassian, A.; Sargent, E. H. Hybrid passivated colloidal quantum dot solids. *Nat. Nanotechnol.* **2012**, *7* (9), 577−582.
(128) Zhitomirsky, D.; Voznyy, O.; Levina, L.; Hoogland, S.; Kemp, K. W.; Ip, A. H.; Thon, S. M.; Sargent, E. H. Engineering colloidal quantum dot solids within and beyond the mobility-invariant regime. *Nat. Commun.* **2014**, *5*, 3803.
(129) Katsiev, K.; Ip, A. H.; Fischer, A.; Tanabe, I.; Zhang, X.; Kirmani, A. R.; Voznyy, O.; Rollny, L. R.; Chou, K. W.; Thon, S. M.; Carey, G. H.; Cui, X.; Amassian, A.; Dowben, P.; Sargent, E. H.; Bakr, O. M. The Complete In-Gap Electronic Structure of Colloidal

Quantum Dot Solids and Its Correlation with Electronic Transport and Photovoltaic Performance. *Adv. Mater.* **2014**, *26* (6), 937−942.
(130) Marshall, A. R.; Young, M. R.; Nozik, A. J.; Beard, M. C.; Luther, J. M. Exploration of Metal Chloride Uptake for Improved Performance Characteristics of PbSe Quantum Dot Solar Cells. *J. Phys. Chem. Lett.* **2015**, *6* (15), 2892−9.
(131) Deng, Z.; Jeong, K. S.; Guyot-Sionnest, P. Colloidal quantum dots intraband photodetectors. *ACS Nano* **2014**, *8* (11), 11707−14.
(132) Jeong, K. S.; Deng, Z.; Keuleyan, S.; Liu, H.; Guyot-Sionnest, P. Air-Stable n-Doped Colloidal HgS Quantum Dots. *J. Phys. Chem. Lett.* **2014**, *5* (7), 1139−43.
(133) Norris, D. J.; Efros, A. L.; Erwin, S. C. Doped nanocrystals. *Science* **2008**, *319* (5871), 1776−9.
(134) Mocatta, D.; Cohen, G.; Schattner, J.; Millo, O.; Rabani, E.; Banin, U. Heavily doped semiconductor nanocrystal quantum dots. *Science* **2011**, *332* (6025), 77−81.
(135) Gresback, R.; Kramer, N. J.; Ding, Y.; Chen, T.; Kortshagen, U. R.; Nozaki, T. Controlled doping of silicon nanocrystals investigated by solution-processed field effect transistors. *ACS Nano* **2014**, *8* (6), 5650−6.
(136) Cargnello, M.; Johnston-Peck, A. C.; Diroll, B. T.; Wong, E.; Datta, B.; Damodhar, D.; Doan-Nguyen, V. V.; Herzing, A. A.; Kagan, C. R.; Murray, C. B. Substitutional doping in nanocrystal superlattices. *Nature* **2015**, *524* (7566), 450−3.
(137) Garcia de Arquer, F. P.; Lasanta, T.; Bernechea, M.; Konstantatos, G. Tailoring the Electronic Properties of Colloidal Quantum Dots in Metal-Semiconductor Nanocomposites for High Performance Photodetectors. *Small* **2015**, *11* (22), 2636−41.
(138) Stavrinadis, A.; Rath, A. K.; de Arquer, F. P.; Diedenhofen, S. L.; Magen, C.; Martinez, L.; So, D.; Konstantatos, G. Heterovalent cation substitutional doping for quantum dot homojunction solar cells. *Nat. Commun.* **2013**, *4*, 2981.
(139) Vlaskin, V. A.; Barrows, C. J.; Erickson, C. S.; Gamelin, D. R. Nanocrystal diffusion doping. *J. Am. Chem. Soc.* **2013**, *135* (38), 14380−9.
(140) Buonsanti, R.; Milliron, D. J. Chemistry of Doped Colloidal Nanocrystals. *Chem. Mater.* **2013**, *25* (8), 1305−1317.
(141) Mikulec, F. V.; Kuno, M.; Bennati, M.; Hall, D. A.; Griffin, R. G.; Bawendi, M. G. Organometallic Synthesis and Spectroscopic Characterization of Manganese-Doped CdSe Nanocrystals. *J. Am. Chem. Soc.* **2000**, *122* (11), 2532−2540.
(142) Shim, M.; Guyot-Sionnest, P. n-type colloidal semiconductor nanocrystals. *Nature* **2000**, *407* (6807), 981−3.
(143) Zhitomirsky, D.; Furukawa, M.; Tang, J.; Stadler, P.; Hoogland, S.; Voznyy, O.; Liu, H.; Sargent, E. H. N-Type Colloidal-Quantum-Dot Solids for Photovoltaics. *Adv. Mater.* **2012**, *24* (46), 6181−6185.
(144) Voznyy, O.; Zhitomirsky, D.; Stadler, P.; Ning, Z.; Hoogland, S.; Sargent, E. H. A Charge-Orbital Balance Picture of Doping in Colloidal Quantum Dot Solids. *ACS Nano* **2012**, *6* (9), 8448−8455.
(145) Adinolfi, V.; Kramer, I. J.; Labelle, A. J.; Sutherland, B. R.; Hoogland, S.; Sargent, E. H. Photojunction Field-Effect Transistor Based on a Colloidal Quantum Dot Absorber Channel Layer. *ACS Nano* **2015**, *9* (1), 356−362.
(146) Balazs, D. M.; Dirin, D. N.; Fang, H. H.; Protesescu, L.; ten Brink, G. H.; Kooi, B. J.; Kovalenko, M. V.; Loi, M. A. Counterion-Mediated Ligand Exchange for PbS Colloidal Quantum Dot Superlattices. *ACS Nano* **2015**, *9* (12), 11951−9.
(147) Bederak, D.; Balazs, D. M.; Sukharevska, N. V.; Shulga, A. G.; Abdu-Aguye, M.; Dirin, D. N.; Kovalenko, M. V.; Loi, M. A. Comparing Halide Ligands in PbS Colloidal Quantum Dots for Field-Effect Transistors and Solar Cells. *ACS Appl. Nano Mater.* **2018**, *1* (12), 6882−6889.
(148) Ning, Z.; Voznyy, O.; Pan, J.; Hoogland, S.; Adinolfi, V.; Xu, J.; Li, M.; Kirmani, A. R.; Sun, J. P.; Minor, J.; Kemp, K. W.; Dong, H.; Rollny, L.; Labelle, A.; Carey, G.; Sutherland, B.; Hill, I.; Amassian, A.; Liu, H.; Tang, J.; Bakr, O. M.; Sargent, E. H. Air-stable n-type colloidal quantum dot solids. *Nat. Mater.* **2014**, *13* (8), 822−8.
(149) Tang, J.; Liu, H.; Zhitomirsky, D.; Hoogland, S.; Wang, X.; Furukawa, M.; Levina, L.; Sargent, E. H. Quantum Junction Solar Cells. *Nano Lett.* **2012**, *12* (9), 4889−4894.
(150) Rath, A. K.; Pelayo Garcia de Arquer, F.; Stavrinadis, A.; Lasanta, T.; Bernechea, M.; Diedenhofen, S. L.; Konstantatos, G. Remote Trap Passivation in Colloidal Quantum Dot Bulk Nanoheterojunctions and Its Effect in Solution-Processed Solar Cells. *Adv. Mater.* **2014**, *26* (27), 4741−4747.
(151) Koh, W.-k.; Koposov, A. Y.; Stewart, J. T.; Pal, B. N.; Robel, I.; Pietryga, J. M.; Klimov, V. I. *Sci. Rep.* **2013**, *3*, 2004.
(152) Engel, J. H.; Surendranath, Y.; Alivisatos, A. P. Controlled Chemical Doping of Semiconductor Nanocrystals Using Redox Buffers. *J. Am. Chem. Soc.* **2012**, *134* (32), 13200−13203.
(153) Nugraha, M. I.; Kumagai, S.; Watanabe, S.; Sytnyk, M.; Heiss, W.; Loi, M. A.; Takeya, J. Enabling Ambipolar to Heavy n-Type Transport in PbS Quantum Dot Solids through Doping with Organic Molecules. *ACS Appl. Mater. Interfaces* **2017**, *9* (21), 18039−18045.
(154) Kirmani, A. R.; García de Arquer, F. P.; Fan, J. Z.; Khan, J. I.; Walters, G.; Hoogland, S.; Wehbe, N.; Said, M. M.; Barlow, S.; Laquai, F.; Marder, S. R.; Sargent, E. H.; Amassian, A. Molecular Doping of the Hole-Transporting Layer for Efficient, Single-Step-Deposited Colloidal Quantum Dot Photovoltaics. *ACS Energy Letters* **2017**, *2* (9), 1952−1959.
(155) Kirmani, A. R.; Kiani, A.; Said, M. M.; Voznyy, O.; Wehbe, N.; Walters, G.; Barlow, S.; Sargent, E. H.; Marder, S. R.; Amassian, A. Remote Molecular Doping of Colloidal Quantum Dot Photovoltaics. *ACS Energy Letters* **2016**, *1* (5), 922−930.
(156) Brown, P. R.; Kim, D.; Lunt, R. R.; Zhao, N.; Bawendi, M. G.; Grossman, J. C.; Bulović, V. Energy Level Modification in Lead Sulfide Quantum Dot Thin Films through Ligand Exchange. *ACS Nano* **2014**, *8* (6), 5863−5872.
(157) Balazs, D. M.; Nugraha, M. I.; Bisri, S. Z.; Sytnyk, M.; Heiss, W.; Loi, M. A. Reducing charge trapping in PbS colloidal quantum dot solids. *Appl. Phys. Lett.* **2014**, *104* (11), 112104.
(158) Speirs, M. J.; Balazs, D. M.; Fang, H. H.; Lai, L. H.; Protesescu, L.; Kovalenko, M. V.; Loi, M. A. Origin of the increased open circuit voltage in PbS-CdS core-shell quantum dot solar cells. *J. Mater. Chem. A* **2015**, *3* (4), 1450−1457.
(159) Speirs, M. J.; Dirin, D. N.; Abdu-Aguye, M.; Balazs, D. M.; Kovalenko, M. V.; Loi, M. A. Temperature dependent behaviour of lead sulfide quantum dot solar cells and films. *Energy Environ. Sci.* **2016**, *9* (9), 2916−2924.
(160) Chuang, C.-H. M.; Maurano, A.; Brandt, R. E.; Hwang, G. W.; Jean, J.; Buonassisi, T.; Bulović, V.; Bawendi, M. G. Open-Circuit Voltage Deficit, Radiative Sub-Bandgap States, and Prospects in Quantum Dot Solar Cells. *Nano Lett.* **2015**, *15* (5), 3286−3294.
(161) Gaulding, E. A.; Hao, J.; Kang, H. S.; Miller, E. M.; Habisreutinger, S. N.; Zhao, Q.; Hazarika, A.; Sercel, P. C.; Luther, J. M.; Blackburn, J. L. Conductivity Tuning via Doping with Electron Donating and Withdrawing Molecules in Perovskite CsPbI3 Nanocrystal Films. *Adv. Mater.* **2019**, *31* (27), No. 1902250.
(162) Luque, A.; Martí, A. Increasing the Efficiency of Ideal Solar Cells by Photon Induced Transitions at Intermediate Levels. *Phys. Rev. Lett.* **1997**, *78* (26), 5014−5017.
(163) Luther, J. M.; Law, M.; Beard, M. C.; Song, Q.; Reese, M. O.; Ellingson, R. J.; Nozik, A. J. Schottky solar cells based on colloidal nanocrystal films. *Nano Lett.* **2008**, *8* (10), 3488−92.
(164) Debnath, R.; Tang, J.; Barkhouse, D. A.; Wang, X.; Pattantyus-Abraham, A. G.; Brzozowski, L.; Levina, L.; Sargent, E. H. Ambient-Processed Colloidal Quantum Dot Solar Cells via Individual Pre-Encapsulation of Nanoparticles. *J. Am. Chem. Soc.* **2010**, *132* (17), 5952−5953.
(165) Piliego, C.; Protesescu, L.; Bisri, S. Z.; Kovalenko, M. V.; Loi, M. A. 5.2% efficient PbS nanocrystal Schottky solar cells. *Energy Environ. Sci.* **2013**, *6* (10), 3054−3059.
(166) Luther, J. M.; Gao, J.; Lloyd, M. T.; Semonin, O. E.; Beard, M. C.; Nozik, A. J. Stability assessment on a 3% bilayer PbS/ZnO quantum dot heterojunction solar cell. *Adv. Mater.* **2010**, *22* (33), 3704−7.

https://dx.doi.org/10.1021/acsenergylett.0c01453
ACS Energy Lett. 2020, 5, 3069−3100

(167) Pattantyus-Abraham, A. G.; Kramer, I. J.; Barkhouse, A. R.; Wang, X.; Konstantatos, G.; Debnath, R.; Levina, L.; Raabe, I.; Nazeeruddin, M. K.; Grätzel, M.; Sargent, E. H. Depleted-Heterojunction Colloidal Quantum Dot Solar Cells. *ACS Nano* **2010**, *4* (6), 3374−3380.
(168) Maraghechi, P.; Labelle, A. J.; Kirmani, A. R.; Lan, X.; Adachi, M. M.; Thon, S. M.; Hoogland, S.; Lee, A.; Ning, Z.; Fischer, A.; Amassian, A.; Sargent, E. H. The Donor-Supply Electrode Enhances Performance in Colloidal Quantum Dot Solar Cells. *ACS Nano* **2013**, *7* (7), 6111−6116.
(169) Carey, G. H.; Levina, L.; Comin, R.; Voznyy, O.; Sargent, E. H. Record Charge Carrier Diffusion Length in Colloidal Quantum Dot Solids via Mutual Dot-To-Dot Surface Passivation. *Adv. Mater.* **2015**, *27* (21), 3325−3330.
(170) Chuang, C.-H. M.; Brown, P. R.; Bulović, V.; Bawendi, M. G. Improved performance and stability in quantum dot solar cells through band alignment engineering. *Nat. Mater.* **2014**, *13*, 796.
(171) Kim, G.-H.; García de Arquer, F. P.; Yoon, Y. J.; Lan, X.; Liu, M.; Voznyy, O.; Yang, Z.; Fan, F.; Ip, A. H.; Kanjanaboos, P.; Hoogland, S.; Kim, J. Y.; Sargent, E. H. High-Efficiency Colloidal Quantum Dot Photovoltaics via Robust Self-Assembled Monolayers. *Nano Lett.* **2015**, *15* (11), 7691−7696.
(172) Zhang, L.; Rao, H.; Pan, Z.; Zhong, X. ZnSxSe1-x Alloy Passivation Layer for High-Efficiency Quantum-Dot-Sensitized Solar Cells. *ACS Appl. Mater. Interfaces* **2019**, *11* (44), 41415−41423.
(173) Bernechea, M.; Miller, N. C.; Xercavins, G.; So, D.; Stavrinadis, A.; Konstantatos, G. Solution-processed solar cells based on environmentally friendly AgBiS2 nanocrystals. *Nat. Photonics* **2016**, *10*, 521.
(174) Ahmad, W.; He, J.; Liu, Z.; Xu, K.; Chen, Z.; Yang, X.; Li, D.; Xia, Y.; Zhang, J.; Chen, C. Lead Selenide (PbSe) Colloidal Quantum Dot Solar Cells with > 10% Efficiency. *Adv. Mater.* **2019**, *31* (33), 1900593.
(175) Leschkies, K. S.; Beatty, T. J.; Kang, M. S.; Norris, D. J.; Aydil, E. S. Solar Cells Based on Junctions between Colloidal PbSe Nanocrystals and Thin ZnO Films. *ACS Nano* **2009**, *3* (11), 3638−3648.
(176) Koleilat, G. I.; Wang, X.; Labelle, A. J.; Ip, A. H.; Carey, G. H.; Fischer, A.; Levina, L.; Brzozowski, L.; Sargent, E. H. A Donor-Supply Electrode (DSE) for Colloidal Quantum Dot Photovoltaics. *Nano Lett.* **2011**, *11* (12), 5173−5178.
(177) Kramer, I. J.; Sargent, E. H. Colloidal Quantum Dot Photovoltaics: A Path Forward. *ACS Nano* **2011**, *5* (11), 8506−8514.
(178) Ning, Z.; Zhitomirsky, D.; Adinolfi, V.; Sutherland, B.; Xu, J.; Voznyy, O.; Maraghechi, P.; Lan, X.; Hoogland, S.; Ren, Y.; Sargent, E. H. Graded Doping for Enhanced Colloidal Quantum Dot Photovoltaics. *Adv. Mater.* **2013**, *25* (12), 1719−1723.
(179) Barkhouse, D. A. R.; Debnath, R.; Kramer, I. J.; Zhitomirsky, D.; Pattantyus-Abraham, A. G.; Levina, L.; Etgar, L.; Grätzel, M.; Sargent, E. H. Depleted Bulk Heterojunction Colloidal Quantum Dot Photovoltaics. *Adv. Mater.* **2011**, *23* (28), 3134−3138.
(180) Kramer, I. J.; Zhitomirsky, D.; Bass, J. D.; Rice, P. M.; Topuria, T.; Krupp, L.; Thon, S. M.; Ip, A. H.; Debnath, R.; Kim, H.-C.; Sargent, E. H. Ordered Nanopillar Structured Electrodes for Depleted Bulk Heterojunction Colloidal Quantum Dot Solar Cells. *Adv. Mater.* **2012**, *24* (17), 2315−2319.
(181) Jean, J.; Chang, S.; Brown, P. R.; Cheng, J. J.; Rekemeyer, P. H.; Bawendi, M. G.; Gradečak, S.; Bulović, V. ZnO Nanowire Arrays for Enhanced Photocurrent in PbS Quantum Dot Solar Cells. *Adv. Mater.* **2013**, *25* (20), 2790−2796.
(182) Rekemeyer, P. H.; Chang, S.; Chuang, C.-H. M.; Hwang, G. W.; Bawendi, M. G.; Gradečak, S. Enhanced Photocurrent in PbS Quantum Dot Photovoltaics via ZnO Nanowires and Band Alignment Engineering. *Adv. Energy Mater.* **2016**, *6* (24), 1600848.
(183) Wang, H.; Gonzalez-Pedro, V.; Kubo, T.; Fabregat-Santiago, F.; Bisquert, J.; Sanehira, Y.; Nakazaki, J.; Segawa, H. Enhanced Carrier Transport Distance in Colloidal PbS Quantum-Dot-Based Solar Cells Using ZnO Nanowires. *J. Phys. Chem. C* **2015**, *119* (49), 27265−27274.
(184) Cheng, J. J.; Chuang, C.-H. M.; Hentz, O.; Rekemeyer, P. H.; Bawendi, M. G.; Gradečak, S. Dimension- and Surface-Tailored ZnO Nanowires Enhance Charge Collection in Quantum Dot Photovoltaic Devices. *ACS Applied Energy Materials* **2018**, *1* (5), 1815−1822.
(185) Shi, G.; Kaewprajak, A.; Ling, X.; Hayakawa, A.; Zhou, S.; Song, B.; Kang, Y.; Hayashi, T.; Altun, M. E.; Nakaya, M.; Liu, Z.; Wang, H.; Sagawa, T.; Ma, W. Finely Interpenetrating Bulk Heterojunction Structure for Lead Sulfide Colloidal Quantum Dot Solar Cells by Convective Assembly. *ACS Energy Letters* **2019**, *4* (4), 960−967.
(186) Rekemeyer, P. H.; Chuang, C.-H. M.; Bawendi, M. G.; Gradečak, S. Minority Carrier Transport in Lead Sulfide Quantum Dot Photovoltaics. *Nano Lett.* **2017**, *17* (10), 6221−6227.
(187) Crisp, R. W.; Kroupa, D. M.; Marshall, A. R.; Miller, E. M.; Zhang, J.; Beard, M. C.; Luther, J. M. Metal halide solid-state surface treatment for high efficiency PbS and PbSe QD solar cells. *Sci. Rep.* **2015**, *5*, 9945.
(188) Lan, X.; Voznyy, O.; Kiani, A.; García de Arquer, F. P.; Abbas, A. S.; Kim, G.-H.; Liu, M.; Yang, Z.; Walters, G.; Xu, J.; Yuan, M.; Ning, Z.; Fan, F.; Kanjanaboos, P.; Kramer, I.; Zhitomirsky, D.; Lee, P.; Perelgut, A.; Hoogland, S.; Sargent, E. H. Passivation Using Molecular Halides Increases Quantum Dot Solar Cell Performance. *Adv. Mater.* **2016**, *28* (2), 299−304.
(189) Azmi, R.; Oh, S.-H.; Jang, S.-Y. High-Efficiency Colloidal Quantum Dot Photovoltaic Devices Using Chemically Modified Heterojunctions. *ACS Energy Letters* **2016**, *1* (1), 100−106.
(190) Shi, G.; Wang, Y.; Liu, Z.; Han, L.; Liu, J.; Wang, Y.; Lu, K.; Chen, S.; Ling, X.; Li, Y.; Cheng, S.; Ma, W. Stable and Highly Efficient PbS Quantum Dot Tandem Solar Cells Employing a Rationally Designed Recombination Layer. *Adv. Energy Mater.* **2017**, *7*, 1602667.
(191) Wang, X.; Koleilat, G. I.; Tang, J.; Liu, H.; Kramer, I. J.; Debnath, R.; Brzozowski, L.; Barkhouse, D. A. R.; Levina, L.; Hoogland, S.; Sargent, E. H. Tandem colloidal quantum dot solar cells employing a graded recombination layer. *Nat. Photonics* **2011**, *5* (8), 480−484.
(192) Pellaroque, A.; Noel, N. K.; Habisreutinger, S. N.; Zhang, Y.; Barlow, S.; Marder, S. R.; Snaith, H. J. Efficient and Stable Perovskite Solar Cells Using Molybdenum Tris(dithiolene)s as p-Dopants for Spiro-OMeTAD. *ACS Energy Letters* **2017**, *2* (9), 2044−2050.
(193) Tavakoli Dastjerdi, H.; Tavakoli, R.; Yadav, P.; Prochowicz, D.; Saliba, M.; Tavakoli, M. M. Oxygen Plasma-Induced p-Type Doping Improves Performance and Stability of PbS Quantum Dot Solar Cells. *ACS Appl. Mater. Interfaces* **2019**, *11* (29), 26047−26052.
(194) Pan, Z.; Rao, H.; Mora-Seró, I.; Bisquert, J.; Zhong, X. Quantum dot-sensitized solar cells. *Chem. Soc. Rev.* **2018**, *47* (20), 7659−7702.
(195) Yang, Z.; Fan, J. Z.; Proppe, A. H.; Arquer, F. P. G. d.; Rossouw, D.; Voznyy, O.; Lan, X.; Liu, M.; Walters, G.; Quintero-Bermudez, R.; Sun, B.; Hoogland, S.; Botton, G. A.; Kelley, S. O.; Sargent, E. H. Mixed-quantum-dot solar cells. *Nat. Commun.* **2017**, *8* (1), 1325.
(196) Kirmani, A. R.; Eisner, F.; Mansour, A. E.; Firdaus, Y.; Chaturvedi, N.; Seitkhan, A.; Nugraha, M. I.; Yarali, E.; García de Arquer, F. P.; Sargent, E. H.; Anthopoulos, T. D.; Amassian, A. Colloidal Quantum Dot Photovoltaics Using Ultrathin, Solution-Processed Bilayer In2O3/ZnO Electron Transport Layers with Improved Stability. *ACS Applied Energy Materials* **2020**, *3* (6), 5135−5141.
(197) Pradhan, S.; Stavrinadis, A.; Gupta, S.; Christodoulou, S.; Konstantatos, G. Breaking the Open-Circuit Voltage Deficit Floor in PbS Quantum Dot Solar Cells through Synergistic Ligand and Architecture Engineering. *ACS Energy Letters* **2017**, *2* (6), 1444−1449.
(198) Rath, A. K.; Bernechea, M.; Martinez, L.; de Arquer, F. P. G.; Osmond, J.; Konstantatos, G. Solution-processed inorganic bulk nano-heterojunctions and their application to solar cells. *Nat. Photonics* **2012**, *6* (8), 529−534.

https://dx.doi.org/10.1021/acsenergylett.0c01453
ACS Energy Lett. 2020, 5, 3069−3100

(199) Zhitomirsky, D.; Kramer, I. J.; Labelle, A. J.; Fischer, A.; Debnath, R.; Pan, J.; Bakr, O. M.; Sargent, E. H. Colloidal Quantum Dot Photovoltaics: The Effect of Polydispersity. *Nano Lett.* **2012**, *12* (2), 1007−1012.
(200) Jo, J. W.; Kim, Y.; Choi, J.; de Arquer, F. P. G.; Walters, G.; Sun, B.; Ouellette, O.; Kim, J.; Proppe, A. H.; Quintero-Bermudez, R.; Fan, J.; Xu, J.; Tan, C. S.; Voznyy, O.; Sargent, E. H. Enhanced Open-Circuit Voltage in Colloidal Quantum Dot Photovoltaics via Reactivity-Controlled Solution-Phase Ligand Exchange. *Adv. Mater.* **2017**, *29* (43), 1703627.
(201) Alimoradi Jazi, M.; Janssen, V. A. E. C.; Evers, W. H.; Tadjine, A.; Delerue, C.; Siebbeles, L. D. A.; van der Zant, H. S. J.; Houtepen, A. J.; Vanmaekelbergh, D. Transport Properties of a Two-Dimensional PbSe Square Superstructure in an Electrolyte-Gated Transistor. *Nano Lett.* **2017**, *17* (9), 5238−5243.
(202) Shulga, A. G.; Kahmann, S.; Dirin, D. N.; Graf, A.; Zaumseil, J.; Kovalenko, M. V.; Loi, M. A. Electroluminescence Generation in PbS Quantum Dot Light-Emitting Field-Effect Transistors with Solid-State Gating. *ACS Nano* **2018**, *12* (12), 12805−12813.
(203) Luo, D.; Su, R.; Zhang, W.; Gong, Q.; Zhu, R. Minimizing non-radiative recombination losses in perovskite solar cells. *Nature Reviews Materials* **2020**, *5* (1), 44−60.
(204) Stolterfoht, M.; Grischek, M.; Caprioglio, P.; Wolff, C. M.; Gutierrez-Partida, E.; Peña-Camargo, F.; Rothhardt, D.; Zhang, S.; Raoufi, M.; Wolansky, J.; Abdi-Jalebi, M.; Stranks, S. D.; Albrecht, S.; Kirchartz, T.; Neher, D. How To Quantify the Efficiency Potential of Neat Perovskite Films: Perovskite Semiconductors with an Implied Efficiency Exceeding 28%. *Adv. Mater.* **2020**, *32* (17), 2000080.
(205) Stolterfoht, M.; Wolff, C. M.; Márquez, J. A.; Zhang, S.; Hages, C. J.; Rothhardt, D.; Albrecht, S.; Burn, P. L.; Meredith, P.; Unold, T.; Neher, D. Visualization and suppression of interfacial recombination for high-efficiency large-area pin perovskite solar cells. *Nature Energy* **2018**, *3* (10), 847−854.
(206) Kim, T.; Firdaus, Y.; Kirmani, A. R.; Liang, R.-Z.; Hu, H.; Liu, M.; El Labban, A.; Hoogland, S.; Beaujuge, P. M.; Sargent, E. H.; Amassian, A. Hybrid Tandem Quantum Dot/Organic Solar Cells with Enhanced Photocurrent and Efficiency via Ink and Interlayer Engineering. *ACS Energy Letters* **2018**, *3* (6), 1307−1314.
(207) Kim, T.; Gao, Y.; Hu, H.; Yan, B.; Ning, Z.; Jagadamma, L. K.; Zhao, K.; Kirmani, A. R.; Eid, J.; Adachi, M. M.; Sargent, E. H.; Beaujuge, P. M.; Amassian, A. Hybrid tandem solar cells with depleted-heterojunction quantum dot and polymer bulk heterojunction subcells. *Nano Energy* **2015**, *17*, 196−205.
(208) Kim, T.; Palmiano, E.; Liang, R. Z.; Hu, H.; Murali, B.; Kirmani, A. R.; Firdaus, Y.; Gao, Y.; Sheikh, A.; Yuan, M.; Mohammed, O. F.; Hoogland, S.; Beaujuge, P. M.; Sargent, E. H.; Amassian, A. Hybrid tandem quantum dot/organic photovoltaic cells with complementary near infrared absorption. *Appl. Phys. Lett.* **2017**, *110* (22), 223903.
(209) Aqoma, H.; Imran, I. F.; Mubarok, M. A.; Hadmojo, W. T.; Do, Y. R.; Jang, S.-Y. Efficient Hybrid Tandem Solar Cells Based on Optical Reinforcement of Colloidal Quantum Dots with Organic Bulk Heterojunctions. *Adv. Energy Mater.* **2020**, *10* (7), 1903294.
(210) Yuan, L.; Michaels, H.; Roy, R.; Johansson, M.; Öberg, V.; Andruszkiewicz, A.; Zhang, X.; Freitag, M.; Johansson, E. M. J. Four-Terminal Tandem Solar Cell with Dye-Sensitized and PbS Colloidal Quantum-Dot-Based Subcells. *ACS Applied Energy Materials* **2020**, *3* (4), 3157−3161.
(211) Crisp, R. W.; Pach, G. F.; Kurley, J. M.; France, R. M.; Reese, M. O.; Nanayakkara, S. U.; MacLeod, B. A.; Talapin, D. V.; Beard, M. C.; Luther, J. M. Tandem Solar Cells from Solution-Processed CdTe and PbS Quantum Dots Using a ZnTe-ZnO Tunnel Junction. *Nano Lett.* **2017**, *17* (2), 1020−1027.
(212) Kim, J.; Ouellette, O.; Voznyy, O.; Wei, M.; Choi, J.; Choi, M.-J.; Jo, J. W.; Baek, S.-W.; Fan, J.; Saidaminov, M. I.; Sun, B.; Li, P.; Nam, D.-H.; Hoogland, S.; Lu, Z.-H.; García de Arquer, F. P.; Sargent, E. H. Butylamine-Catalyzed Synthesis of Nanocrystal Inks Enables Efficient Infrared CQD Solar Cells. *Adv. Mater.* **2018**, *30* (45), 1803830.
(213) Kim, Y.; Che, F.; Jo, J. W.; Choi, J.; García de Arquer, F. P.; Voznyy, O.; Sun, B.; Kim, J.; Choi, M.-J.; Quintero-Bermudez, R.; Fan, F.; Tan, C. S.; Bladt, E.; Walters, G.; Proppe, A. H.; Zou, C.; Yuan, H.; Bals, S.; Hofkens, J.; Roeffaers, M. B. J.; Hoogland, S.; Sargent, E. H. A Facet-Specific Quantum Dot Passivation Strategy for Colloid Management and Efficient Infrared Photovoltaics. *Adv. Mater.* **2019**, *31* (17), 1805580.
(214) Sun, B.; Ouellette, O.; García de Arquer, F. P.; Voznyy, O.; Kim, Y.; Wei, M.; Proppe, A. H.; Saidaminov, M. I.; Xu, J.; Liu, M.; Li, P.; Fan, J. Z.; Jo, J. W.; Tan, H.; Tan, F.; Hoogland, S.; Lu, Z. H.; Kelley, S. O.; Sargent, E. H. Multibandgap quantum dot ensembles for solar-matched infrared energy harvesting. *Nat. Commun.* **2018**, *9* (1), 4003.
(215) Che, X.; Li, Y.; Qu, Y.; Forrest, S. R. High fabrication yield organic tandem photovoltaics combining vacuum- and solution-processed subcells with 15% efficiency. *Nature Energy* **2018**, *3* (5), 422−427.
(216) Meng, L.; Zhang, Y.; Wan, X.; Li, C.; Zhang, X.; Wang, Y.; Ke, X.; Xiao, Z.; Ding, L.; Xia, R.; Yip, H.-L.; Cao, Y.; Chen, Y. Organic and solution-processed tandem solar cells with 17.3% efficiency. *Science* **2018**, *361* (6407), 1094−1098.
(217) Fan, B.; Zhang, D.; Li, M.; Zhong, W.; Zeng, Z.; Ying, L.; Huang, F.; Cao, Y. Achieving over 16% efficiency for single-junction organic solar cells. *Sci. China: Chem.* **2019**, *62* (6), 746−752.
(218) An, Q.; Ma, X.; Gao, J.; Zhang, F. Solvent additive-free ternary polymer solar cells with 16.27% efficiency. *Science Bulletin* **2019**, *64* (8), 504−506.
(219) Tan, L.; Li, P.; Sun, B.; Chaker, M.; Ma, D. Stabilities Related to Near-Infrared Quantum Dot-Based Solar Cells: The Role of Surface Engineering. *ACS Energy Letters* **2017**, *2* (7), 1573−1585.
(220) Hassinen, A.; Moreels, I.; De Nolf, K.; Smet, P. F.; Martins, J. C.; Hens, Z. Short-Chain Alcohols Strip X-Type Ligands and Quench the Luminescence of PbSe and CdSe Quantum Dots, Acetonitrile Does Not. *J. Am. Chem. Soc.* **2012**, *134* (51), 20705−20712.
(221) Lu, K.; Wang, Y.; Liu, Z.; Han, L.; Shi, G.; Fang, H.; Chen, J.; Ye, X.; Chen, S.; Yang, F.; Shulga, A. G.; Wu, T.; Gu, M.; Zhou, S.; Fan, J.; Loi, M. A.; Ma, W. High-Efficiency PbS Quantum-Dot Solar Cells with Greatly Simplified Fabrication Processing via "Solvent-Curing. *Adv. Mater.* **2018**, *30* (25), 1707572.
(222) Song, J. H.; Choi, H.; Kim, Y.-H.; Jeong, S. High Performance Colloidal Quantum Dot Photovoltaics by Controlling Protic Solvents in Ligand Exchange. *Adv. Energy Mater.* **2017**, *7* (15), 1700301.
(223) Aqoma, H.; Jang, S.-Y. Solid-state-ligand-exchange free quantum dot ink-based solar cells with an efficiency of 10.9%. *Energy Environ. Sci.* **2018**, *11* (6), 1603−1609.
(224) Deng, Y.; Zheng, X.; Bai, Y.; Wang, Q.; Zhao, J.; Huang, J. Surfactant-controlled ink drying enables high-speed deposition of perovskite films for efficient photovoltaic modules. *Nature Energy* **2018**, *3* (7), 560−566.
(225) Chen, W.; Tang, H.; Li, N.; Scheel, M. A.; Xie, Y.; Li, D.; Körstgens, V.; Schwartzkopf, M.; Roth, S. V.; Wang, K.; Sun, X. W.; Müller-Buschbaum, P. Colloidal PbS quantum dot stacking kinetics during deposition via printing. *Nanoscale Horizons* **2020**, *5* (5), 880−885.
(226) Aqoma, H.; Mubarok, M. A.; Lee, W.; Hadmojo, W. T.; Park, C.; Ahn, T. K.; Ryu, D. Y.; Jang, S.-Y. Improved Processability and Efficiency of Colloidal Quantum Dot Solar Cells Based on Organic Hole Transport Layers. *Adv. Energy Mater.* **2018**, *8* (23), 1800572.
(227) Mubarok, M. A.; Aqoma, H.; Wibowo, F. T. A.; Lee, W.; Kim, H. M.; Ryu, D. Y.; Jeon, J.-W.; Jang, S.-Y. Molecular Engineering in Hole Transport π-Conjugated Polymers to Enable High Efficiency Colloidal Quantum Dot Solar Cells. *Adv. Energy Mater.* **2020**, *10* (8), 1902933.
(228) Zhang, Y.; Kan, Y.; Gao, K.; Gu, M.; Shi, Y.; Zhang, X.; Xue, Y.; Zhang, X.; Liu, Z.; Zhang, Y.; Yuan, J.; Ma, W.; Jen, A. K. Y. Hybrid Quantum Dot/Organic Heterojunction: A Route to Improve Open-Circuit Voltage in PbS Colloidal Quantum Dot Solar Cells. *ACS Energy Letters* **2020**, *5*, 2335−2342.

https://dx.doi.org/10.1021/acsenergylett.0c01453
ACS Energy Lett. 2020, 5, 3069−3100

(229) Chernomordik, B. D.; Marshall, A. R.; Pach, G. F.; Luther, J. M.; Beard, M. C. Quantum Dot Solar Cell Fabrication Protocols. *Chem. Mater.* **2017**, *29* (1), 189−198.
(230) Abbas, M. A.; Basit, M. A.; Yoon, S. J.; Lee, G. J.; Lee, M. D.; Park, T. J.; Kamat, P. V.; Bang, J. H. Revival of Solar Paint Concept: Air-Processable Solar Paints for the Fabrication of Quantum Dot-Sensitized Solar Cells. *J. Phys. Chem. C* **2017**, *121* (33), 17658−17670.
(231) Genovese, M. P.; Lightcap, I. V.; Kamat, P. V. Sun-Believable Solar Paint. A Transformative One-Step Approach for Designing Nanocrystalline Solar Cells. *ACS Nano* **2012**, *6* (1), 865−872.
(232) Kramer, I. J.; Moreno-Bautista, G.; Minor, J. C.; Kopilovic, D.; Sargent, E. H. Colloidal quantum dot solar cells on curved and flexible substrates. *Appl. Phys. Lett.* **2014**, *105* (16), 163902.
(233) Tang, J.; Brzozowski, L.; Barkhouse, D. A. R.; Wang, X.; Debnath, R.; Wolowiec, R.; Palmiano, E.; Levina, L.; Pattantyus-Abraham, A. G.; Jamakosmanovic, D.; Sargent, E. H. Quantum Dot Photovoltaics in the Extreme Quantum Confinement Regime: The Surface-Chemical Origins of Exceptional Air- and Light-Stability. *ACS Nano* **2010**, *4* (2), 869−878.
(234) Silbergeld, E. K.; Waalkes, M.; Rice, J. M. Lead as a carcinogen: Experimental evidence and mechanisms of action. *Am. J. Ind. Med.* **2000**, *38* (3), 316−323.
(235) Zhang, S.; Ye, L.; Zhang, H.; Hou, J. Green-solvent-processable organic solar cells. *Mater. Today* **2016**, *19* (9), 533−543.
(236) Ma, Z.; Zhao, B.; Gong, Y.; Deng, J.; Tan, Z. a. Green-solvent-processable strategies for achieving large-scale manufacture of organic photovoltaics. *J. Mater. Chem. A* **2019**, *7* (40), 22826−22847.
(237) Tian, S.; Li, J.; Li, S.; Bu, T.; Mo, Y.; Wang, S.; Li, W.; Huang, F. A facile green solvent engineering for up-scaling perovskite solar cell modules. *Sol. Energy* **2019**, *183*, 386−391.
(238) Jessop, P. G. Searching for green solvents. *Green Chem.* **2011**, *13* (6), 1391−1398.
(239) Byrne, F. P.; Jin, S.; Paggiola, G.; Petchey, T. H. M.; Clark, J. H.; Farmer, T. J.; Hunt, A. J.; Robert McElroy, C.; Sherwood, J. Tools and techniques for solvent selection: green solvent selection guides. *Sustainable Chem. Processes* **2016**, *4* (1), 7.
(240) Shen, Y.; Weeranoppanant, N.; Xie, L.; Chen, Y.; Lusardi, M. R.; Imbrogno, J.; Bawendi, M. G.; Jensen, K. F. Multistage extraction platform for highly efficient and fully continuous purification of nanoparticles. *Nanoscale* **2017**, *9* (23), 7703−7707.
(241) Shen, Y.; Abolhasani, M.; Chen, Y.; Xie, L.; Yang, L.; Coley, C. W.; Bawendi, M. G.; Jensen, K. F. In-Situ Microfluidic Study of Biphasic Nanocrystal Ligand-Exchange Reactions Using an Oscillatory Flow Reactor. *Angew. Chem., Int. Ed.* **2017**, *56* (51), 16333−16337.
(242) MacLeod, B. P.; Parlane, F. G. L.; Morrissey, T. D.; Häse, F.; Roch, L. M.; Dettelbach, K. E.; Moreira, R.; Yunker, L. P. E.; Rooney, M. B.; Deeth, J. R.; Lai, V.; Ng, G. J.; Situ, H.; Zhang, R. H.; Elliott, M. S.; Haley, T. H.; Dvorak, D. J.; Aspuru-Guzik, A.; Hein, J. E.; Berlinguette, C. P. Self-driving laboratory for accelerated discovery of thin-film materials. *Science Advances* **2020**, *6* (20), No. eaaz8867.
(243) Niu, G.; Zhang, L.; Ruditskiy, A.; Wang, L.; Xia, Y. A Droplet-Reactor System Capable of Automation for the Continuous and Scalable Production of Noble-Metal Nanocrystals. *Nano Lett.* **2018**, *18* (6), 3879−3884.
(244) Li, S.; Baker, R. W.; Lignos, I.; Yang, Z.; Stavrakis, S.; Howes, P. D.; deMello, A. J. Automated microfluidic screening of ligand interactions during the synthesis of cesium lead bromide nanocrystals. *Molecular Systems Design & Engineering* **2020**, *5* (6), 1118−1130.
(245) Bezinge, L.; Maceiczyk, R. M.; Lignos, I.; Kovalenko, M. V.; deMello, A. J. Pick a Color MARIA: Adaptive Sampling Enables the Rapid Identification of Complex Perovskite Nanocrystal Compositions with Defined Emission Characteristics. *ACS Appl. Mater. Interfaces* **2018**, *10* (22), 18869−18878.
(246) Voznyy, O.; Levina, L.; Fan, J. Z.; Askerka, M.; Jain, A.; Choi, M.-J.; Ouellette, O.; Todorović, P.; Sagar, L. K.; Sargent, E. H. Machine Learning Accelerates Discovery of Optimal Colloidal Quantum Dot Synthesis. *ACS Nano* **2019**, *13* (10), 11122−11128.
(247) Kirmani, A. R. Commercializing colloidal quantum dot photovoltaics. *MRS Bull.* **2019**, *44* (7), 524−525.
(248) Yuan, J.; Hazarika, A.; Zhao, Q.; Ling, X.; Moot, T.; Ma, W.; Luther, J. M. Metal Halide Perovskites in Quantum Dot Solar Cells: Progress and Prospects. *Joule* **2020**, *4* (6), 1160−1185.
(249) Wang, Y.; Yuan, J.; Zhang, X.; Ling, X.; Larson, B. W.; Zhao, Q.; Yang, Y.; Shi, Y.; Luther, J. M.; Ma, W. Surface Ligand Management Aided by a Secondary Amine Enables Increased Synthesis Yield of CsPbI3 Perovskite Quantum Dots and High Photovoltaic Performance. *Adv. Mater.* **2020**, *32*, 2000449.

https://dx.doi.org/10.1021/acsenergylett.0c01453
ACS Energy Lett. 2020, 5, 3069−3100